Earth-Science Reviews 239 (2023) 104359

Contents lists available at ScienceDirect

Earth-Science Reviews

journal homepage: www.elsevier.com/locate/earscirev

Quantitative and mechanistic understanding of the open ocean carbonate pump - perspectives for remote sensing and autonomous in situ observation

G. Neukermans [a,f,*], L.T. Bach [b], A. Butterley [b], Q. Sun [a,e], H. Claustre [c], G.R. Fournier [d]

[a] Ghent University, Biology Department, MarSens Research Group, Krijgslaan 281 – S8, 9000 Ghent, Belgium
[b] Institute for Marine and Antarctic Studies, University of Tasmania, Hobart, TAS 7004, Australia
[c] Sorbonne Université, CNRS, Laboratoire d'Océanographie de Villefranche, LOV, F-06230 Villefranche-sur-Mer, France
[d] DRDC Valcartier Research Laboratory, Québec, Québec G3J1X5, Canada
[e] Ghent University, ELIS department, Liquid Crystals and Photonics Group, Technologiepark Zwijnaarde 15, 9052 Zwijnaarde, Belgium.
[f] Flanders Marine Institute (VLIZ), InnovOcean Campus, Jacobsenstraat 1, 8400 Ostend, Belgium

ARTICLE INFO

Keywords:
Ocean carbon cycle
Biological carbon pump
Carbonate pump
Alkalinity pump
Planktonic calcification
Calcium carbonate flux
Autonomous observations
Ocean colour remote sensing

ABSTRACT

The open ocean carbonate pump represents the production and downward flux of particulate inorganic carbon (PIC) in the form of calcium carbonate synthesized by calcifying plankton. This pump operates alongside the organic carbon pump, which concerns the production and downward flux of organic carbon, mostly in the form of particles (POC). While the organic carbon pump draws down atmospheric carbon dioxide, the carbonate pump causes an increase in surface ocean carbon dioxide (CO_2), thereby counteracting the organic carbon pump. However, PIC produced by the carbonate pump is of high-density and has been hypothesized to enhance the downward flux of organic carbon, increasing the efficiency of the organic carbon pump. Here, we review our current quantitative and mechanistic understanding of the contemporary open ocean carbonate pump, its counter- and ballast effects. We first examine the relative contributions of the various calcifying plankton groups (coccolithophores, foraminifera, and pteropods) to PIC production and flux based on a global compilation of PIC flux observations. Next, we compare spatial patterns in calcification rates from remote sensing with observations of PIC flux at depth obtained from sediment traps and radiochemical tracers. We then review estimates of the counter effect of the carbonate pump on the partial pressure of CO_2, pCO_2, in surface waters based on remote sensing studies and estimates of the rain ratio of exported carbon and the amount of CO_2 released per PIC precipitated, Ψ. Next, we review our understanding of the PIC ballast effect and implementations in biogeochemical models. Lastly, we discuss observations of the organic carbon pump with autonomous BioGeoChemical-Argo (BGC-Argo) profiling floats and perspectives for extending observations to the carbonate pump.

1. Introduction

The ocean's biological carbon pump (BCP) is a combination of sequential processes that collectively transfer biogenic carbon from the surface ocean to deeper layers (Volk and Hoffert, 1985). The first process is the production of particulate organic and inorganic carbon (POC, PIC) and dissolved organic carbon (DOC) in the euphotic zone (Fig. 1). POC and DOC are formed photosynthetically by phytoplankton while PIC in the form of calcium carbonate ($CaCO_3$) is formed through calcification by various autotrophic and heterotrophic taxa. The second process is the downward flux of some of the POC, PIC, and DOC after their production in the surface ocean. The downward flux is driven by three mechanisms: gravitational sinking of POC and PIC, physical downwelling of PIC, POC and dissolved organic carbon (DOC), and active transport mediated by zooplankton and nekton (Boyd et al., 2019). While being transferred to deeper ocean waters, most of the POC and DOC become respired (75%–93% of exported POC; Boyd et al., 2019) and a significant fraction of PIC dissolves (12%–60% of exported PIC, reviewed in detail in section 3.2) (Fig. 1). The remineralized products are transported back to the surface ocean via ocean currents on timescales that depend on how fast water masses move, but generally range from months to millenia (Siegel et al., 2021).

The BCP leads to a depletion of dissolved inorganic carbon (DIC) and nutrients in the surface ocean and an enrichment in the deep ocean, thereby enabling the oceans to store more CO_2 than without the BCP. Indeed, model simulations under pre-industrial conditions have found

* Corresponding author.
E-mail address: griet.neukermans@ugent.be (G. Neukermans).

https://doi.org/10.1016/j.earscirev.2023.104359
Received 25 July 2022; Received in revised form 10 February 2023; Accepted 11 February 2023
Available online 18 February 2023

that the atmospheric CO_2 mixing ratio would increase from 280 ppm to about 500 ppm within 250 years when the BCP is "switched off" (Maier-Reimer et al., 1996). The BCP is currently assumed to be in steady state, meaning that the downward flux of carbon is in equilibrium with the upward flux of carbon (DeVries et al., 2017). Or in other words, the BCP maintains an established surface-to-depth gradient in DIC but does not further increase or weaken it. The surface-to-depth gradient in DIC is thought to be maintained to 70% by the "organic carbon pump" (POC and DOC) and to 20% by the carbonate pump (PIC). The remaining 10% are due to the "solubility pump", an abiotic process where excess DIC is taken up in cold water at high latitudes and transported in deep-water formation regions (Sarmiento and Gruber, 2006), which will not be further considered in this review.

While both the organic carbon and carbonate pumps contribute to the surface-to-depth DIC gradient, they have opposite effects on atmospheric CO_2. This is also the reason why the carbonate pump is occasionally referred to as the "carbonate counter pump" (Rost and Riebesell, 2004). Its opposing effect on atmospheric CO_2 is due to a chemical feedback during $CaCO_3$ formation where CO_2 is ultimately generated. In the following we will introduce the chemistry driving this process in more detail.

When CO_2 dissolves in seawater it reacts with water (H_2O) to form carbonic acid (H_2CO_3). Carbonic acid dissociates to form bicarbonate (HCO_3^-), carbonate (CO_3^{2-}) and protons (H^+):

$$CO_2 + H_2O \leftrightarrow HCO_3^- + H^+ \leftrightarrow CO_3^{2-} + 2H^+ \quad (1)$$

(Note that H_2CO_3 is omitted in this equilibrium as it usually considered as part of dissolved CO_2) (Zeebe and Wolf-Gladrow, 2001). The relative concentrations of dissolved CO_2, HCO_3^- and CO_3^{2-} depend on the proton concentration in seawater, commonly referred to as pH (i.e. $10^{-[H+]}$). At a typical seawater pH on the total pH scale of 8.1, CO_2, HCO_3^-, and CO_3^{2-} contribute 1, 90, and 9%, respectively. When $CaCO_3$ is precipitated, Ca^{2+} ions react with CO_3^{2-}. The removal of CO_3^{2-} due to calcification reduces the buffering capacity of the carbonate system (Eq. 1), enabling protons to react with the remaining CO_3^{2-} and HCO_3^- which leads to a shift in the carbonate system (Eq. 1) towards CO_2, thus increasing the partial pressure of CO_2 in seawater, pCO_2.

The amount of CO_2 released per $CaCO_3$ precipitated, denoted Ψ (mol: mol, $\Psi \leq 1$), is controlled by seawater carbonate chemistry, temperature, and salinity (Frankignoulle et al., 1994; Smith and Gattuso, 2011). Contemporary global mean surface values of Ψ are ~0.66 (Smith and Mackenzie, 2016), with values tending towards 1 as seawater cools and pCO_2 increases (Smith and Gattuso, 2011). Surface values range from 0.56 to 0.80 from the tropical to the polar oceans (driven by temperature differences) and with depth from 0.66 at the surface to 0.85 at 1000 m (driven mostly by pCO_2 differences) (Smith, 2013; Smith and Gattuso, 2011).

The ratio of PIC to POC in biogenic particles that "rain" to the deep ocean is referred to as the rain ratio (dimensionless) (Archer and Maier-Reimer, 1994). The rain ratio of particles exported from the euphotic zone to the deeper ocean layers reflects the strength of the carbonate pump relative to the organic carbon pump. The counter effect of the carbonate pump on CO_2 drawdown by the organic carbon pump can be expressed as (Rembauville et al., 2016; Salter et al., 2014):

$$CounterEffect(\%) = \Psi \times FPIC_{>EZ}/FPOC_{>EZ} \times 100 \quad (2)$$

where $FPOC_{>EZ}$ and $FPIC_{>EZ}$ are the respective annual export flux of POC and PIC from the euphotic zone (or alternatively, a fixed reference depth of 100 m; see Buesseler et al., 2020 for discussion on depth horizon for carbon export). Estimates for global POC export based on sediment traps, radiochemical tracers, and biogeochemical models range between 4 and 12 Pg C y^{-1} (DeVries and Weber, 2017; Henson et al., 2012; Siegel et al., 2016) (Fig. 1), a broad range of uncertainty almost as large as current annual anthropogenic CO_2 emissions of 10.2 ± 0.8 Pg C y^{-1} (Friedlingstein et al., 2022). Global PIC export estimates vary over a factor of four, 0.4–1.8 Pg C y^{-1} (Berelson et al., 2007) (Fig. 1). With a global surface ocean mean Ψ of 0.66, a median open ocean PIC export of 1 Pg C y^{-1} results in a net CO_2 production of 0.26–1.19 Pg C y^{-1}, which is equivalent to 3–12% of current annual anthropogenic CO_2 emissions. In section 3.3, we review global and regional estimates of the counter

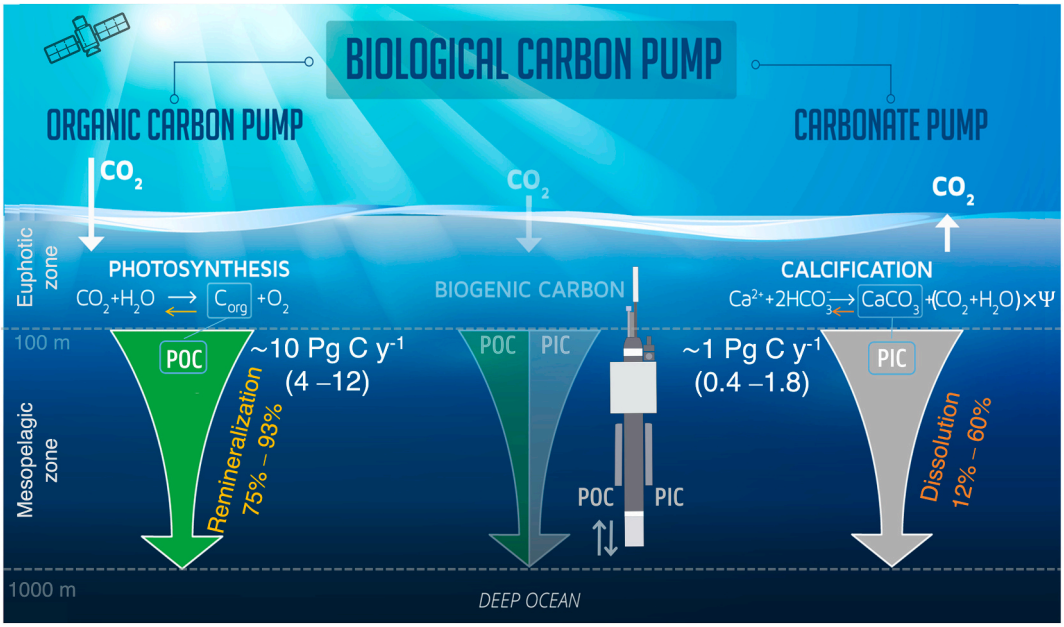

Fig. 1. The components of the biological carbon pump: (left) the organic carbon pump (driven by photosynthesis-remineralization processes) and (right) the carbonate pump (driven by calcification-dissolution processes), which have opposite effects on the partial pressure of CO_2 in the surface ocean. Calcification reaction: $Ca^{2+} + 2HCO_3^- \rightarrow CaCO_3 + \psi(CO_2 + H_2O) + (1-\psi)(CH_2O + O_2)$ (Smith and Gattuso, 2011) Median and range of global annual POC and PIC export flux. Middle: a BioGeoChemical-Argo float equipped with POC and PIC sensors to monitor the organic and carbonate pumps in concert (image credits: Thomas Jessin @oceanshape, satellite: Nick Bluth@noun-project).

effect based on in situ and remote sensing observations.

The changes in carbonate chemistry induced by calcification thus weaken CO_2 drawdown by the BCP. However, the formed $CaCO_3$ has a high density ($\rho = 2.7$ g cm^{-3}) compared to POC ($\rho = 1.06$ g cm^{-3}; Aas, 1996) and may therefore enhance the sinking speed of POC aggregates (Armstrong et al., 2001). Earlier evidence from sediment traps suggested that this ballast effect drives the POC flux to large depths (Armstrong et al., 2001; Francois et al., 2002; Klaas and Archer, 2002). However, the so-called ballast hypothesis, proposed twenty years ago, remains controversial today as will be discussed in more detail in section 3.4.

This review paper is organized as follows: first we introduce the calcifying plankton groups and examine their relative contributions to PIC production and flux (section 3.1). In section 3.2, we review our current quantitative understanding of the carbonate pump, including global estimates of PIC export and dissolution in the mesopelagic ocean. In section 3.3, we review estimates of the counter effect of the carbonate pump on pCO_2 in surface waters based on remote sensing studies and estimates of the rain ratio of exported carbon and Ψ. Then, we review our understanding of the PIC ballast effect and implementations in biogeochemical models (section 3.4). Lastly, we discuss observations of the BCP with autonomous BioGeoChemical-Argo (BGC-Argo) profiling floats and perspectives for extending observations to the carbonate pump (section 3.5).

2. Materials and methods

2.1. Compilation of PIC flux estimates with contributions from calcifying plankton groups

A literature search for observations of PIC flux from different taxa of calcifying plankton was done using Google Scholar. The first 150 hits for the keywords "PIC" or "$CaCO_3$" or "aragonite" or "calcite" or "inorganic carbon" or "carbonate" and "flux" combined with either "coccolithophores", "foraminifera", or "pteropods" were included in this review. Where available, the relative contribution of the three taxa to total PIC flux is reported.

2.2. PIC and POC flux from sediment traps and radiochemical tracers

Mass fluxes of PIC and POC were obtained from the compilation of observations from sediment traps that collect sinking particles by Torres Valdés et al. (2014). The compilation covers a latitudinal gradient across the Atlantic Ocean and spans the period 1982 till 2011. The original dataset contains 5202 observations of POC flux (mg C m^{-2} d^{-1}), 2649 observations of $CaCO_3$ flux (mg $CaCO_3$ m^{-2} d^{-1}) and 1048 observations of PIC flux spanning a depth range from 15 m to 5031 m. $CaCO_3$ mass flux was multiplied by a factor 0.12 to convert into PIC mass flux (mg C m^{-2} d^{-1}). Most sediment trap deployment times ranged from <1 to 61 days, reflecting daily to seasonal mean mass fluxes. In a minority of cases, traps were deployed for longer term (>250 days), giving $n = 134$ observations of annual mean fluxes. For a detailed description of the dataset, the reader is referred to Torres Valdés et al. (2014).

PIC and POC export flux out of the euphotic zone were also obtained from the Thorium-234 isotope technique (Buesseler et al., 1998). The radioactive short-lived Thorium-234 (^{234}Th, $t_{1/2} = 24.1$ days) is the daughter isotope of naturally occurring Uranium-238 (^{238}U, $t_{1/2} = 4.47 \times 10^9$ years). Unlike ^{238}U, ^{234}Th is insoluble in seawater and adheres to particles as they form. Particle export flux can then be estimated from the ^{234}Th export rate, obtained from disequilibrium between ^{238}U and ^{234}Th in the water column. POC and PIC export flux are obtained by multiplying ^{234}Th export rate by an estimate of the ratio of ^{234}Th/POC and ^{234}Th/PIC on sinking particles that are characteristic of those carrying these elements below the euphotic zone (Buesseler et al., 1998; Le Moigne et al., 2013b). This provides an integrated estimate of POC and PIC export over a timescale of several weeks. Whereas ^{234}Th is commonly used to quantify POC export flux and global compilations of such datasets exist (Ceballos-Romero et al., 2022; Le Moigne et al., 2013b; Puigcorbé et al., 2020), PIC flux estimates are more rare. To the best of our knowledge, the only published datasets of ^{234}Th-derived POC export flux that also include PIC export flux are the ones in Le Moigne et al. (2014; their supplementary table S1) and Rosengard et al. (2015; their Table 3). The dataset of Le Moigne et al. (2014) comprises 95 observations, mostly from the Atlantic Ocean, while the dataset of Rosengard et al. (2015) comprises 27 observations from the Atlantic and Indian sectors of the Southern Ocean.

2.3. Ocean colour remote sensing data

PIC concentration from ocean colour satellites is derived from a hybrid of two independent approaches, one that uses two spectral bands (blue and green band) and a pre-computed look-up-table derived from in situ measurements (Balch et al., 2005) and another that uses three spectral bands (red and near-infrared bands; Gordon et al., 2001). Both approaches estimate the backscattering coefficient of calcite particles b_{bc} (m^{-1}). PIC concentration (mol m^{-3}) is then estimated by dividing b_{bc} by the calcite-specific backscattering coefficient b_{bc}(546 nm)/PIC which equals 1.628 m^2 mol^{-1} as obtained from regression analyses of concomitant in situ b_{bc}(546) and PIC measurements (Balch et al., 1996a). We note that in the reprocessing of NASA ocean colour satellite data version R2022 (being implemented at the time of publication of this manuscript), the constant value for b_{bc}(546 nm)/PIC = 1.628 m^2 mol^{-1} was changed to a variable value based on results from the field that show a strong relationship between high b_{bc}/PIC values in regions of low coccolithophore abundance and lower b_{bc}/PIC values in regions of high coccolithophore abundance (Balch and Mitchell, 2023). The ocean colour satellite PIC concentration represents coccolith and coccosphere calcite concentrations at the surface of the ocean, PICsurface. POC concentration from ocean colour satellites, denoted POCsurface,was derived using the retrieval algorithm of Stramski et al. (2008), based on empirical relationships derived from in situ measurements of POC and blue-to-green band ratios of ocean colour remote sensing reflectances.

Surface satellite PIC and POC concentrations were depth integrated to 100 m to using empirical relationships based on in situ measurements across the Atlantic ocean (Balch et al., 2018):

$$PIC_{100m}\left(mmol\ C\ m^{-2}\right) = 40.555 \times PIC_{surface}\left(mmol\ C\ m^{-3}\right)^{0.560} \quad (3)$$

$$POC_{100m}\left(mmol\ C\ m^{-2}\right) = 164.376 \times POC_{surface}\left(mmol\ C\ m^{-3}\right)^{0.617} \quad (4)$$

The PIC/POC ratio of the standing stock in the top 100 m of the ocean (dimensionless) was then obtained by dividing PIC100m by POC100m.

Remotely sensed seasonal coccolithophore calcification rates integrated over the euphotic zone were obtained from (Hopkins and Balch, 2018) (their Fig. 3). This approach models calcification rate as a function of PIC concentration, a temperature-dependent growth rate function, irradiance, and depth. Remotely sensed calcification rates were validated using an extensive database of calcification rates with slope = 0.98, $R^2 = 0.28$; $p < 0.05$; RMSE = 0.53 mg C m^{-3} d^{-1} (Hopkins and Balch, 2018). This satellite based approach gives an average global euphotic zone depth-integrated calcification production of 1.42 ± 1.69 Pg C y^{-1}.

For a review of the history and uncertainties on ocean colour satellite algorithms for PIC concentration and production, the reader is referred to Balch and Mitchell (2023).

2.4. Optical model of the PIC-specific backscattering by coccolithophores and foraminifera

We developed a model for the backscattering cross-section of coccolithophores and foraminifera of different sizes based on Mie scattering theory for coated spherical particles with coating thickness τ_c and index of refraction relative to seawater of $n_{coat} = 1.2$ (calcite coating). The

backscattering cross-section is the product of the geometric cross-section of the particle and the dimensionless efficiency factor for backscattering of the particle, where the efficiency factor is the ratio of radiant power backscattered by the particle to radiant power intercepted by the geometric cross-section of the particle (Morel and Bricaud, 1986). Multiplication of the backscattering cross-section of a particle by the number density (number of individuals per m^3 volume of seawater) gives the backscattering coefficient of the particle population (units m^{-1}).

For coccolithophores, we first established a relationship between τ_c and the radius of the coccosphere covered with elliptical coccoliths of longest dimension L and aspect ratio ν. The volume of a coccolith of dimension L can be expressed as $V_c = k_s L^3$, where k_s is a species-specific shape constant (Young and Ziveri, 2000). This gives:

$$\tau_c = \left(\frac{4k_s}{\pi\nu}\right)L \tag{5}$$

For the aspect ratio we used that of the *Emiliana huxleyi* coccolith, $\nu = 1.2$ (Young et al., 2014), with radius of the coccosphere core approximately equal to L (Zhai et al., 2013). As a result, each coccosphere is comprised of approximately 16 coccoliths in a single layer coat over the core, consistent with coccosphere 3-D imagery. The real part of the relative index of refraction of the core was estimated as $n_{core} = 1.03$ and the imaginary part was set at $\kappa_{core} = 0.004$ at a wavelength of 550 nm (Fournier and Neukermans, 2017; Neukermans and Fournier, 2018). We included all coccolithophore species reported in Young and Ziveri (2000) and report backscattering cross-sections normalized by PIC weight.

We modeled foraminifera as prolate (elongated) spheroids with an aspect ratio of 1.1 based on the relationship between silhouette area vs. size reported by (Schiebel and Movellan, 2012). We estimated foraminiferan shell thickness from the relationship between foraminiferan test weight vs. size (Schiebel and Movellan, 2012) (their Fig. 4b) for prolate spheroids of aspect ratio 1.1. The average foraminifera shell thickness obtained was 9.5 ± 1.0 microns and, contrary to coccolithophores, this thickness was independent of size. We report modeled backscattering cross sections normalized by PIC weight over the typical foraminiferan size range of Schiebel and Movellan (2012).

The wavelength used for the computations was 550 nm *in vacuo*. We assumed that the surfaces of the calcite coatings were optically smooth in the sense that all voids, mounds, and asperities had characteristic dimensions smaller than ¼ the wavelength in water (Fournier and Neukermans, 2017). For surfaces with features larger than ¼ the wavelength in water (such as the voids between the spokes of *E. huxleyi* coccoliths), the backscattering increases by up to a factor of eight (Fournier and Neukermans, 2017).

3. Results and discussion

3.1. Planktonic calcifying organisms: PIC production and contributions to PIC flux

PIC production in open oceans is predominantly driven by three calcifying planktonic taxa (Fig. 2). Two of these, coccolithophores and foraminifera, precipitate $CaCO_3$ as calcite whereas the third taxon, pteropods, produce a less stable form of $CaCO_3$, aragonite (Mucci, 1983). The relative contributions to global $CaCO_3$ production and sinking $CaCO_3$ flux by these planktonic groups is poorly constrained. Understanding the contribution of each group is important as predicted ocean change will affect the ecology and biogeochemistry of calcifying plankton taxa differently (Doney et al., 2009; Grigoratou et al., 2019), which will in turn affect the magnitude of the open ocean carbonate pump.

3.1.1. Coccolithophores

Coccolithophores are calcifying phytoplankton forming calcite platelets, or coccoliths, organized around the cell in a so-called coccosphere (Fig. 2a). Coccosphere diameters mostly range between 5 and 30 μm (Monteiro et al., 2016) and come in a wide variety of shapes and sizes (Fig. 2a). Coccolithophores are ubiquitous in tropical to subpolar oceans, contributing 1–10% of global primary production (Poulton et al., 2007), with global average monthly PIC standing stock in the top 100 m estimated to be 27.04 ± 4.33 Tg C and with turnover times (the time taken to replace the biomass of the given population) of 3–7 days (Hopkins and Balch, 2018). Coccolithophore diversity is highest in oligotrophic subtropical regions (Winter et al., 2014; Winter and Siesser, 1994) with the globally most abundant coccolithophore species, *E. huxleyi* (shown in top left panel of Fig. 2a, the smallest species), forming enormous blooms from temperate to subpolar regions (Balch et al., 1991; Garcia et al., 2011; Holligan et al., 1983; Winter et al., 2014). The global production of coccolithophore PIC exhibits strong seasonal and interannual variability due to seasonality in light intensity, water column stability, nutrient availability, El Nino/La Nina and dust

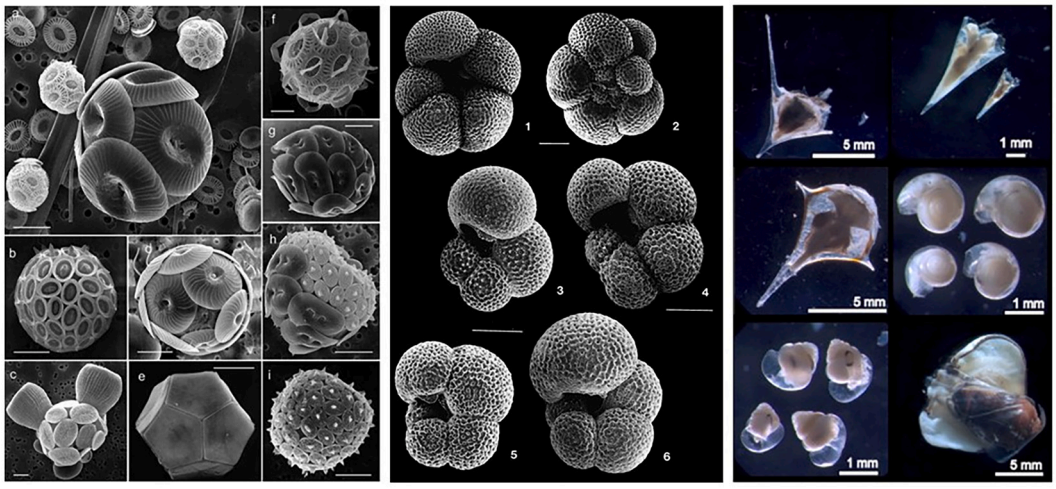

Fig. 2. Main calcifying plankton groups in the open ocean. a) Coccolithophores imaged with SEM. Scale bars 5 μm (reprinted from Eikrem et al., 2017 with permission), b) Foraminifera from the Arabian Sea. Scale bar 100 μm (reprinted from Peeters et al., 1999, with permission), and c) Pteropods from the Southern Antarctic Zone (image adapted from Howard et al., 2011 with permission).

events, which are all factors that have been shown to influence the regional biomass of coccolithophores, in turn influencing the carbonate counter pump (Balch, 2018; Guerreiro et al., 2019; Iglesias-Rodriguez et al., 2002; Köbrich and Baumann, 2009; Poulton et al., 2017).

Globally, coccolithophores are considered to be a main contributor to PIC production and flux, with microscopic studies of seafloor sediments revealing a large component of PIC consisting of coccoliths (Broecker and Clark, 2009; Haidar et al., 2000; Honjo, 1978). The flux of coccolithophores is thought to account for ~50% of open ocean PIC found in sediments (Broecker and Clark, 2009) with regional studies showing they contribute to up to 59% to deep sea PIC flux in the Atlantic Ocean (Honjo, 1978), 51.5% in the Indian Ocean (Ramaswamy and Gaye, 2006), 31% in the Pacific Ocean (Ziveri et al., 2007), with a lesser extent in polar regions where PIC flux is likely to be dominated by foraminifera and pteropods (Manno et al., 2018).

3.1.2. Foraminifera

Planktic foraminifera are unicellular protozoans with calcite shells and chambered tests (Fig. 2b). Adult test diameters mostly range in size between 100 and 1000 μm with an average diameter of 250 μm, and in CaCO3 weight between 0.3 μg to 100 μg, with an average of 2.5 μg (Schiebel and Movellan, 2012). Most species are found in the top 100 m of the global ocean, but some species are intermediate (500–1000 m) to deep-dwelling (1000–2000 m), which indicates that not all foraminiferan PIC flux originates from the surface ocean (Schiebel and Movellan, 2012). Roughly half of foraminifera species develop $CaCO_3$ spines (spinose). These species are predominantly carnivorous and most abundant in oligotrophic regions (Schiebel and Hemleben, 2017). The other half are non-spinose species which mostly feed on phytoplankton, but may also feed on marine snow and zooplankton (Anderson et al., 1979; Greco et al., 2021; Schiebel and Hemleben, 2017), and are most abundant in highly productive areas (Grigoratou et al., 2019). Foraminifera geographical and seasonal abundance distribution broadly reflects global patterns of temperature and primary productivity (Schiebel, 2002) and abundance generally decreases by two orders of magnitude from the surface to the bottom of the twilight zone (Schiebel and Movellan, 2012). The predicted turnover time for planktic foraminifera is one month, aligning with their lunar reproductive cycle, with global estimates of foraminifera biomass production between 0.025 and 0.1 Pg C y^{-1} (Schiebel and Movellan, 2012).

They play an important role in PIC production and flux, especially in polar regions such as in the Arctic Ocean where they account for up to 34% of PIC surface flux, and in the Southern Ocean where Salter et al. (2014) found they dominate deep sea flux (22%) compared to other contributors. Other region-specific studies show highly variable results on the contribution of foraminifera to PIC flux, such as 10–40% in the North Atlantic (Salmon et al., 2015), 15% for the Indian Ocean (Rembauville et al., 2016), 22% for the Sargasso Sea (Deuser and Ross, 1989), and 30% in the south-west Pacific (Marchant et al., 1998). Global estimates generally fall between 3 and 30% (Buitenhuis et al., 2019; Kiss et al., 2021), but substantially higher contributions (56–88%) have also been estimated (Honjo et al., 2008; Schiebel, 2002).

3.1.3. Pteropods

Thecosomata (shelled body) pteropods, also known as sea butterflies, are free-swimming pelagic sea snails and secrete $CaCO_3$ as aragonite to form a thin, delicate shell (Fig. 2c). The diameter of these shells range from 1000 to 3000 μm and can be either coiled or bilaterally symmetrical (Gilmer and Harbison, 1986). Pteropods are found in all major oceans with an estimated global carbon (POC) production between 0.444 and 0.505 Pg C y^{-1} (Bednaršek et al., 2012). Highest abundances are found at high latitudes while the highest species diversity is found in tropical and subtropical regions (Fabry et al., 2008). They are largely distributed within the upper 300 m of the water column being mostly located in surface waters (0–10 m), with observations down to 2000 m (Bednaršek et al., 2012) and many species undergoing diel vertical migrations. The thecosomatous pteropods are mainly herbivorous with populations increasing during spring spawning events in response to increasing primary productivity. The average life cycle for pteropods is around one year, although it varies with species from higher latitudes generally living longer eg. *Limacina helicina* antarctica spanning over three years (Bednaršek et al., 2012).

The contribution of pteropods to global PIC production and flux is generally considered to be small, even though one modeling study argues that their contribution in the global budget has been underrepresented (Buitenhuis et al., 2019). Pteropods may however be seasonally and regionally highly important contributors to PIC production and flux. For example in polar regions -where coccolithophores are less abundant- pteropods can dominate PIC production and shallow flux (Bednaršek et al., 2012; Collier et al., 2000). In the Arctic, pteropods have been found to contribute up to 77% to annual carbonate flux (Bauerfeind et al., 2014), and in the Southern Ocean, nearly all PIC export south of the Antarctic polar front is due to pteropods (Accornero et al., 2003). However, at lower latitudes and at great depths, pteropods have shown to be of lesser importance where the PIC flux is dominated by coccolithophores and foraminifera (Table 1).

3.1.4. Other contributors to the carbonate pump

A potential fourth main contributor to the open ocean carbonate production is pelagic fish. A byproduct of fish filtering sea water is the excretion of magnesium enriched calcium carbonate crystals (Wilson et al., 2009). Due to the high dissolution rate of Mg $CaCO_3$, these carbonates might undergo rapid dissolution throughout the water column. This process still lacks empirical data linking fish carbonates to open oceans, even with papers hypothesizing this process could be adding up to 15% to surface carbonate production (Wilson et al., 2009). Other calcifying organisms, including ostracods, heteropods, calcifying dinoflagelletes, and ciliates also contribute but to a lesser extent (Manno et al., 2018). Schiebel (2002) showed that dinoflagellates could be contributing up to 3.5% while Manno et al. (2018) showed ostracods are an important component over winter in the Southern Ocean becoming the dominant calcifying taxa in the region, although they generally play a relatively minor role. With few studies on these organisms, their actual contributions remains unclear.

3.1.5. Relative contributions of coccolithophores, foraminifera, and pteropods to PIC mass flux

We compiled literature data of PIC mass flux by coccolithophores, foraminifera, and pteropods to the mesopelagic (200–1000 m) and bathypelagic (>1000 m) in Table 1. The contribution to the total PIC flux by coccolithophores, planktic foraminifera, and pteropods exhibits strong regional, seasonal, and interannual variations (Table 1). Both coccolithophores and foraminifera comprise nearly all deep-sea PIC flux in tropical and subtropical regions, while pteropod contributions to PIC flux are mostly restricted to the polar regions (Table 1, Fig. 3). Pteropods may well account for a higher proportion of global PIC production (up to 89%; Buitenhuis et al., 2019) owing to their larger size and mass flux events. However, due to their aragonitic shells, they are more susceptible to dissolution than coccolithophores and foraminifera, and are only infrequently present in deep ocean sediment traps (Schiebel, 2002).

We note that a large proportion of PIC flux is often not attributable to any planktonic group of calcifiers, termed “unspecified PIC flux” in Fig. 3 and Table 1. The majority of this unspecified PIC is attributed to the fine fraction or “biogenic carbonate powder” which comprises damaged coccoliths, broken shells, and juvenile foraminifera (Guerreiro et al., 2021; Ziveri et al., 2007). This unspecified PIC flux is reported in about half of the studies in which it represents 69% of the total (specified + unspecified) PIC flux on average, but can be as low as 0% and as high as 96% of total PIC flux (Table 1).

Fig. 4a, b illustrates large variability in the PIC flux in the meso- and bathypelagic ocean associated with each of the three groups of calcifying taxa. The relative contributions of each group to the total specified

Table 1
Overview of published global and regional estimates of PIC flux and relative contributions by various groups of calcifying plankton.

	Region	Latitude (°N)	Longitude (°E)	Season	Depth (m)	PIC flux (g m^{-2} y^{-1})	% of PIC	Unspecified PIC flux (g m^{-2} y^{-1})	References
Shallow Foraminifera	Arctic Ocean	81	22–32	August-Sept	100	0.1–0.35	4–34		Anglada-Ortiz et al. (2021)
	Atlantic Ocean	47	−20	Summer	100	2.689			Schiebel and Hemleben (2000)*
	Indian Ocean	−35	53.3	Summer	90	0.003			Meilland et al. (2018)*
	Indian Ocean	−45	52.06	Summer	90	0.050			Meilland et al. (2018)*
	Indian Ocean	−47.4	58	Summer	90	0.723			Meilland et al. (2018)*
	Indian Ocean	−50.4	68.25	Summer	50	1.172			Meilland et al. (2018)*
	Indian Ocean	−56.3	63	Summer	90	0.032			Meilland et al. (2018)*
Pteropods	Arctic Ocean	79.43	4.3	Annual	200	0.32–0.53	56–74	0.186–0.249	Busch et al. (2015)
	Arctic Ocean	79	4.2	Annual	200	0.11–0.53	14–74	0.235–0.656	Busch et al. (2015)
	Arctic Ocean	81	22–32	August-Sept	100	0.27–9.97	66–96		Anglada-Ortiz et al. (2021)
	Pacific Ocean	15–50	153–156	May–June	100	1.315			Betzer et al. (1984)
Mesopelagic Coccolithophores	Atlantic Ocean	29	−15	Annual	976	0.171	33.4	0.341	Sprengel et al. (2000)
	Atlantic Ocean	26.4	−78.5	Feb-April	500	0.612	29	1.499	Pilskaln et al. (1989)
	Atlantic Ocean	34	−21	Annual	1000	0.612	24	1.939	Broerse et al. (2000a)
	Atlantic Ocean	48	−21	Annual	1000	0.324	34	0.629	Broerse et al. (2000a)
	Atlantic Ocean	−23	12.59	Sept-Jan	544	1.37	21.7	4.943	Giraudeau et al. (2000)
	Indian Ocean	15.34	68.36	Annual	963	1.261	53.1		Ramaswamy and Gaye (2006)
	Indian Ocean	3.34	77.46	Annual	912	0.516	31.4		Ramaswamy and Gaye (2006)
	Indian Ocean	13.09	84.2	Annual	893	0.780	52.8		Ramaswamy and Gaye (2006)
	Indian Ocean	−50.38	72.02	Annual	289	0.067	85.2		Rembauville et al. (2016)
	Pacific Ocean	−37.05	−74.5	Dec-Oct	1000	0.131	4.8	2.598	Menschel et al. (2016)
	Pacific Ocean	27	−111	Annual	500	0.372	17	1.817	Ziveri and Thunell (2000)
	Pacific Ocean	33.33	−118.3	Jan/July	500	3.500	90	0.389	Ziveri et al. (1995)
	Pacific Ocean	34	−120	Annual	610	0.276	4	6.627	Ziveri et al. (2007)
	Pacific Ocean	53.19	149.5	Annual	258	0.048	3.6	1.286	Broerse et al. (2000b)
	Southern Ocean	−46.56	142.15	Annual	1000	1.080	58	0.768	Rigual Hernández et al. (2020)
Foraminifera	Atlantic Ocean	33	−22	Annual	1000	1.818	15	10.299	Honjo and Manganini (1993)
	Atlantic Ocean	47	−20	Annual	1000	0.220	17	1.073	Honjo and Manganini (1993)
	Atlantic Ocean	47	−20	Summer	500	1.200			Schiebel and Hemleben (2000)*
	Indian Ocean	−50.38	72.02	Annual	289	0.012	14.8		Rembauville et al. (2016)
	Indian Ocean	15.34	68.36	Annual	963	0.984	46.9		Ramaswamy and Gaye (2006)
	Indian Ocean	3.34	77.46	Annual	912	1.128	68.6		Ramaswamy and Gaye (2006)
	Indian Ocean	13.09	84.2	Annual	893	0.696	47.2		Ramaswamy and Gaye (2006)

(*continued on next page*)

Table 1 (*continued*)

	Region	Latitude (°N)	Longitude (°E)	Season	Depth (m)	PIC flux (g m^{-2} y^{-1})	% of PIC	Unspecified PIC flux (g m^{-2} y^{-1})	References
Pteropods	Arctic Ocean	79	4	Annual	200–300	0.212 (0.024–0.791)	39 (7–73)	0.247 (0.128–0.478)	Bauerfeind et al. (2014)
	Atlantic Ocean	13.3	−54	Nov-Feb	1000	0.149	12.5	1.042	Berner and Honjo (1981)
	Pacific Ocean	15–50	153–156	May–June	400	0.212			Betzer et al. (1984)
	Pacific Ocean	15–50	153–156	May–June	900	0.079			Betzer et al. (1984)
	Atlantic Ocean	31.5	−64.1	Annual	500	0.140	17	0.686	Fabry and Deuser (1992)
	Southern Ocean	−47	142	Annual	1000	0.01–0.22			Roberts et al. (2011)
	Southern Ocean	−54	140	Annual	800	0.02–0.6			Roberts et al. (2014)
	Southern Ocean	−75.06	164.13	Annual	180	0–2.06	78–100		Accornero et al. (2003)
Bathypelagic Coccolithophores	Arctic Ocean	69	10	Annual	2600	0.801	57	0.563	Samtleben and Bickert (1990)
	Arctic Ocean	75	11	Annual	1700	0.631	73	0.163	Samtleben and Bickert (1990)
	Arctic Ocean	78	1	Annual	2000	0.077	54	0.056	Samtleben and Bickert (1990)
	Atlantic Ocean	31.45	−64.21	Annual	3200	0.53 (0.22–0.07)			Haidar et al. (2000)
	Atlantic Ocean	31.32	−55	Annual	5367	0.214	59		Honjo (1978)
	Atlantic Ocean	20.45	−19.44	Annual	2195	0.584 (0.171–0.999)	18 (7–35)	2.660	Köbrich and Baumann (2009)
	Atlantic Ocean	20	−21	Annual	1214	0.348	8.5	3.748	Guerreiro et al. (2021)
	Atlantic Ocean	14	−37	Annual	1235	0.216	22.5	0.744	Guerreiro et al. (2021)
	Atlantic Ocean	12	−23	Annual	1150	0.216	12.9	1.458	Guerreiro et al. (2021)
	Atlantic Ocean	12	−49	Annual	1130	0.696	38.7	1.102	Guerreiro et al. (2021)
	Atlantic Ocean	0.1	−10	Apr-Nov	1097	0.444	31	0.989	Ziveri et al. (2007)
	Atlantic Ocean	−29	−13	Annual	2516	1.212	47	1.367	Ziveri et al. (2007)
	Atlantic Ocean	29	−15	Annual	3000	0.434	41.4	0.614	Sprengel et al. (2000)
	Atlantic Ocean	47	−21	Annual	1018–1202	0.564	41	0.812	Ziveri et al. (2000)
	Atlantic Ocean	47	−21	Annual	3718–3749	0.828	46	0.972	Ziveri et al. (2000)
	Atlantic Ocean	45	−2.5	Annual	2300	0.294	12	2.156	Beaufort and Heussner (1999)
	Indian Ocean	16.18	60.3	Annual	1200	2.089	44.6		Ramaswamy and Gaye (2006)
	Indian Ocean	16.13	60.19	Annual	3007	2.881	51.2		Ramaswamy and Gaye (2006)
	Indian Ocean	14.28	64.35	Annual	1018	0.026–0.053			Mergulhao et al. (2006)
	Indian Ocean	15.34	68.36	Annual	3189	1.248	51.5		Ramaswamy and Gaye (2006)
	Indian Ocean	3.34	77.46	Annual	2394	0.720	33		Ramaswamy and Gaye (2006)
	Indian Ocean	5.01	87.09	Annual	3010	0.708	47.6		Ramaswamy and Gaye (2006)
	Indian Ocean	13.09	84.2	Annual	2282	0.912	56		Ramaswamy and Gaye (2006)
	Indian Ocean	15.31	89.13	Annual	1131	0.684	43.8		Ramaswamy and Gaye (2006)
	Indian Ocean	15.31	89.13	Annual	2120	0.576	44.9		Ramaswamy and Gaye (2006)
	Indian Ocean	5.03	87.03	Annual	1518	1.633			Mergulhao et al. (2013)
	Indian Ocean	11.01	84.26	Annual	1588	1.5			Mergulhao et al. (2013)
	Indian Ocean	15.44	88.58	Annual	1156	0.6			Mergulhao et al. (2013)
	Indian Ocean	10	53	Annual	1032	0.348	13.2	2.288	Broerse et al. (2000c)

(*continued on next page*)

Table 1 (*continued*)

	Region	Latitude (°N)	Longitude (°E)	Season	Depth (m)	PIC flux (g m^{-2} y^{-1})	% of PIC	Unspecified PIC flux (g m^{-2} y^{-1})	References
	Indian Ocean	10	53	Annual	3000	1.080	17.3	5.165	Ziveri et al. (2007)
	Pacific Ocean	2.59	135.1	June–March	1592	0.727	23.3	2.393	Tanaka and Kawahata (2001)
	Pacific Ocean	2.59	135.1	June–March	3902	0.784	27.9	2.026	Tanaka and Kawahata (2001)
	Pacific Ocean	53.19	149.5	Annual	1061	0.009	0.8	1.087	Broerse et al. (2000b)
	Pacific Ocean	−5	−140	Annual	2209	0.156	31	0.347	Ziveri et al. (2007)
	Southern Ocean	−46.56	142.15	Annual	2000	1.200	58	0.864	Rigual Hernández et al. (2020)
	Southern Ocean	−46.56	142.15	Annual	3800	1.200	56	0.913	Rigual Hernández et al. (2020)
	Southern Ocean	−46.4	178.3	Annual	1500	0.480	28	1.187	Rigual Hernández et al. (2020)
	Southern Ocean	−52.43	−40.08	Annual	2000	0.980	~33		Manno et al. (2018)
	Southern Ocean	−55.11	−40.07	Annual	1500	0.361	~18		Manno et al. (2018)
	Southern Ocean	−44.29	59.92	Annual	2000	0.084	15	0.032	Salter et al. (2014)
	Southern Ocean	−46	56.05	Annual	3195	0.084	10	0.423	Salter et al. (2014)
	Southern Ocean	−49	51.3	Annual	3160	0.012	14	0.035	Salter et al. (2014)
Foraminifera	Atlantic Ocean	54	−21	Summer	2200	3.553			Schiebel et al. (1995)
	Atlantic Ocean	50	−145	Annual	3800	0.264	20	1.056	Reynolds and Thunell (1985)
	Atlantic Ocean	50	−145	Annual	3800	0.264	18.8	1.141	Thunell and Honjo (1987)
	Atlantic Ocean	32.5	−64.15	Annual	3200	0.120	22	0.426	Deuser and Ross (1989)
	Atlantic Ocean	31.5	−61.4	Annual	1500	0.388	<10–40		Salmon et al. (2015)
	Atlantic Ocean	31.32	−55	Annual	5367	0.106	29		Honjo (1978)
	Atlantic Ocean	21.28	−20.8	Annual	1222	0.394	17 (2–50)	1.922	Kiss et al. (2021)
	Atlantic Ocean	13.31	−54	Annual	3755	0.583	88.1	0.079	Thunell and Honjo (1981)
	Atlantic Ocean	13.31	−54	Annual	5068	0.321	64.6	0.176	Thunell and Honjo (1981)
	Indian Ocean	16.18	60.3	Annual	1200	2.593	55.4		Ramaswamy and Gaye (2006)
	Indian Ocean	16.13	60.19	Annual	3007	2.749	48.8		Ramaswamy and Gaye (2006)
	Indian Ocean	15.34	68.36	Annual	3189	1.176	48.5		Ramaswamy and Gaye (2006)
	Indian Ocean	3.34	77.46	Annual	2394	1.465	67		Ramaswamy and Gaye (2006)
	Indian Ocean	5.01	87.09	Annual	3010	0.780	52.4		Ramaswamy and Gaye (2006)
	Indian Ocean	13.09	84.2	Annual	2282	0.720	44		Ramaswamy and Gaye (2006)
	Indian Ocean	15.31	89.13	Annual	1131	0.876	56.2		Ramaswamy and Gaye (2006)
	Indian Ocean	15.31	89.13	Annual	2120	0.708	55.1		Ramaswamy and Gaye (2006)
	Indian Ocean	12.25	64.35	Annual	2986	0.852			Koppelmann et al. (2000)
	Pacific Ocean	39.5	−128	Annual	4050	0.168	38	0.274	Fischer et al. (1988)
	Pacific Ocean	15.21	−151.28	Annual	2778	0.088	47.6	0.096	Thunell and Honjo (1981)
	Pacific Ocean	15.21	−151.28	Annual	4280	0.074	42.5	0.101	Thunell and Honjo (1981)
	Pacific Ocean	15.21	−151.28	Annual	5582	0.096	100	0.000	Thunell and Honjo (1981)
	Pacific Ocean	5.21	−81.53	Annual	3560	0.228	11	1.845	Thunell and Reynolds (1984)
	Pacific Ocean	−30.1	−73.11	Annual	2173	0.960	29.5	2.295	Marchant et al. (1998)

(*continued on next page*)

Table 1 (*continued*)

	Region	Latitude (°N)	Longitude (°E)	Season	Depth (m)	PIC flux (g m^{-2} y^{-1})	% of PIC	Unspecified PIC flux (g m^{-2} y^{-1})	References
	Southern Ocean	−52.43	−40.08	Annual	2000	0.391	~22		Manno et al. (2018)
	Southern Ocean	−55.11	−40.07	Annual	1500	0.219	~23		Manno et al. (2018)
	Southern Ocean	−60.55	−57.6	Annual	3625	0.792			Wefer et al. (1982)
	Southern Ocean	−44.29	59.92	Annual	2000	0.180	33	0.032	Salter et al. (2014)
	Southern Ocean	−46	56.05	Annual	3195	0.252	33	0.423	Salter et al. (2014)
	Southern Ocean	−49	51.3	Annual	3160	0.034	42	0.035	Salter et al. (2014)
Pteropods	Arctic Ocean	79.43	4.3	Annual	2400	0.039–0.12	4–8	0.951–1.381	Busch et al. (2015)
	Arctic Ocean	79	4.2	Annual	1250	0.03–0.06	5–8	0.593–0.704	Busch et al. (2015)
	Arctic Ocean	79	4.2	Annual	2400	0.01–0.09	2–10	0.684–0.959	Busch et al. (2015)
	Arctic Ocean	78.51	1.22	Annual	2000	0.156	11.5	1.201	Meinecke and Wefer (1990)
	Arctic Ocean	75.51	11.28	Annual	1700	0.003	0.38	0.787	Meinecke and Wefer (1990)
	Arctic Ocean	70.01	4.2	Annual	2550	0.071 (0.001–0.108)	3.4 (<1–5)	1.735 (0.119–2.762)	Bauerfeind et al. (2014)
	Arctic Ocean	69.3	10	Annual	2761	0.003	1.7	0.160	Meinecke and Wefer (1990)
	Atlantic Ocean	31.5	−64.1	Annual	1500	0.140	15	0.796	Fabry and Deuser (1992)
	Atlantic Ocean	31.5	−64.2	Annual	3200	0.127	13	0.852	Fabry and Deuser (1992)
	Atlantic Ocean	31.32	−55	Annual	5367	0.026	7		Honjo (1978)
	Atlantic Ocean	21.08	−20.41	Spring/ Summer	3502	1.080			Kalberer et al. (1993)
	Indian Ocean	10.43	53.34	June-Feb	1032	0.789	22.5	2.717	Singh and Conan (2008)
	Pacific Ocean	15–50	153–156	May–June	2200	0.039			Betzer et al. (1984)
	Pacific Ocean	50	−145	Annual	3800	0.300			Tsurumi et al. (2005)
	Southern Ocean	−47	142	Annual	2000	0.007–0.113			Roberts et al. (2011)
	Southern Ocean	−52.43	40.08	Annual	2000	0.873	~40		Manno et al. (2018)
	Southern Ocean	−55.11	−40.07	Annual	1500	0.595	~50		Manno et al. (2018)
	Southern Ocean	−44.29	59.92	Annual	2000	0.024	4	0.032	Salter et al. (2014)
	Southern Ocean	−46	56.05	Annual	3195	0.024	3	0.423	Salter et al. (2014)
	Southern Ocean	−49	51.3	Annual	3160	0.000	<1	0.035	Salter et al. (2014)

* Tow net data.

meso- and bathypelagic PIC flux in individual studies is also strongly variable (Table 1). To calculate the mean relative contribution of each group to the total specified PIC flux across collated studies, we first calculated the average PIC flux for each group (F_{cocco}, F_{foram}, F_{ptero}) and then divided by the sum of the average PIC fluxes. This gives, for example for pteropods:

$$Contrib_{ptero}(\%) = 100 \times F_{ptero} / \left(F_{cocco} + F_{foram} + F_{ptero}\right) \quad (6)$$

Our estimates show that coccolithophores, foraminifera, and pteropods contribute respectively 38%, 42%, and 20% to the total specified mesopelagic flux, and respectively 46%, 41%, and 13% to the total specified bathypelagic flux (Fig. 4c). The decline of pteropod contribution in the bathypelagic could be due to the higher solubility of aragonite of the pteropod shells, relative to calcitic coccolithophore and foraminifera shells (Mucci, 1983). The comparable contributions by coccolithophores and foraminifera to PIC flux in the meso-and bathypelagic ocean is also reflected in deep sea sediments, where coccolithophores and foraminifera contribute roughly the same on a global average (Broecker and Clark, 2009).

It is important to note, however, that there are significant uncertainties in estimates of relative contributions of the different taxa to total PIC mass flux because a large proportion of PIC flux is often not attributable to any planktonic group of calcifiers (Fig. 3, Table 1). In order to increase the accuracy of relative contributions to PIC flux by the various calcifying groups, this unspecified flux would also need to be attributed (Guerreiro et al., 2021). We also note that the above calculation neglects the contribution to PIC flux by taxa other than coccolithophores, foraminifera and pteropods. While the available evidence

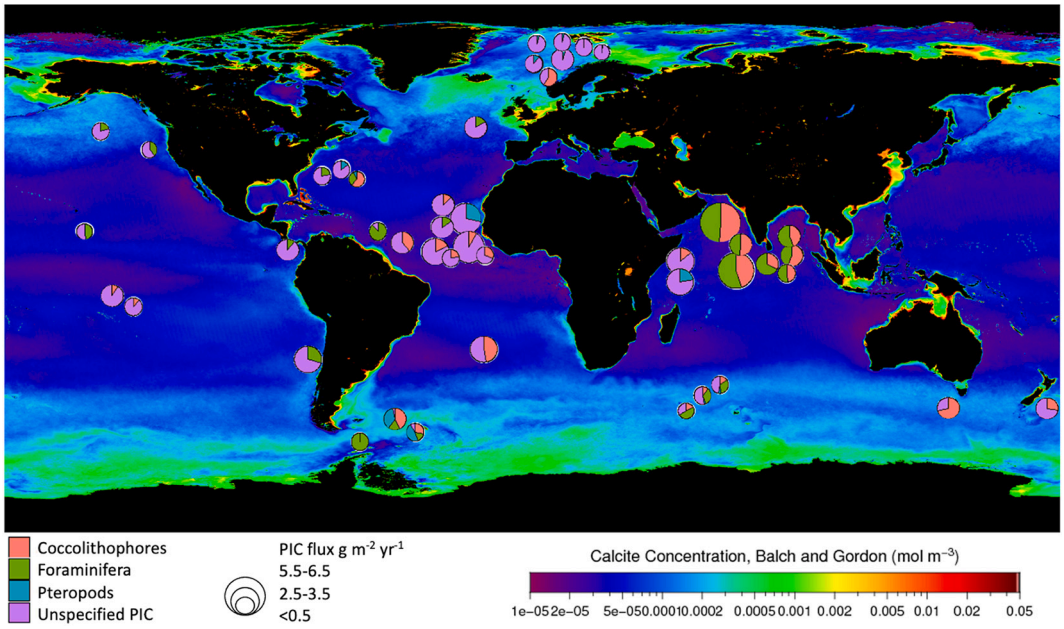

Fig. 3. Pie graphs depicting relative contributions of main taxa to total PIC flux (g m^{-2} yr^{-1}) from bathypelagic sediment trap data (Table 2). Geographic coordinates were slightly adapted where necessary to improve visibility. Background image showing satellite PIC climatology from the SeaWiFS ocean colour satellite mission, 1997-09-04 to 2010-12-11. (note: High PIC satellite values in shallow waters are caused by resuspended sediments, not PIC).

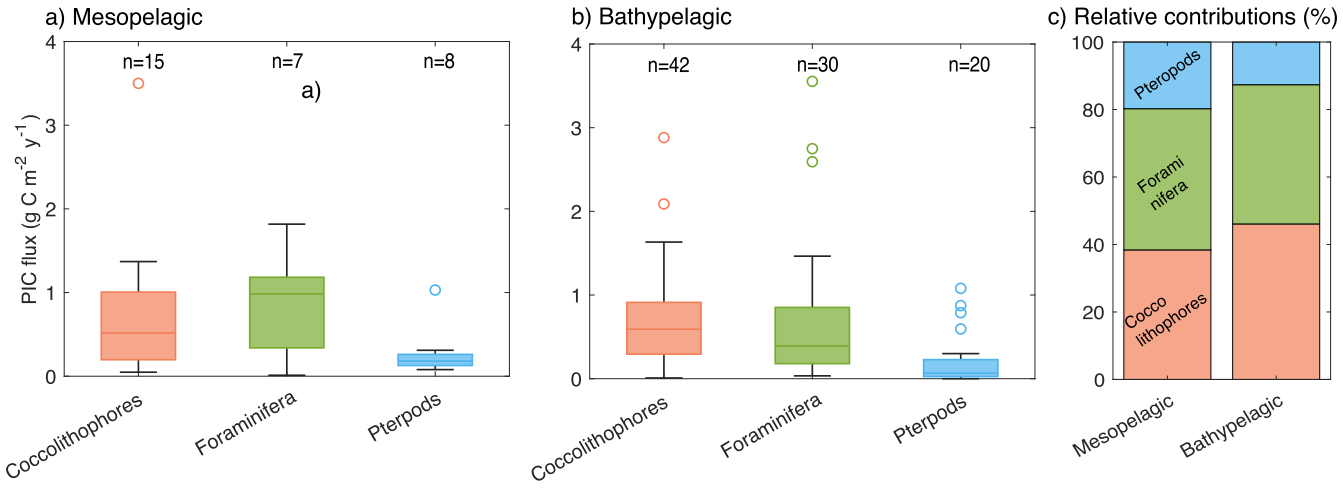

Fig. 4. PIC flux associated with three calcifying plankton groups collected in sediment traps in the a) mesopelagic (200-1000 m) and b) bathypelagic (>1000 m). Boxes span lower to upper quartiles with line indicating the median, whiskers extend to non-outlier minimum and maximum and circles indicate outliers. n is the number of observations. c) global mean relative contributions to PIC mass flux in the mesopelagic and bathypelagic.

does not suggest that other groups could be as important as these three on a global scale (see section 3.1.4), other groups may be important under certain settings.

3.1.6. Implications for remote sensing estimates of PIC concentration and production

A comprehensive, in-depth discussion of the limitations and uncertainties of ocean colour satellite algorithms for PIC concentration and production is provided by Balch and Mitchell (2023). A complete review of remote sensing techniques to monitor the BCP, including gaps and needs was provided earlier in this Journal (Brewin et al., 2021). Here, we would briefly like to emphasize a few important aspects to be able to understand the potential connection between remotely sensed PIC concentration, production, and PIC mass fluxes obtained from sediment traps.

First, ocean colour satellite products for PIC concentration or standing stock mainly include PIC from coccoliths and coccolithophores. The reason is that the mass-specific backscattering-cross section of a $CaCO_3$ particle is strongly size-dependent, and is generally orders of magnitude higher for coccolithophores than for foraminifera and pteropods, as shown by the modeling results (Fig. 5). The contribution from larger $CaCO_3$ particles (foraminifera and pteropods) to the backscattering coefficient, which is a first order determinant of remote sensing reflectance measured by ocean colour satellites, is therefore generally negligible. The PIC-specific backscattering coefficient of NASA's standard PIC satellite product is 1.355×10^{-4} m^2 (mg C)$^{-1}$, approximately in the middle (in log scale) of the modeled values for a range of coccolithophore species (Fig. 5). The modeling result in Fig. 5 also implies that only in the unrealistic scenario that the number densities of larger $CaCO_3$ particles would be over two orders of magnitude

higher than those of coccolithophores, these particles would contribute a non-negligible signal to backscattering and hence remote sensing reflectance.

Second, 90% of the signal detected by ocean colour satellites emerges from water depths shallower than the depth where photosynthetic available radiation (PAR) has dropped to 37% of its surface value (Gordon and McCluney, 1975). This implies that ocean colour satellites only "see" down to a few meters in turbid waters (such as coccolithophore blooms) to up to roughly 60 m in the clearest ocean waters (depths given for 450 nm light wavelength) (Gordon and McCluney, 1975). This depth is thus much shallower than the euphotic zone depth, which reflects the depth where PAR is 1% of its surface value (Lee et al., 2007). As a consequence, coccolithophore species residing in the lower euphotic zone or even the sub-euphotic zone (Guerreiro et al., 2019; Poulton et al., 2017), do not contribute to the ocean colour satellite signal.

To summarize, ocean colour satellite data of PIC concentration reflect calcite concentrations from coccoliths and coccolithophores from the upper euphotic zone. This limitation is to some extent overcome by depth-integration of PIC concentration in the upper 100 m using the empirical approach of (Balch et al., 2018) as expressed in Eqs. (3–4). Because of the size-sensitivity of mass-specific backscattering cross section (Fig. 5), satellite PIC concentration is biased towards smaller coccolithophore species, notably the ubiquitous species *E. huxleyi*. Lastly, satellite calcification rates are derived from a model specifically accounting for the physiological characteristics of *E. huxleyi* (Hopkins and Balch, 2018). We have shown earlier that the global contribution of coccolithophores to PIC mass flux amounts to 38% in the mesopelagic and 46% in the bathypelagic on average (Fig. 4c), but that their relative contribution is also highly variable in time and space (Table 1, Fig. 3).

3.2. Quantitative understanding of the carbonate pump

The development of a quantitative understanding of the carbonate pump involves estimating PIC production in the euphotic zone, PIC export below the euphotic zone, dissolution in the water column and lastly seafloor dissolution and burial. Estimates of global PIC production range widely, from 0.5 to 1.6 Pg C y^{-1} (Berelson et al., 2007; Sulpis et al., 2021) with a median value of 1.2 Pg C y^{-1} (Fig. 6). This includes two ocean colour satellite based estimates of euphotic zone depth-integrated values of 1.6 Pg PIC y^{-1} and 1.4 Pg PIC y^{-1} (Balch et al., 2007; Hopkins and Balch, 2018). For a review of the history and uncertainties on ocean colour satellite algorithms for PIC concentration and production, the reader is referred to Balch and Mitchell (2023). In what follows, we focus on PIC export and pelagic dissolution.

Like PIC production, the quantitative assessment of pelagic PIC export flux into the deep ocean is associated with large uncertainty. A compilation of estimated PIC export flux by Sulpis et al. (2021), built upon earlier work by Berelson et al. (2007), found PIC export to range from 0.45 to 1.80 Pg C y^{-1} with a median value of 1.00 Pg C y^{-1} (Fig. 6). These estimates were obtained with different methodologies, including modeling, direct observations of PIC fluxes, and tracer-based approaches (Sulpis et al., 2021 and references therein). Since the attempt of Berelson et al. (2007) to constrain the global ocean carbonate budget, two new global assessments have been undertaken. (Battaglia et al., 2016) used data constrained modeling to estimate a global PIC export flux at 75 m depth of 0.9 (0.72–1.05) Pg C y^{-1}. Sulpis et al. (2021) used an alkalinity-tracer based approach to estimate a PIC export flux at 300 m depth of 0.91 (0.72–1.08) Pg C y^{-1}. These similar estimates are within the range of values reported by Berelson et al. (2007), with most estimates now clustered around 1.00 Pg C y^{-1}, the median value from 19 studies (Fig. 6).

Variability in global PIC export estimates is partially due to the dynamic nature of export fluxes with large seasonal (e.g. Guerreiro et al., 2021; Lampitt et al., 2010) and spatial variations (e.g., Le Moigne et al., 2014), which are difficult and expensive to measure. Indeed, direct observations of export flux using sediment traps are labour-intensive, require ship support, and provide limited spatial and temporal coverage (Buesseler and Boyd, 2009; Honjo et al., 2008). Furthermore, there is uncertainty from the largely unknown collection efficiency of moored sediment traps, which may underestimate total fluxes considerably (Baker et al., 1988), particularly in traps shallower than 1000 m (Scholten et al., 2001). To circumvent the lack of direct flux estimates, scientists used tracer-based approaches such as in the above mentioned study by Sulpis et al. (2021) or more recently the study by (Subhas et al., 2022). However, the development of autonomous profiling floats

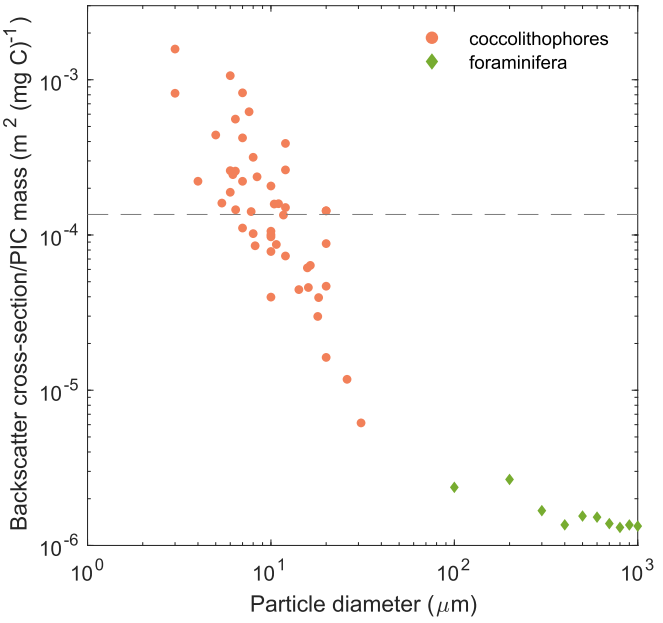

Fig. 5. Modeled backscattering cross-section per unit PIC mass for coccolithophores and foraminiferans of varying sizes. The dashed line represents the value used in NASA's standard ocean colour PIC algorithm (=1.628 m^2 mol^{-1} = 1.355 10^{-4} m^2 $(mg\ C)^{-1}$).

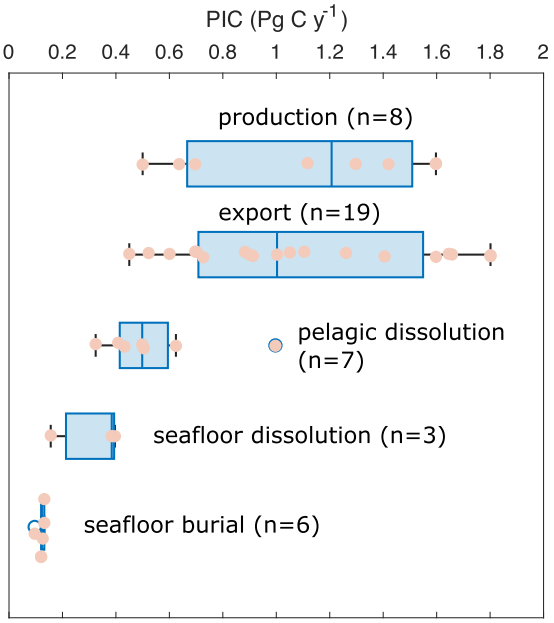

Fig. 6. Literature compilation of global open ocean estimates of annual planktonic PIC production, export, pelagic dissolution, seafloor dissolution, and seafloor burial. Adapted from Sulpis et al. (2021, see references therein).

equipped with instruments for the measurement of PIC concentration and flux will accelerate observations of the carbonate pump from the surface down to 2000 m depth, discussed in detail in section 3.5.4. The proliferation of such observation tools is expected to help narrow down uncertainties in the carbonate pump budget and functioning.

Among the most noticeable recent advancements in our understanding of pelagic PIC export is the improved understanding of water column dissolution above sub-saturated water, contrary to the widespread assumption that PIC dissolution occurs primarily below the calcite and aragonite lysoclines. The lysocline represents the depth below which the rate of dissolution of calcite increases substantially, and is typically situated around 4000–4500 m in the Atlantic and < 2000 m in the Pacific. There has been early evidence for substantial PIC dissolution above the saturation horizon for $CaCO_3$ minerals (Bishop et al., 1980; Milliman et al., 1999). This was attributed to sub-saturated microenvironments in more corrosive zooplankton guts or within organic aggregates and/or a more widespread occurrence of more soluble mineral carbonates such as aragonite or Magnesium calcite (Bishop et al., 1980; Milliman et al., 1999). While Bishop et al. (1980) still considered such dissolution a "probably rare and local phenomenon", Milliman and Droxler (1996) suggested that >50% of pelagic carbonate formation dissolves above 1000 m, broadly consistent with Koeve (2002) who estimated 31–59% dissolution between 125 and 1000 m depth. Battaglia et al. (2016) estimated a global mean dissolution between 75 m and 1500 m of 36 ± 20%, with 24–28% for the Atlantic. Based on the sediment trap PIC flux data from the Atlantic, we obtain an estimate of dissolution between 200 m and 1000 m of 60% (as 1 minus the ratio of median PIC flux in the 1000–2000 m depth bin to median PIC flux in the 100–200 m bin), consistent with Koeve (2002) and Milliman and Droxler (1996).

The recent global assessment of PIC export and dissolution by Sulpis et al. (2021) estimated a global PIC export below 300 m of 0.91 Pg PIC y^{-1}, of which 12% dissolves in the mesopelagic (between 300 and 1000 m depth), much lower than previous mesopelagic dissolution estimates (note that the estimate of pelagic dissolution in Fig. 6 encompasses dissolution in the entire water column, including depths below the calcite and aragonite lysocline). Subhas et al. (2022) determined coccoliths as the predominant source for dissolution in the North Pacific and designate metabolic CO_2 as the cause for sub-saturation in microenvironments where the dissolution occurs. Through in situ dissolution experiments they found a critical saturation state threshold of 0.75, below which dissolution rates rapidly increase (Subhas et al., 2022). Knowledge of such a critical saturation state threshold is an important step forward as it enables the assessment of how widespread such conditions occur within microenvironments.

We compared seasonal depth-integrated calcification rates over the euphotic zone obtained from remote sensing with seasonal PIC fluxes obtained from radiochemical tracers and sediment traps along a latitudinal gradient across the Atlantic Ocean (Fig. 7). Estimates of (coccolithophore) PIC production rates modeled with input from satellite data suggest that PIC production rates vary with latitude by over two orders of magnitude (Fig. 7a). There is a clear pattern of highest calcification rates in the Northern and Southern subtropical gyres in the respective hemispheric summer season, and generally low calcification rates around the equator and at high latitudes (Fig. 7a). Please note that satellite data is missing at higher latitudes (>45°) due to low sun angles in the hemispheric autumn and winter seasons (Hopkins and Balch, 2018). The latitudinal pattern in PIC production from remote sensing is roughly in agreement with the latitudinal pattern of PIC export (Fig. 7b) and fluxes from traps in and below the mesopelagic (100–1000 m depth) (Fig. 7c, d). This observation is in contrast with an earlier comparison of satellite-derived PIC euphotic zone standing stock and PIC flux showed very poor coherence (Berelson et al., 2007). Indeed, annual mean PIC standing stocks generally decrease from the higher latitudes towards the equator (Fig. 3), while the reverse pattern was seen for PIC flux across the Atlantic, Pacific, and Indian ocean basins (Berelson et al., 2007). However, we argue that it is PIC production rate that is the quantity of relevance to PIC flux at depth and calcification rate is not only determined by PIC standing stock, but also by temperature-driven growth rate and by irradiance (Hopkins and Balch, 2018).

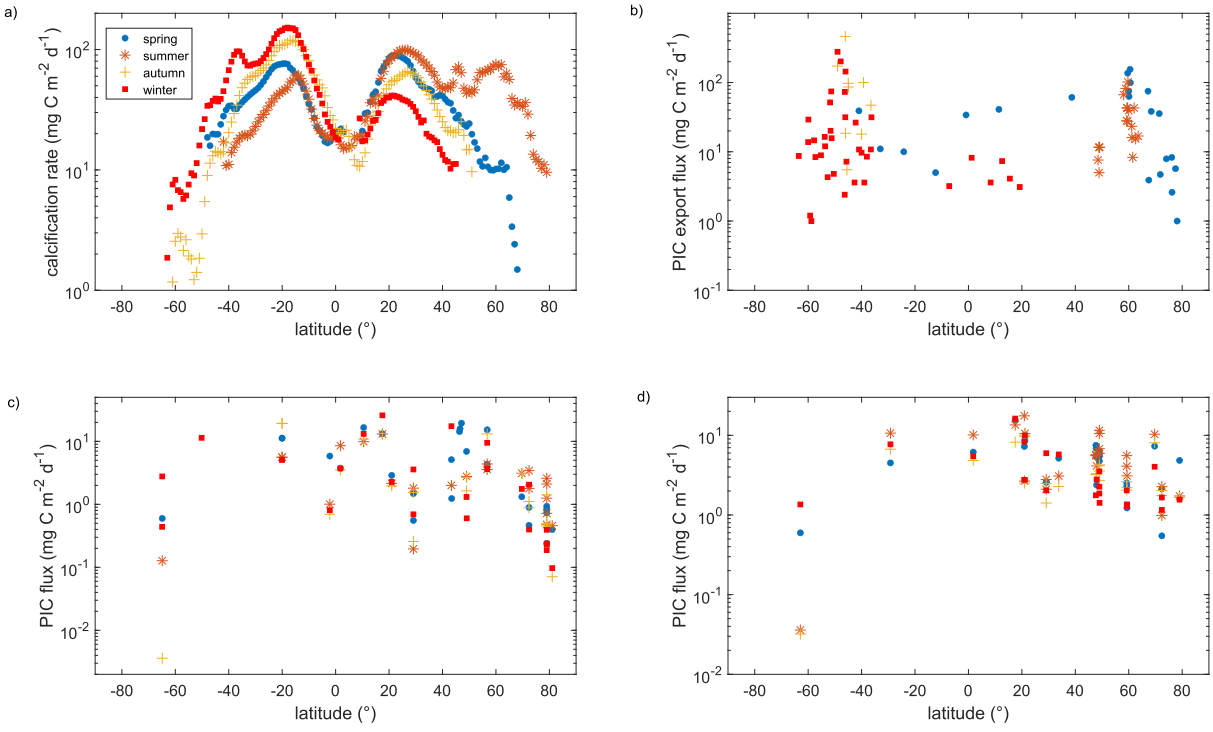

Fig. 7. a) Zonally averaged seasonal depth-integrated calcification rate across a latitudinal gradient in the Atlantic obtained from remote sensing (Hopkins and Balch, 2018). b) Zonally averaged Thorium-derived PIC export flux (Le Moigne et al., 2014; Rosengard et al., 2015). PIC flux from sediment traps across the Atlantic Ocean for traps located c) between 100 m and 1000 m, and d) below 2000 m.

We re-emphasize that satellite products have limitations (section 3.1.6), that remotely sensed calcification rates reflect depth-integrated PIC production in the euphotic zone by coccolithophores only and that the model parametrization for calcification rates was derived for the fast-growing species *E. huxleyi*, the most ubiquitous coccolithophore. Despite these limitations, the latitudinal patterns of satellite calcification rates and PIC flux are broadly coherent (Fig. 7).

3.3. The Counter effect of the carbonate pump

3.3.1. Global and regional estimates based on the rain ratio of exported particles

Using global median estimates of POC and PIC flux below the euphotic zone of 10 Pg C y^{-1} and 1 Pg C y^{-1} (section 3.2) this would give a global rain ratio of annual exported carbon of 0.1. Considering the wide range in estimates of POC flux of 4–12 Pg C y^{-1} and 0.45–1.8 Pg C for PIC flux, global mean values of the rain ratio for exported carbon would range by over an order of magnitude between 0.04 and 0.45. This range is slightly broader than the range of values in the global mean rain ratio of annual export found in the literature, between 0.06 and 0.25 (Table 2, but also note large regional differences as discussed below). Using a global mean value for Ψ of 0.66 and a mean rain ratio of annual export of 0.1 (range: 0.04–0.45), the BCP would be weakened by 7% on average due to the strength of the carbonate counter pump, with a range in the global counter effect between 3% and 30%.

The rain ratio of export was found to differ among ocean basins, with generally greater mean ratios in the Pacific and the Indian Ocean compared to the Atlantic (Table 2). However, there are strong disagreements in mean rain ratios reported for some ocean basins. For example, for the Atlantic Ocean Koeve (2002) reports a mean value of 0.23, much higher than estimates by Sarmiento et al. (2002) and Jin et al. (2006) (Table 2). Our own analyses of annual export rain ratios based on sediment trap data in the Atlantic Ocean shows better agreement with Koeve's high estimates of export rain ratio (Fig. 8a, Table 2). Also, we emphasize that the spatiotemporal and methodological limitations of flux estimates may bias calculations of global annual mean fluxes (Baker et al., 1988; Honjo et al., 2008). Despite strong differences, all studies are broadly consistent: there is a pronounced latitudinal gradient in rain ratios with values in the tropics and southern hemisphere subtropics up to four times higher than values in the high latitudes and northern subtropics (Jin et al., 2006; Koeve, 2002; Pinsonneault et al., 2012; Sarmiento et al., 2002). The latitudinal pattern in rain ratio found in these studies is also broadly reflected in the rain ratio obtained from long-term trap data shown in Fig. 9, which also shows the rain ratio of the carbon standing stock in the top 100 m obtained from remote sensing.

Table 2
Estimates of the PIC/POC rain ratio of exported carbon at global or basin-scales obtained from the literature using different approaches.

Reference	Global or Basin mean rain ratio of annual export	Approach
Li et al. (1969)	0.25 global, 0.21 Atlantic, 0.27 Pacific	alkalinity and nitrate tracer distribution
Broecker (1971)	0.11 Atlantic, 0.33 Pacific	alkalinity and nitrate tracer distribution
Broecker and Peng (1982)	0.25 global	alkalinity and nitrate tracer distribution
Lee (2001)	0.10–0.12 global	alkalinity and nitrate tracer in the mixed layer
Yamanaka and Tajika (1996)	0.08 global	Observations and modeling
Murnane et al. (1999)	0.16 global	Observations and modeling
Sarmiento et al. (2002)	0.06 ± 0.03 global 0.01–0.08 Atlantic, 0.03–0.1 Indian, 0.05–0.09 Pacific	alkalinity and nitrate tracer distribution
Koeve (2002)	0.23 (0.14–0.33) Atlantic	Observations of particle flux, tracers and modeling
Jin et al. (2006)	0.09 ± 0.02 global 0.03–0.13 Atlantic, 0.06–0.17 Indian, 0.06–0.23 Pacific	alkalinity and nitrate tracer distribution
This study	0.4 (0.15–0.55, Fig. 8a) Atlantic	Long-term sediment traps (100–500 m depth)
	0.2 (0.07–0.45, Fig. 8b) Atlantic	Thorium-based export

As the latitudinal pattern in rain ratios is opposite to the pattern of Ψ (Smith, 2013), the overall global counter effect of the carbonate pump will be subdued somewhat by the Ψ factor. However, Ψ varies only by a factor 1.4 in surface water (0.56 in the tropics to 0.80 at high latitudes; Smith, 2013), while the rain ratio of annual export varies latitudinally by a factor 3–4. Therefore, we expect the carbonate counter effect to exhibit latitudinal variations by a factor 2–3 with counter strength decreasing from low to high latitudes.

To the best of our knowledge only three regional in situ studies, all located in the Southern Ocean, have quantified the counter effect of the carbonate pump based on annual cycles of PIC and POC flux observations using Eq. 2. Rembauville et al. (2016) used time series of PIC and POC export flux collected from shallow sediment traps on the Kerguelen Plateau and found the counter effect to be low, 5%. Salter et al. (2014) found a significantly stronger counter pump effect of 6-32% in an iron fertilized area vs. 1-4% in a non-fertilized area, with intermediate values of 4–18% found by Manno et al. (2018) in the Scotia Sea. The latter two studies measured PIC flux from deep-moored traps and assumed that the deep PIC flux equaled PIC export flux. Given recent knowledge on important shallow PIC dissolution, these estimates of the counter pump are very likely underestimated (by up to 60%). Lastly, Koeve (2002) used observations of PIC and POC flux and modeling to obtain an Atlantic basin-scale average counter effect estimate of 13–16%.

3.3.2. Remote sensing studies of the counter effect in coccolithophore blooms

The counter effect has also been quantified using multi-year time series of ocean colour satellite observations of blooms of the coccolithophore species *E. huxleyi*. This species forms extensive blooms in the temperate and subpolar surface ocean in summer, potentially reaching cell densities $>10^9$ cells m^{-3} and characterized by detachment and overproduction of coccoliths in the bloom decline phase (Balch et al., 1996a; Balch et al., 1993). The resulting accumulated *E. huxleyi* coccospheres and detached coccoliths in surface waters increase the light backscattered from the ocean, coloring the water bright milky-turquoise. This typical coloration of seawater due to *E. huxleyi* bloom formation has been quantitatively assessed by using in situ radiometry (Cazzaniga et al., 2021), as well as observed (Kondrik et al., 2019; Moore et al., 2012) and modeled (Neukermans and Fournier, 2018) ocean colour satellite reflectance.

First, Shutler et al. (2013) estimated *E. huxleyi* bloom-induced increase in seawater pCO_2 and associated decrease in air-sea CO_2 flux in the North Atlantic (40° – 70°N). The overall approach was to estimate PIC production in blooms, multiply by an estimate of Ψ, and then quantify the calcification-induced increase in seawater pCO_2 relative to a baseline derived from monthly seawater pCO_2 climatologies (Takahashi et al., 2014). To estimate the total seasonal PIC production, Shutler et al. (2013) assessed the monthly aerial extent of the bloom from the SeaWiFS ocean colour satellite and made the following assumptions: (i) blooms extend down to 20 m depth, (ii) PIC concentration in all blooms was set to an average value obtained from in situ measurements in the North Atlantic, (iii) PIC turnover time was one month. Their results show that over the period 1998–2007 *E. huxleyi* blooms covered an annual mean area of $474 \pm 10^4 \times 10^3$ km^2. These blooms were shown to increase the monthly local seawater pCO_2 by an average 14% (up to 35%), which reduced the monthly air-sea pCO_2 difference by 77% (up to

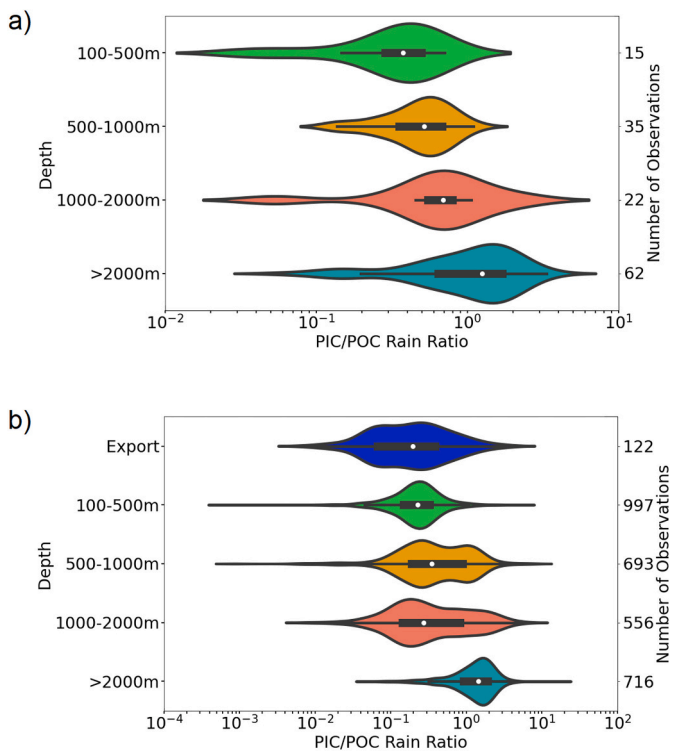

Fig. 8. Violin plots of PIC/POC rain ratio obtained from sediment traps deployed a) long-term (>250 days) and b) short-term (<250 days) binned in depth intervals. "Export" in panel b) refers to PIC/POC rain ratio obtained from Thorium-derived PIC and POC Export flux (Le Moigne et al., 2014; Rosengard et al., 2015).

231%), and the monthly air-sea CO_2 flux by 55% (up to 155%). Due to the slow equilibration time between the surface ocean and the atmosphere (Jones et al., 2014), increased seawater pCO_2 due to calcification can persist for many months, thereby reducing the total annual drawdown of CO_2 from the atmosphere. Particularly since *E. huxleyi* blooms typically occur during the summer, when seawater temperatures are high, which decreases the solubility of the CO_2 gas, thus increasing the seawater pCO_2. Thus, *E. huxleyi* blooms will block a large portion of the annual CO_2 sink (Robertson et al., 1994). Assuming an air-sea equilibration time of six months, Shutler et al. (2013) estimated that *E. huxleyi* blooms decrease the annual net sink for atmospheric CO_2 by $\sim 3-28\%$ in the North Atlantic.

Kondrik et al. (2018) extended estimation of the local *E. huxleyi* bloom-induced increase in seawater pCO_2 to the North Pacific, the Nordic and the Barents Seas through linear regression with ocean colour remote sensing reflectance at 8-day frequency covering the period 1998–2015. Their results show large differences in bloom-induced increases in seawater pCO_2 among the ocean basins, giving lowest mean increases of 21% (up to 32%) in the Greenland Sea and highest mean increase of 43% (up to 63%) in the Barents Sea. However, no estimate of the actual counter effect of the carbonate pump was made in this study.

Remote sensing studies of the counter effect are thus limited to *E. huxleyi* blooms, which can be easily observed from ocean colour satellites. One of the main limitations of these remote sensing approaches is that they do not account for calcite dissolution that may occur in the euphotic zone, which would "neutralize" the rise in pCO_2 due to calcification. In fact, it is only PIC exported from the euphotic zone that contributes to a longer-term effect on pCO_2 in the surface ocean. This is analogous to the fact that it is only POC that escapes remineralization in the euphotic zone and gets exported below the euphotic zone that contributes to a drawdown of pCO_2 in water, and hence the atmosphere. The depth at which sinking POC is remineralized in the mesopelagic broadly determines the sequestration time of CO_2 in the ocean (Nowicki et al., 2022; Siegel et al., 2021). Analogously, the depth at which PIC dissolves in the mesopelagic controls the longevity of the carbonate counter effect. One can think of two extreme situations to illustrate this: 1) PIC produced in the euphotic zone is dissolved entirely in the euphotic zone, which would imply a zero counter pump effect on annual timescales; 2) all PIC produced in the euphotic zone sinks through the abyss and is buried in the sediments without undergoing any dissolution. The second scenario implies a quasi-permanent (millennial scale) counter pump effect by the PIC formed in the surface ocean.

3.4. The PIC ballast effect

3.4.1. The ballast hypothesis

The ballast hypothesis posits that POC fluxes are largely controlled by the availability of high-density minerals, particularly $CaCO_3$ and to a lesser extent opal and lithogenic material (Armstrong et al., 2001; Francois et al., 2002; Klaas and Archer, 2002). These mineral particles are hypothesized to be a major driver of POC flux by increasing the density of aggregates and thus their sinking speed (Klaas and Archer, 2002), or by physically protecting the more labile POC in aggregates from degradation while sinking to the deep ocean (Armstrong et al., 2001). Indeed, according to Stokes Law, the sinking velocity of a spherical particle can be expressed as:

$$V_p = {}^{2}\!/_{9}\left(\rho_p - \rho_w\right) g R^2 \Big/ \mu \tag{7}$$

where μ is the dynamic viscosity of seawater (1.07 g m^{-1} s^{-1} at ~25 °C), g the Earth's gravitational acceleration (9.81 m s^{-2}), R the radius of the spherical particle, and ρ_p and ρ_w are the density of the particle and seawater respectively. The density of seawater is a function of temperature and salinity, ranging between 1.020 g cm^{-3} to 1.029 g cm^{-3} with a typical value of ρ_w= 1.027 g cm^{-3}, while typical densities of organic material are 1.06 g cm^{-3} (Aas, 1996) and mineral densities are 2.71 g cm^{-3} for $CaCO_3$, 2.1 g cm^{-3} for opal, and 2.65 g cm^{-3} for lithogenic material such as quartz (Aas, 1996). All else equal, the sinking velocity of an aggregate is proportional to its density in excess of seawater, which is in turn strongly influenced by the makeup of the aggregate in terms of mineral and organic material as well as its porosity.The ballast hypothesis was proposed as a mechanism to explain the strong quantitative relationship between annual POC and PIC mass fluxes in deep (> 1000 m) particle traps obtained from n = 107 observations throughout the global ocean (Klaas and Archer, 2002). However, the existence of a strong globally uniform relationship between POC and PIC flux was later re-examined using a more advanced statistical approach on a larger dataset which revealed substantial regional variability in the relationship between deep fluxes of POC and minerals, as well as in the PIC/POC rain ratio (Wilson et al., 2012). Similar statistical analyses on an Atlantic ocean dataset of observations of ^{234}Th-drived POC and mineral export fluxes from the surface ocean (n = 95) also revealed spatial variability in the association of POC export flux with minerals, with highest PIC-associated POC export in the high-latitude North Atlantic and lowest in the Southern Ocean (Le Moigne et al., 2014). Since the proposition of the ballast hypothesis twenty years ago, it seems now more widely accepted that i) there is no simple global ballasting mechanism, ii) there is no globally constant PIC/POC rain rate in export nor deep particle fluxes, iii) ballasting of POC flux by high-density PIC can be regionally very important, but that iv) ecosystem processes in the EZ and TZ should also be taken into account to examine POC flux and the efficiency of POC transfer (Buesseler et al., 2007; Buesseler and Boyd, 2009; Le Moigne et al., 2014).

3.4.2. Laboratory and mesocosm experiments

The mechanistic underpinnings for the ballast effect are mainly (1) the acceleration of organic matter sinking velocities when associated

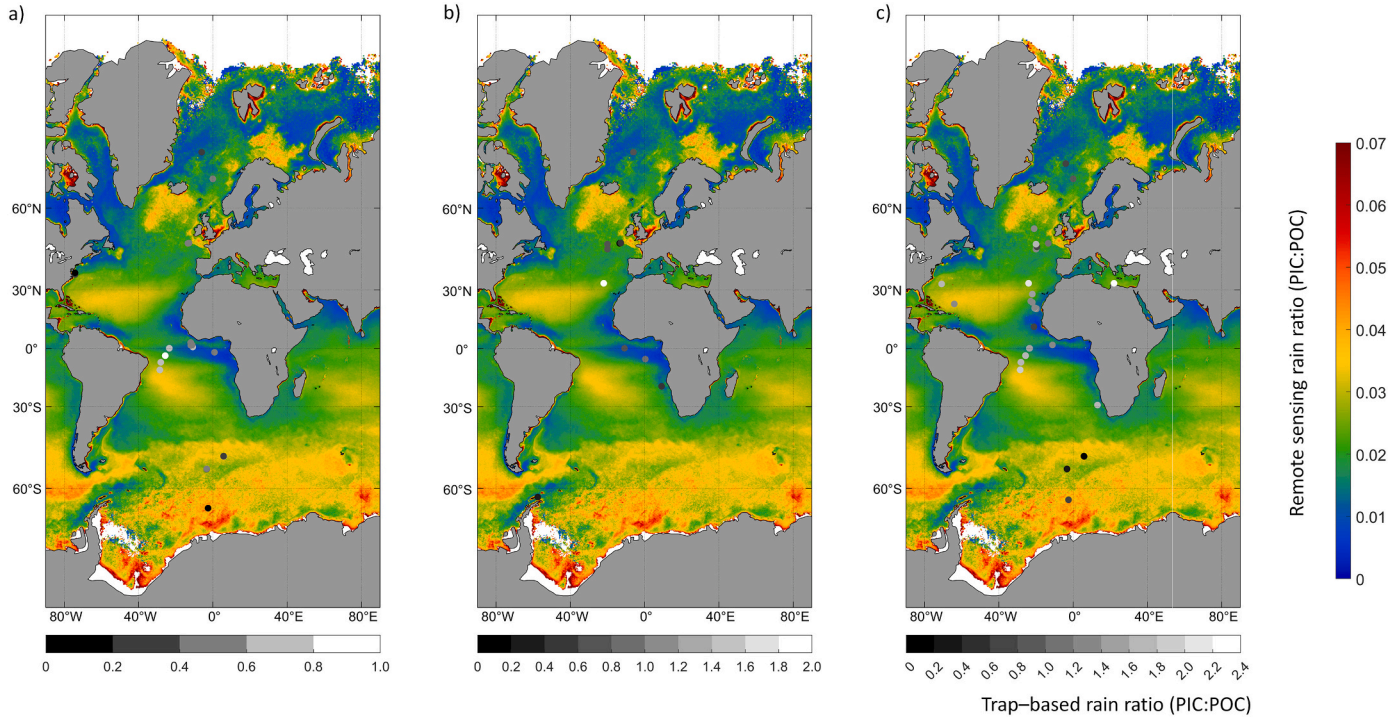

Fig. 9. Remote sensing data of PIC/POC rain ratio of 100 m depth-integrated standing stock derived from climatologies of SeaWiFS ocean colour satellite PIC and POC concentration (using Eqs. 3–4). Circles show the rain ratio obtained from sediment traps deployed long-term (>250 days) at depths a) between 100 and 1000 m depth, b) between 1000 and 2000 m depth, and c) deeper than 2000 m.

with $CaCO_3$ and (2) that the association of organic matter with $CaCO_3$ reduces remineralization rates (Francois et al., 2002).

The acceleration of sinking velocity by ballast has been demonstrated in countless studies, ranging from laboratory experiments with cell cultures (Iversen and Ploug, 2010; Ploug et al., 2008), studies with natural communities (Bach et al., 2016; Iversen and Robert, 2015), and observational field studies (Fischer et al., 2009). $CaCO_3$ is generally a more effective ballasting mineral than biogenic silica from diatoms frustules because it has a much higher density (2.7 vs. 2.1 g cm^{-3}) (Aas, 1996). However, various lithogenic minerals e.g. provided as dust to the open ocean, have also been shown to substantially accelerate organic matter sinking velocity (Passow and De La Rocha, 2006). Next to the density of the ballasting mineral, it is also crucial how the minerals integrate into the matrix of an organic matter aggregate. For example, large calcite tests (several hundred μm in diameter, Fig. 2) formed by foraminifera were shown to integrate less well into aggregates than the much smaller calcitic coccoliths (~3 μm) formed by *E. huxleyi* (Schmidt et al., 2014). Thus, even under conditions where most of the PIC is provided as large particles, smaller ones which contribute less to overall PIC production may still dominate the ballasting effect on organic matter flux. Mineral particle interactions with organic matter can also influence the dynamics of organic matter aggregation and potentially alter their compactness. For example, aggregation rates can be increased by the presence of minerals such as coccoliths (Engel et al., 2009). However, as shown by Passow and De La Rocha (2006), effective absorbance of minerals (illite and $CaCO_3$ in their case) into organic matter aggregates can also lead to a higher degree of fragmentation into larger numbers of dense but smaller aggregates. This effect of minerals has implications for sinking velocities, which are difficult to predict because decreasing size and increasing density of opposite effects on sinking velocities (Laurenceau-Cornec et al., 2020, see also Eq. 7).

The reduction of remineralization rates due to ballast minerals is substantially less investigated than the ballast effect on sinking velocities. As key proponents of the ballast hypothesis, Armstrong et al. (2001) argue that ballast minerals determine deep-water POC fluxes. They speculated that minerals protect POC from remineralization by an 'internal' and/or and 'external' process. The internal process would work by POC being entombed in biogenic mineral shells, such as coccospheres, thereby restricting its access to decomposing enzymes (Lowenstam and Weiner, 1989). The external process refers to POC being adsorbed onto mineral particles and into pores, again reducing the exposure to decomposing enzymes (Mayer, 1994). Experimental studies investigating the protection by minerals against POC remineralization found mixed evidence. Ploug et al. (2008) found no systematic differences in POC remineralization rates in fecal pellets containing biogenic silica ballast (BSi), $CaCO_3$ ballast, or no mineral ballast. The same outcome was also reported for BSi-, $CaCO_3$-, or no mineral-containing aggregates formed in roller tanks from monoclonal phytoplankton cultures (Iversen and Ploug, 2010) and natural phytoplankton communities from the North Sea where aggregates without mineral addition were compared to aggregates enriched in non-biogenic smectite (Iversen and Robert, 2015). However, another roller tank study with aggregates reported lower remineralization rates in aggregates composed of a calcifying *E. huxleyi* strain, relative to aggregates composed of a non-calcifying strain (Engel et al., 2009). Similar to that, (Arnarson and Keil, 2007) compared organic matter remineralization rates in a dinoflagellate culture with and without non-biogenic montmorillonite additions and found a reduction in organic carbon remineralization when the mineral particles were present. Their explanation for this difference was the adsorption of labile components onto mineral particles, which protected them from remineralization. Le Moigne et al. (2013a) found that aggregate remineralisation was lower in aggregates with added $CaCO_3$ than in aggregates without $CaCO_3$. The key difference in the study by Le Moigne et al. (2013a) relative to those mentioned above was that remineralization was predominantly performed by added microzooplankton (rotifers), not by bacteria. Overall the mixed evidence reported in various studies suggests that there is no simple mechanism for a protection by mineral particles against organic matter remineralisation. Instead, this mechanism appears to depend on the source of organic matter, characteristics of the minerals, and on the community

decomposing the organic matter.

3.4.3. Implementation in biogeochemical models

The ballast hypothesis has been highly influential in the design of biogeochemical models implemented into Earth System Models, which are important tools to predict the response of the ocean's BCP to a changing climate (IPCC, 2013). The ability to make accurate predictions relies on adequate parameterizations of biogeochemical processes. Among the most challenging tasks is the modeling of POC fluxes in the twilight zone where they are attenuated most strongly. Following the ballast hypothesis that PIC may be an important carrier of POC through the twilight zone (Armstrong et al., 2001; Francois et al., 2002; Klaas and Archer, 2002), a ballasting and carbon protection mechanism was included in a wide range of biogeochemical models (DeVries et al., 2014; Gehlen et al., 2006; Hofmann and Schellnhuber, 2009; Kwon et al., 2009).

Numerical models show the wide-ranging implications of PIC ballasting of POC, including a positive feedback on climate change through reduced calcification by calcifying phytoplankton (i.e. coccolithophores) in response to ocean acidification (Heinze, 2004; Hofmann and Schellnhuber, 2009; Krumhardt et al., 2019; Kwon et al., 2009; Orr et al., 2005), overriding the negative feedback due to decreased production of CO_2 from reduced PIC production and export from the euphotic zone. The quantitative importance of $CaCO_3$ as ballast for sinking POC in the global ocean is crucial for determining the efficiency of the BCP and the sign of the climate change ocean-acidification feedback on the BCP (Heinze, 2004; Riebesell et al., 2009). However, the parameterization of PIC flux and the ballast effect is based on simplifying assumptions and many unknowns, for example by assuming a globally constant PIC/POC ratio of particles exported out of the euphotic zone (Kwon et al., 2009), parametrizing coccolithophores as a certain proportion of the bulk phytoplankton (Hense et al., 2017), or assigning a carbon protection for a fixed fraction of the POC flux (DeVries et al., 2014). Current parameterizations of the ballast effect are derived from small datasets of POC and PIC fluxes from sediment traps, and much of the lack of consensus within the biogeochemical modeling community stems from the fact that there is very limited in situ observational evidence for the ballast effect and a lack of mechanistic understanding (Aumont et al., 2017).

3.5. Towards autonomous observations of the carbonate pump from BioGeoChemical-Argo floats

3.5.1. Limitations of traditional observations of the biological carbon pump

Traditional observations of the biological carbon pump rely on (i) direct measurement of sinking POC and PIC flux from sediment traps operating at discrete depths (Buesseler et al., 2007; Lampitt et al., 2010), (ii) water column measurement of the $^{238}U/^{234}Th$ isotope disequilibrium to estimate POC and PIC flux at discrete depths (Le Moigne et al., 2014; Rosengard et al., 2015), (iii) measurements of particle size distributions converted into POC flux using a size-dependent particle sinking speed (Fender et al., 2019; Guidi et al., 2015), (iv) high temporal frequency time series observations of carbon flux and biogeochemical parameters at a limited number of locations (Emerson, 2014; Lutz et al., 2007; Wong et al., 1999), or (v) empirical algorithms using satellite observations of the surface ocean (Henson et al., 2012; Marsay et al., 2015; Siegel et al., 2014). Approaches (i)-(iii) require intensive ship support, have limited spatial coverage and temporal resolution, and exhibit strong temporal bias (Buesseler and Boyd, 2009; Henson et al., 2015).

3.5.2. Autonomous observations of the biological carbon pump

Since the past decade, a growing global network of autonomous profiling floats equipped with bio-optical and biogeochemical sensors, so-called BioGeoChemical-Argo (BGC-Argo) floats (Fig. 10), is driving a transformative shift in our ability to observe the BCP (Boyd et al., 2019; Claustre et al., 2021). BGC-Argo floats are free-drifting, battery-powered profiling platforms that provide vertically resolved biogeochemical observations at unprecedented time and space scales (Claustre et al., 2020). These platforms allow quantification of particle fluxes due to gravitational sinking, the dominant mechanism of the BCP (Boyd et al., 2019), but also due to horizontal advection processes (see Claustre et al., 2021 and references therein). BGC-Argo floats generally profile 0–1000 m at 5–10 day intervals, and 0–2000 m at least every 30 days (targeting 0–2000 m every 10 days in accordance with the Argo mission) (Bittig et al., 2019; Owens et al., 2022; Roemmich et al., 2019). In between profiles, these quasi-Lagrangian platforms drift at a parking depth of ~1000 m. The sampling strategy of BGC-Argo floats is however highly flexible, allowing for adjustments in profiling frequency and vertical resolution of data acquisition during the float mission via two-way iridium satellite communication. For example, sampling frequency was increased to every 2 days and 1 m vertical resolution to estimate fluxes of rapidly settling particles associated with spring and summer phytoplankton blooms in the high latitude oceans (Briggs et al., 2020).

The BGC-Argo program, established in 2016, selected six core variables (Fig. 10): pH, downwelling irradiance, and the concentration of dissolved oxygen, nitrate, chlorophyll-a (Chl-a), and suspended particles (Claustre et al., 2020). The selection of these variables was based on sensor availability and maturity level at the time and relevance to the research and management themes of the BGC-Argo program: ocean biogeochemistry, marine ecosystem health and management, and ocean colour validation (Johnson and Claustre, 2016). Through a flexible community and data management system, the program anticipates the integration of new and improved sensors to extend the observational capacity of the network (Claustre et al., 2020; Roemmich et al., 2019). The most recent sensor developments include a particle camera for imaging, counting, and identification of zooplankton and large particles (UVP6-LP Hydroptics) (Picheral et al., 2022) and hyperspectral radiometers to better characterize the downwelling light field (TrioS GmBh) (Jemai et al., 2021) and potentially also phytoplankton communities (Organelli et al., 2021). In what follows we discuss the feasibility of examining the carbonate pump using existing sensors on BGC-Argo floats and the need for an Argo-float-fitting sensor for autonomous detection of PIC concentration and flux.

Two core BGC-Argo measurements can be used to assess the concentration of various oceanic particle stocks. Chlorophyll-a fluorescence (FChl-*a*) is used to derive the concentration of chlorophyll-*a*, the primary photosynthetic pigment in phytoplankton cells, as a proxy for phytoplankton biomass (but see Behrenfeld et al., 2005). This requires i) correcting FChl-*a* for non-photochemical quenching, a photo-protective mechanism of phytoplankton cells that depresses FChl-*a* per unit chlorophyll-*a*n under high light conditions (Terrats et al., 2020; Xing et al., 2018), and ii) applying regional calibration coefficients to convert corrected FChl-*a* into chlorophyll-*a* concentration (Roesler et al., 2017). The particulate backscattering coefficient $b_{bp}(\lambda)$ (in m^{-1}, at a wavelength λ *in vacuo*) is, to first order, driven by the mass concentration of suspended particles, both organic and inorganic (Neukermans et al., 2012, 2016; Reynolds et al., 2016). In the open ocean where POC$>>$PIC, $b_{bp}(\lambda)$ varies broadly proportional to POC concentration (Allison et al., 2010; Cetinić et al., 2012; Johnson et al., 2017; Loisel et al., 2011; Stramski et al., 1999, 2008), albeit with substantial variability in the $b_{bp}(\lambda)$/POC ratio (see below). In coccolithophore blooms, on the other hand, $b_{bp}(\lambda)$ is mainly driven by PIC concentration, with PIC contributing up to 90% of the $b_{bp}(546)$ signal (Balch et al., 1996b; Balch et al., 1991; Garcia et al., 2011). This forms the basis of the standard PIC remote sensing algorithm for intense, turbid coccolithophore blooms (Gordon et al., 2001) which is essentially a retrieval of $b_{bp}(\lambda)$, converted into PIC when PIC >3 mmol m^{-3} (=36 mg C m^{-3}).

3.5.3. Observations of coccolithophore blooms with BioGeoChemical-Argo floats

Coccolithophore blooms commonly occur in the temperate and

subpolar surface ocean in summer, formed by the species *E. huxleyi* (Balch et al., 1996b; Balch et al., 1991; Garcia et al., 2011; Holligan et al., 1993), one of the smallest members in the coccolithophore family (Fig. 2). *E. huxleyi* blooms are uniquely characterized by overproduction and release of coccoliths into the water at the final bloom stage (Paasche, 2001). Ship-based studies of the bio-optical properties of *E. huxleyi* bloom waters have shown that the accumulation of these calcite particles of high refractive index ($n_{calcite} = 1.20$ relative to seawater) results in increasing $b_{bp}(\lambda)$ in proportion to PIC, as well as in elevated ratios of $b_{bp}(\lambda)$/Chl-a and $b_{bp}(\lambda)/b_p(\lambda)$ in surface waters (Balch et al., 1991; Balch et al., 1996b; Garcia et al., 2011), where $b_p(\lambda)$ is the scattering coefficient of particles (in m^{-1}). The $b_{bp}(\lambda)/b_p(\lambda)$ ratio is the so-called backscattering ratio and represents the proportion of particle scattering in the back direction. The $b_{bp}/b_p(\lambda)$ ratio can be related to the bulk refractive index of the particle population, based on optical Mie theory simulations for homogenous spherical particle populations (Twardowski et al., 2001), albeit with some sensitivity to changes in particle size distribution (Ulloa et al., 1994). Ship-based bio-optical studies have shown that b_{bp}/b_p (660 nm) increases with PIC/POC ratio in an *E. huxleyi* bloom on the Patagonian shelf (Garcia et al., 2011) or with PIC/(POC + PIC) ratio in Atlantic waters (Neukermans et al., 2012), thus holding promise as a proxy for the bulk carbon composition of the particle assemblage (see below).

The $b_{bp}(\lambda)/b_p(\lambda)$ ratio has been retrieved from a minority of BGC-Argo floats equipped with a beam transmissometer in addition to a backscattering sensor (Estapa et al., 2019; Terrats et al., 2020; Xing et al., 2014). Beam transmissometers measure the particulate beam attenuation coefficient ($c_p(\lambda)$ in m^{-1}), typically at a red wavelength (e.g. $\lambda = 660$ nm) where particle scattering, b_p (in m^{-1}), dominates the c_p signal (Loisel and Morel, 1998; Neukermans et al., 2012). The float-derived backscattering ratio from concurrent measurement of c_p and b_{bp} was shown to be a good indicator for coccolithophore blooms in subpolar surface waters as observed from ocean colour satellite remote sensing (Terrats et al., 2020; Xing et al., 2014). Terrats et al. (2020) further demonstrated that surface ocean coccolithophore blooms could also be successfully identified from the global fleet of BGC-Argo floats equipped with only $b_{bp}(\lambda)$ and FChl-*a* sensors based on basin-specific thresholds on the $b_{bp}(\lambda)$/Chl-*a* ratio and $b_{bp}(\lambda)$ reflecting the fact that coccolithophore bloom waters are both relatively turbid and comprised of a particle population with high backscattering per unit Chl-*a*.

Identification of coccolithophore blooms from BGC-Argo floats is thus feasible, but estimating the actual PIC and POC concentration associated with these blooms is very challenging, let alone estimating PIC and POC concentration in non-bloom conditions and in the mesopelagic zone. It is generally assumed that PIC<<POC, so that float-based $b_{bp}(\lambda)$ can serve as a proxy for POC (Dall'Olmo and Mork, 2014; Lacour et al., 2019). Even if POC dominates the particle assemblage, converting $b_{bp}(\lambda)$ into POC is challenging because of the sensitivity of $b_{bp}(\lambda)$ to particle size, composition, and internal structure (Gordon and Du, 2001; Kitchen and Zaneveld, 1992; Organelli et al., 2018). As a result, $b_{bp}(\lambda)$/POC varies among ocean basins, seasons, and with depth in the mesopelagic. Mean surface values for b_{bp}/POC(λ) at λ =700 nm (a standard wavelength for BGC-Argo floats) vary by a factor two from 0.0170 m^2 g^{-1} C in the low latitude Pacific and Atlantic (Stramski et al., 2008) to 0.0321 ± 0.0025 m^2 g^{-1} C in the Subantarctic (Johnson et al., 2017). Measurements of $b_{bp}(\lambda)$ and POC in the mesopelagic ocean are limited. In one study in the North Atlantic, it was shown that b_{bp}/POC(700 nm) was significantly higher in the mesopelagic zone than in the productive surface ocean (0.0266 m^2 g^{-1} C vs. 0.0316 m^2 g^{-1} C; Cetinić et al., 2012). To account for the effects of particle composition on the relationship between POC and $b_{bp}(\lambda)$, a multivariate empirical algorithm was recently proposed that estimates POC from $b_{bp}(\lambda)$ and $b_{bp}(\lambda)$/Chla (Koestner et al., 2022), which is expected to reduce uncertainties in POC estimates derived from BGC-Argo floats.

Except for coccolithophore blooms, the assumption PIC<<POC may be acceptable in the surface ocean. However, our analyses of rain ratios obtained from sediment traps suggest a majority of PIC/POC values above 0.15 in the upper mesopelagic and above 0.20 in the lower mesopelagic ocean (Fig. 8). Furthermore, because of their high refractive index, inorganic carbon particles backscatter more light per unit

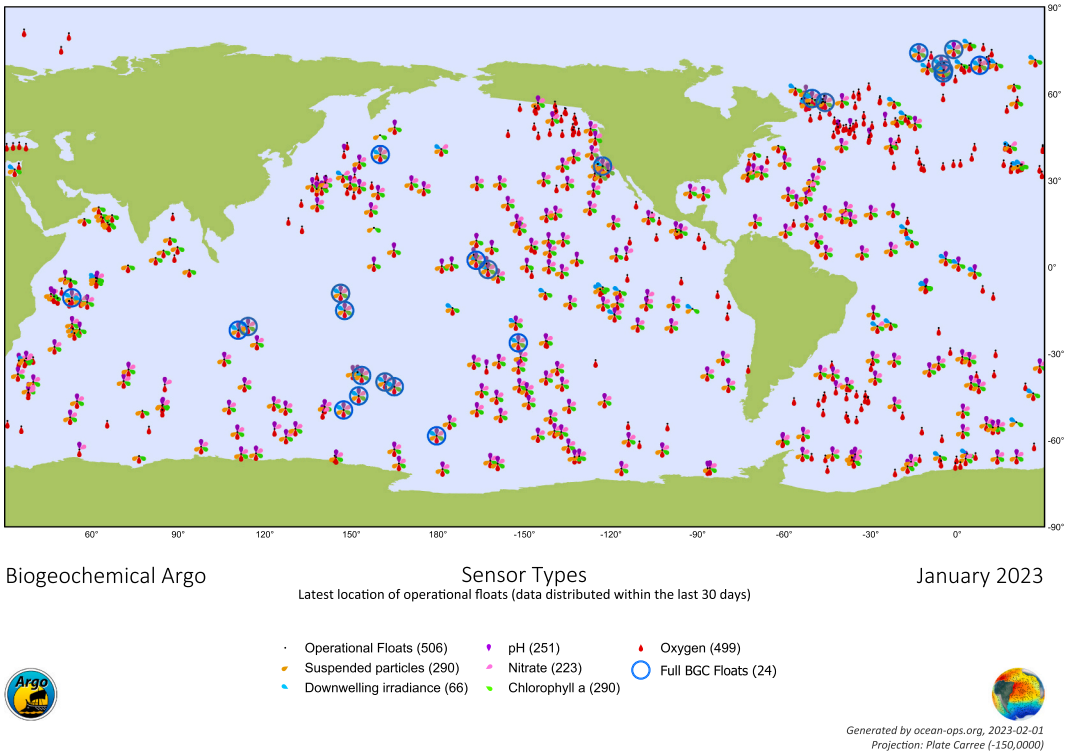

Fig. 10. Status map of the Biogeochemical-Argo network of profiling floats for January 2023, indicating the core-variables and the number of floats measuring them (source: https://biogeochemical-argo.org/float-map-network-status-maps.php, updated monthly).

carbon than organic carbon particles. Indeed, at green wavelengths (±550 nm) mean b_{bpic}/PIC equals 1.628 m^2 (mol C)$^{-1}$ (Balch et al., 2005) which is about five times higher than mean b_{bp}/POC in Mediterranean waters (0.320 m^2 (mol C)$^{-1}$; Loisel et al., 2011) and seven times higher than mean b_{bp}/POC in the low latitude Atlantic and Pacific waters (0.224 m^2 (mol C)$^{-1}$; Stramski et al., 2008). This implies that neglecting PIC contribution to b_{bp} can lead to overestimation of POC by a factor 1.6 when PIC/POC = 0.1 to a factor 5 when PIC/POC = 0.7, both probable values in the mesopelagic (Fig. 8, 9). This could be the cause of observed overestimations of mesopelagic POC from BGC-Argo float $b_{bp}(\lambda)$ compared to modelled POC in the global ocean (Galí et al., 2022).

To summarize, a quantitative examination of the carbonate pump with current sensors on BGC-Argo is limited by our inability to quantify PIC. Moreover, this has knock-on effects on our ability to quantify POC, particularly deeper in the mesopelagic as the PIC/POC rain ratio increases with depth (Fig. 8), which leads to high uncertainties in the quantification of the organic carbon pump from BGC-Argo floats.

3.5.4. An Argo-float-fitting sensor for autonomous detection of PIC concentration and flux

The concept for autonomous measurement of suspended PIC in seawater based on the intrinsic birefringence of calcite and aragonite minerals was first formulated by Guay and Bishop (2002). Birefringence is an inherent property of optically anisotropic materials indicating the ability of the material to split an incident ray of light into two rays (termed the ordinary and extraordinary ray), each with a different index of refraction and each refracted at a different angle. Therefore, birefringence is also referred to as double refraction. The two rays respond to the polarization state of the incident light beam in a different manner. For the ordinary ray the index of refraction is independent of the direction of polarization while for the extraordinary ray the index of refraction varies as a function of the polarization direction. The maximum difference in refractive index occurs for polarization states which are perpendicular to one another. This maximum difference in refractive index between the two beams traveling at different velocities through the material is also termed birefringence, B (dimensionless). The absolute value of B is 0.172 for calcite and 0.155 for aragonite, much higher than for any other mineral or organic material in the ocean (with B typically <0.04) (Guay and Bishop, 2002). It is therefore assumed that PIC is the dominant source of birefringence signal in the ocean, even though certain dinoflagellate thecae, zooplankton carapaces, and lipid globules may also be birefringent (e.g., Balch and Fabry, 2008).

As a consequence of birefringence, a polarized light beam traveling through birefringent material will change polarization state. This effect occurs because any light beam can be decomposed into two perpendicular (orthogonal) polarization components each propagating at different speeds in the material. This means that the relative amplitudes of both these perpendicular (orthogonal) components will go out of synchronization and that the net polarization state which is the vector sum of both components will rotate as a function of the propagation difference accumulated in passing through the birefringent material. This change in polarization state can be detected when analyzing birefringent particles through crossed polarizers. With no depolarization occurring in the medium between the crossed polarizers the transmitted signal is in theory zero for perfect polarizers and very small for high quality polarizers. The ratio of the remaining signal after the second polarizer to the incoming signal before the first polarizer is called the rejection ratio. High quality stretched glass linear polarizers can achieve a rejection ratio of 10^{-6}. This baseline signal defines the minimum amount of depolarization that can be measured.

Birefringence and its effect on polarized light is commonly used for qualitative and quantitative analyses of coccoliths and coccolithophores. Light microscopes equipped with crossed polarizers on source and detector are used to identify coccoliths and quantify their thickness and calcite mass (Beaufort, 2005; Beaufort et al., 2021; Fuertes et al., 2014; González-Lemos et al., 2018; Hermoso and Minoletti, 2018). Further, polarization-sensitive flow cytometers have been used to differentiate calcite-containing phytoplankton cells from others based on the measurement of depolarization of forward scattered light (Balch et al., 1999; Olson et al., 1989; von Dassow et al., 2012). Most recently, an imaging flow cytometer equipped with crossed polarizers was developed to size and count fossilized coccoliths and coccolithophores in marine sediment samples (Langley et al., 2020).

Guay and Bishop (2002) demonstrated that the concentration of coccolith PIC suspended in water could be detected with a benchtop spectrophotometer with 10 cm pathlength sample cell and crossed linear polarizers. They showed a linear response of the birefringence signal over the range of PIC 0.08 to 450 mmol PIC m^{-3} using purified $CaCO_3$ particles. Their work served as the basis for the development of a submersible PIC sensor that measures the birefringence signal and consisted of the modification of a commercially available 25 cm pathlength beam transmissometer to accommodate crossed linear polarizers on source and detector (Bishop, 2009). This cross-polarized transmissometer was designed to detect PIC over the oceanic concentration range, 0.005 to 40 mmol PIC m^{-3}, from oligotrophic or deep waters to the densest coccolithophore blooms (Bishop, 2009; Balch et al., 2005). It is worth noting that beam transmissometers detect scattering in the near-forward direction (Boss et al., 2009), where depolarization by amorphous (non-birefringent) organic and inorganic particles is negligible, and where the majority of depolarization is caused by the presence of birefringent particles.

A first prototype cross-polarized transmissometer or PIC sensor was deployed in 2003 in the North Atlantic ocean in profiling mode from a ship's CTD-Rosette frame and exhibited severe instabilities due to thermal and pressure effects (Bishop, 2009). Since then, the PIC sensor was re-engineered several times. The latest prototypes were deployed from ship CTD frames in the California coastal current in 2017 and in clear waters across the North Pacific ocean in 2018 (Bishop et al., 2022). These prototypes were extensively profiled from the surface to depths below 2000 m and the birefringence signal was compared to PIC concentration measurements obtained from large volume in situ filtration systems. The birefringence signal showed a linear response to PIC over the range 0.01 to 0.1 mmol PIC m^{-3}, albeit with large scatter around the regression lines (Bishop et al., 2022). Comparison of near-surface measurements with satellite PIC showed mixed results. The authors report further re-engineering needs including corrections for thermal and pressure effects, as well as drift potentially owing to misalignment of the linear polarizers (Bishop et al., 2022).

A new measurement concept based on cross-polarized near-forward scattered light with circular polarization was recently proposed by Neukermans and Fournier (2022) and is depicted in Fig. 11. Circular polarization states can be thought of as composed of two coupled perpendicular polarization states oscillating with a phase difference of +90 degrees for right circular polarization and − 90 degrees for left circular polarization. The model of Fournier and Neukermans (2018) for light scattering by birefringent coccoliths (Young et al., 1992) indicates that the depolarization of circularly polarized light is twice as strong than for linearly polarized light. This finding is in line with recent studies showing the advantage of using light microscopes equipped with circular polarizers compared to linear polarizers to estimate coccolith calcite mass (Beaufort et al., 2014; Bollmann, 2014; Fuertes et al., 2014; González-Lemos et al., 2018). Moreover, circular polarizers are much less sensitive to their relative orientation and thus alleviate the alignment problems that plague linear polarizers (Bishop et al., 2022). Prototypes of such instruments are under development.

A notable advantage of beam transmissometers on profiling floats is that they intercept sinking particles while the float drifts at parking depth (typically around 1000 m), acting as "optical sediment traps" (Bishop, 2009; Bishop et al., 2004; Bishop and Wood, 2009; Estapa et al., 2013, 2017, 2019). Particles, both large and small, settle onto the upward facing window of an unpolarized beam transmissometer and give

rise to a measurable change in beam attenuation during parking time (typically several days). The rate of change in beam attenuation over time can be considered as an optical proxy for particle flux. It was shown that this transmissometer-based particle flux method, pioneered by Bishop et al. (2004), correlated well with concurrent particle flux measurements obtained from sediment traps in the subtropical North Atlantic (Estapa et al., 2017). A cross-polarized beam transmissometer would thus not only provide estimates of water column PIC concentration, but also allow the estimation of PIC flux at float parking depths. Such an approach would be simpler than the estimation of PIC flux from an upward-facing cross-polarized camera at the base of a sediment trap in a voluminous module connected sideways to a profiling float (Bishop et al., 2016).

Even though beam transmissometers are not part of the core instrument package on BGC-Argo floats they offer i) a proxy of particle stock based on c_p, ii) a proxy of particle composition based on the backscattering ratio, and iii) a proxy for particle flux at parking depth. The latter has several advantages compared to other methods that have been developed to estimate export and mesopelagic flux from BGC-Argo floats. For example, the method to estimate particle export flux and transfer efficiency from temporal changes in vertically integrated particle stocks derived from float timeseries of b_{bp} (Dall'Olmo et al., 2016; Dall'Olmo and Mork, 2014). This approach assumes negligible particle flux at 1000 m, underestimates export flux due to missing contributions of particle flux in steady-state, and the contribution of large particles to flux (Dall'Olmo and Mork, 2014).

4. Conclusions

The carbonate pump represents an important, yet poorly understood and poorly constrained component of the open ocean biological carbon pump. The pump is mainly driven by calcification from coccolithophores, foraminifera, and pteropods and potentially to some extent by other calcifiers that have been considered equally thoroughly in this context. The contribution of these three groups to PIC mass flux varies spatially and temporarily. Utilizing our compilation of global sediment trap data we estimate that coccolithophores, foraminifera and pteropods contribute 46%, 41% and 13%, respectively, to the global mass flux of PIC at depths >1000 m.

Current estimates of PIC production range between 0.5 and 1.6 Pg C y^{-1} with a median value of 1.2 Pg C y^{-1}, while estimates of PIC export range between 0.45 and 1.80 Pg C y^{-1} with a median value of 1.00 Pg C y^{-1}. These estimates are poorly constrained, diverging by a factor of 4 and mostly overlapping each other. Comparison of median estimates of PIC production and export suggests that ~20% of PIC dissolves in the sunlit surface ocean. Whereas it was often assumed that PIC particles exported from the euphotic zone sink unaffected until the calcite or aragonite lysocline is reached, it is now increasingly recognized that there is major dissolution of PIC in the upper ocean, notably the mesopelagic zone in which 12% to 60% of exported PIC flux dissolves. The proposed mechanisms for shallow dissolution are either dissolution in microenvironments of high pCO_2 from intense remineralization of organic carbon (e.g. fecal pellets or marine snow), or dissolution of more soluble $CaCO_3$ mineral phases, such as aragonite or Mg calcites. Even though mesopelagic dissolution appears critically important to the overall carbonate budget, our mechanistic understanding of shallow dissolution is still quite limited.

The downward flux of PIC produced in the euphotic zone increases the pCO_2 in the surface ocean because alkalinity is consumed. This chemical feedback counters the reduction of pCO_2 by the organic carbon pump, thus weakening the drawdown of atmospheric CO_2 by the organic carbon pump. This counter effect of the carbonate pump depends on the PIC/POC rain ratio of annual exported carbon and the molar ratio of CO_2 produced per mole of $CaCO_3$ precipitated, Ψ. While Ψ can be accurately quantified from temperature, salinity, and carbonate chemistry, the rain ratio of carbon export is more difficult to measure and is therefore much more poorly constrained. Indeed, we found the global annual rain ratio to range by over an order of magnitude between 0.04 and 0.45. Using a global average value of Ψ, we estimated that the carbonate pump counters CO_2 drawdown by 7%, with range between 3 and 30%. Due to the opposite latitudinal patterns in rain ratios and Ψ, we expect the carbonate counter effect to exhibit latitudinal variations by a factor 2–3 with counter strength decreasing from low to high latitudes. Only few in situ studies have quantified the counter effect of the carbonate pump, relying on the assumption that the observed deep PIC flux equals PIC export (Manno et al., 2018; Salter et al., 2014). However, given recent knowledge on important shallow PIC dissolution, this approach will lead to potentially severe underestimation of the counter effect. An accurate quantification of the carbonate counter effect requires observations of Ψ, as well as annually integrated observations of PIC and POC export flux. Estimating the longevity of the counter effect, ranging from seasonal to centennial time scales, will require estimates of dissolution and the depth at which this occurs in the mesopelagic ocean.

Besides countering atmospheric CO_2 drawdown by the organic carbon pump, the carbonate pump has been proposed to enhance the transfer efficiency of the organic carbon pump by increasing the sinking speed of

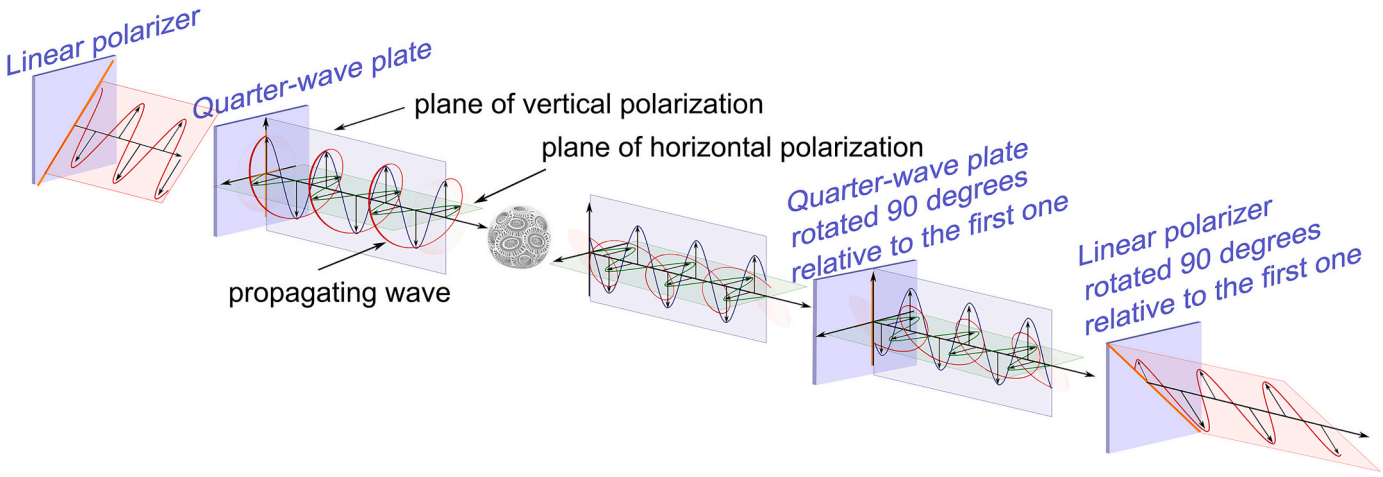

Fig. 11. Schematic diagram of the detection of birefringent particles using a cross-polarized transmissometer with circular polarizers. At the source end, a linear polarizer is aligned with the plane of polarization of the input light. The axes of the quarter-wave plate are at 45° to the polarization axis, thus converting the linear polarization to circular polarization. On the receiver end, a quarter-wave plate and a linear polarizer are at 90° to the first ones. Adapted from open source figure on wikipedia.org.

organic aggregates and faecal pellets, while reducing their remineralization rate. This so-called PIC ballast hypothesis has remained controversial since its proposition twenty years ago. While it was initially hypothesized that PIC is responsible for carrying 83% of POC to the deep ocean, more recent evidence suggests that a globally uniform ballast mechanism is unlikely to exist and that the PIC/POC rain ratio is highly variable. Ballasting of POC flux by coccolithophore PIC and the associated increase in POC sinking velocity has been confirmed through many experimental studies and the knowledge base is comparatively strong. Hence, although there may not be a uniform ballast effect, PIC ballasting of POC is still thought to be regionally important. Ocean biogeochemical models have included various parameterizations of the ballast effect, but there is a lack of consensus in the modeling community that mainly stems from the lack of direct in situ observations of ballasted fluxes.

Improving our mechanistic and quantitative understanding of the carbonate pump component of the BCP at global scale will require large-scale vertically-resolved observations at high temporal frequency of PIC and POC stocks, fluxes, and processes, which lie beyond the reach of traditional observations with sediment traps or ship-based sampling. Autonomous observations from BGC-Argo profiling floats equipped with bio-optical and physicochemical sensors have already provided new insights in the organic carbon pump component of the BCP, including environmental control of phytoplankton growth (Lacour et al., 2015, 2017; Mignot et al., 2018), prevalence and environmental drivers of deep chlorophyll maxima (Cornec et al., 2021), seasonal dynamics of phytoplankton size and community composition (Rembauville et al., 2017; Terrats et al., 2020), export and mesopelagic fluxes of small and large POC (Dall'Olmo et al., 2016; Dall'Olmo and Mork, 2014; Estapa et al., 2017), and a better understanding of mesopelagic flux attenuation (Briggs et al., 2020). The development of a BGC-Argo float-fitting autonomous sampling device to measure the concentration and flux of PIC will enable observations of the two components of the biological carbon pump in concert and shed new light on the counter and ballast effect of the carbonate pump.

While BGC-Argo floats offer vertically-resolved observations of ocean biogeochemical parameters from the surface down to the bottom of the mesopelagic zone at sub-weekly frequency, ocean colour satellites offer global coverage of carbon and phytoplankton stocks in the near-surface ocean at daily frequency. The synergistic combination of these observation platforms allows i) cross-validation and quality control of observations from both platforms in the global ocean (Roesler et al., 2017; Xing et al., 2020), ii) filling observational gaps in satellite data due to clouds or low sun angle (Terrats et al., 2020), and iii) building a dynamical three-dimensional view of ocean carbon pools and biogeochemistry.

Author contributions

G.N. conceptualized and coordinated the review. G.N. and L.B. wrote the first draft; A.B. and L.B. investigated calcifier contributions; G.N and Q. S. conducted the sediment trap and Thorium-derived flux analyses and match up with satellite products; G. F. contributed the backscattering cross section modeling; all authors contributed to reviewing and editing the final manuscript.

Declaration of Competing Interest

The authors declare the following financial interests/personal relationships which may be considered as potential competing interests: Griet Neukermans reports financial support was provided by European Research Council. Griet Neukermans has patent issued to Ghent University.

Data availability

Data availability statement is included in the manuscript

Acknowledgements

Catherine Mitchell and Barney Balch are kindly thanked to provide satellite data of calcification rates. We thank NASA Goddard Space Flight Center, Ocean Ecology Laboratory, Ocean Biology Processing Group for Ocean Color Data from the SeaWiFS and MODIS Aqua satellite missions. This review paper is part of a project that has received funding from the European Research Council (ERC) under the European Union's Horizon 2020 research and innovation programme (Grant agreement No. 853516 CarbOcean). The technological development of a cross-polarized transmissometer has also received funding from UGent's Industrial Research Fund (F2020/IOF-StarTT/088) and Special Research Fund (BOF/STA/202002/011).

References

Aas, E., 1996. Refractive index of phytoplankton derived from its metabolite composition. J. Plankton Res. 18, 2223–2249. https://doi.org/10.1093/plankt/18.12.2223.

Accornero, A., Manno, C., Esposito, F., Gambi, M., 2003. GambiThe vertical flux of particulate matter in the polynya of Terra Nova Bay.Part II. Biological components. Antarct. Sci. 15, 175–188.

Allison, D.B., Stramski, D., Mitchell, B.G., 2010. Empirical Ocean color algorithms for estimating particulate organic carbon in the Southern Ocean. J. Geophys. Res. Ocean. 115 https://doi.org/10.1029/2009JC006040.

Anderson, O.R., Spindler, M., Bé, A.W.H., Hemleben, C., 1979. Trophic activity of planktonic foraminifera. J. Mar. Biol. Assoc. United Kingdom 59, 791–799. https://doi.org/10.1017/S002531540004577X.

Anglada-Ortiz, G., Zamelczyk, K., Meilland, J., Ziveri, P., Chierici, M., Fransson, A., Rasmussen, T.L., 2021. Planktic foraminiferal and pteropod contributions to carbon dynamics in the Arctic Ocean (North Svalbard Margin). Front. Mar. Sci. 8 https://doi.org/10.3389/fmars.2021.661158.

Archer, D., Maier-Reimer, E., 1994. Effect of deep-sea sedimentary calcite preservation on atmospheric CO2 concentration. Nature 367, 260–263. https://doi.org/10.1038/367260a0.

Armstrong, R.A., Lee, C., Hedges, J.I., Honjo, S., Wakeham, S.G., 2001. A new, mechanistic model for organic carbon fluxes in the ocean based on the quantitative association of POC with ballast minerals. Deep Sea ResPart II Top. Stud. Oceanogr. 49, 219–236. https://doi.org/10.1016/S0967-0645(01)00101-1.

Arnarson, T.S., Keil, R.G., 2007. Changes in organic matter-mineral interactions for marine sediments with varying oxygen exposure times. Geochim. Cosmochim. Acta 71, 3545–3556. https://doi.org/10.1016/J.GCA.2007.04.027.

Aumont, O., van Hulten, M., Roy-Barman, M., Dutay, J.-C., Éthé, C., Gehlen, M., 2017. Variable reactivity of particulate organic matter in a global ocean biogeochemical model. Biogeosciences 14, 2321–2341. https://doi.org/10.5194/bg-14-2321-2017.

Bach, L.T., Boxhammer, T., Larsen, A., Hildebrandt, N., Schulz, K.G., Riebesell, U., 2016. Influence of plankton community structure on the sinking velocity of marine aggregates. Glob. Biogeochem. Cycles 30, 1145–1165. https://doi.org/10.1002/2016GB005372.

Baker, E.T., Milburn, H.B., Tennant, D.A., 1988. Field assessment of sediment trap efficiency under varying flow conditions. J. Mar. Res. 46, 573–592. https://doi.org/10.1357/002224088785113522.

Balch, W., Drapeau, D., Bowler, B., Booth, E., 2007. Prediction of pelagic calcification rates using satellite measurements. DeepRes. Part II Top. Stud. Oceanogr. 54, 478–495. https://doi.org/10.1016/J.DSR2.2006.12.006.

Balch, W., Kilpatrick, K.A., Holligan, P., Harbour, D., Fernandez, E., 1996. The 1991 coccolithophore bloom in the Central North Atlantic. 2. Relating optics to coccolith concentration. Limnol. Oceanogr. 41, 1684–1696. https://doi.org/10.4319/lo.1996.41.8.1684.

Balch, W.M., 2018. The Ecology.Biogeochemistry, and Optical Properties of Coccolithophores, 10.1146/annurev-marine-121916-063319 10, 71-98. doi: 10.1146/ANNUREV-MARINE-121916-063319.

Balch, W.M., Bowler, B.C., Drapeau, D.T., Lubelczyk, L.C., Lyczkowski, E., 2018. Vertical distributions of coccolithophores, PIC, POC, biogenic silica, and chlorophyll a throughout the global ocean. Glob. Biogeochem. Cycles 32, 2–17. https://doi.org/10.1002/2016GB005614.

Balch, W.M., Drapeau, D.T., Cucci, T.L., Vaillancourt, R.D., Kilpatrick, K.A., Fritz, J.J., 1999. Optical backscattering by calcifying algae: separating the contribution of particulate inorganic and organic carbon fractions. J. Geophys. Res. Ocean. 104, 1541–1558. https://doi.org/10.1029/1998jc900035.

Balch, W.M., Gordon, H.R., Bowler, B.C., Drapeau, D.T., Booth, E.S., 2005. Calcium carbonate measurements in the surface global ocean based on Moderate-Resolution Imaging Spectroradiometer data. J. Geophys. Res. 110, C07001. https://doi.org/10.1029/2004JC002560.

Balch, W.M., Holligan, P.M., Ackleson, S.G., Voss, K.J., 1991. Biological and optical properties of mesoscale coccolithophore blooms in the Gulf of Maine. Limnol. Oceanogr. 36, 629–643. https://doi.org/10.4319/lo.1991.36.4.0629.

Balch, W.M., Kilpatrick, K., Holligan, P.M., Cucci, T., 1993. Coccolith production and detachment by Emiliania huxleyi (Prymnesiophyceae). J. Phycol. 29, 566–575. https://doi.org/10.1111/j.0022-3646.1993.00566.x.

Balch, W.M., Kilpatrick, K.A., Trees, C.C., 1996. The 1991 coccolithophore bloom in the Central North Atlantic. 1. Optical properties and factors affecting their distribution. Limnol. Oceanogr. 41, 1669–1683. https://doi.org/10.4319/lo.1996.41.8.1669.
Balch, W.M., Mitchell, C., 2023. Remote sensing algorithms for particulate inorganic carbon (PIC) and the global cycle of PIC this issue.
Balch, W.M., Fabry, V.J., 2008. Ocean acidification: documenting its impact on calcifying Phytoplankton at Basin Scales. Mar. Ecol. Prog. Ser. 373, 239–248.
Battaglia, G., Steinacher, M., Joos, F., 2016. A probabilistic assessment of calcium carbonate export and dissolution in the modern ocean. Biogeosciences 13, 2823–2848. https://doi.org/10.5194/bg-13-2823-2016.
Bauerfeind, E., Nöthig, E.M., Pauls, B., Kraft, A., Beszczynska-Möller, A., 2014. Variability in pteropod sedimentation and corresponding aragonite flux at the Arctic deep-sea long-term observatory HAUSGARTEN in the eastern Fram Strait from 2000 to 2009. J. Mar. Syst. 132, 95–105. https://doi.org/10.1016/J.JMARSYS.2013.12.006.
Beaufort, L., 2005. Weight estimates of coccoliths using the optical properties (birefringence) of calcite. Micropaleontology 51, 289–297. https://doi.org/10.2113/gsmicropal.51.4.289.
Beaufort, L., Barbarin, N., Gally, Y., 2014. Optical measurements to determine the thickness of calcite crystals and the mass of thin carbonate particles such as coccoliths. Nat. Protoc. 9, 633–642. https://doi.org/10.1038/nprot.2014.028.
Beaufort, L., Gally, Y., Suchéras-Marx, B., Ferrand, P., Duboisset, J., 2021. Technical note: a universal method for measuring the thickness of microscopic calcite crystals, based on bidirectional circular polarization. Biogeosciences 18, 775–785. https://doi.org/10.5194/BG-18-775-2021.
Beaufort, L., Heussner, S., 1999. Coccolithophorids on the continental slope of the Bay of Biscay – production, transport and contribution to mass fluxes. Deep Sea ResPart II Top. Stud. Oceanogr. 46, 2147–2174. https://doi.org/10.1016/S0967-0645(99)00058-2.
Bednaršek, N., Mozina, J., Vogt, M., O'Brien, C., Tarling, G.A., 2012. The global distribution of pteropods and their contribution to carbonate and carbon biomass in the modern ocean. Earth Syst. Sci. Data 4, 167–186. https://doi.org/10.5194/ESSD-4-167-2012.
Behrenfeld, M.J., Boss, E., Siegel, D.A., Shea, D.M., 2005. Carbon-based ocean productivity and phytoplankton physiology from space. Glob. Biogeochem. Cycles 19, GB1006. https://doi.org/10.1029/2004GB002299.
Berelson, W.M., Balch, W.M., Najjar, R., Feely, R.A., Sabine, C., Lee, K., 2007. Relating estimates of CaCO 3 production, export, and dissolution in the water column to measurements of CaCO 3 rain into sediment traps and dissolution on the sea floor: a revised global carbonate budget. Glob. Biogeochem. Cycles 21. https://doi.org/10.1029/2006GB002803.
Berner, Robert A., Honjo, S., 1981. Pelagic sedimentation of aragonite: its geochemical significance. Science 211 (4485), 940–942.
Betzer, P.R., Byrne, R.H., Acker, J.G., Lewis, C.S., Jolley, R.R., Feely, R.A., 1984. The. Science 226 (4678), 1074–1077.
Bishop, J., 2009. Autonomous observations of the ocean biological carbon pump. Oceanography 22, 182–193. https://doi.org/10.5670/oceanog.2009.48.
Bishop, J.K.B., Amaral, V.J., Lam, P.J., Wood, T.J., Lee, J.-M., Laubach, A., Barnard, A., Derr, A., Orrico, C., 2022. Transmitted cross-polarized light detection of particulate inorganic carbon concentrations and fluxes in the ocean water column: ships to ARGO floats. Front. Remote Sens. 4. https://doi.org/10.3389/FRSEN.2022.837938.
Bishop, J.K.B., Collier, R.W., Kettens, D.R., Edmond, J.M., 1980. The chemistry, biology, and vertical flux of particulate matter from the upper 1500 m of the Panama Basin. Deep Sea Res.Part A. Oceanogr. Res. Pap. 27, 615–640. https://doi.org/10.1016/0198-0149(80)90077-1.
Bishop, J.K.B., Fong, M.B., Wood, T.J., 2016. Robotic observations of high wintertime carbon export in California coastal waters. Biogeosciences 13, 3109–3129. https://doi.org/10.5194/BG-13-3109-2016.
Bishop, J.K.B., Wood, T.J., 2009. Year-round observations of carbon biomass and flux variability in the Southern Ocean. Glob. Biogeochem. Cycles 23, GB2019. https://doi.org/10.1029/2008GB003206.
Bishop, J.K.B., Wood, T.J., Davis, R.E., Sherman, J.T., 2004. Robotic observations of enhanced carbon biomass and export at 55 degrees during SOFeX. Science 304, 417–420. https://doi.org/10.1126/science.1087717.
Bittig, H.C., Maurer, T.L., Plant, J.N., Schmechtig, C., Wong, A.P.S., Claustre, H., Trull, T.W., Udaya Bhaskar, T.V.S., Boss, E., Dall'Olmo, G., Organelli, E., Poteau, A., Johnson, K.S., Hanstein, C., Leymarie, E., Le Reste, S., Riser, S.C., Rupan, A.R., Taillandier, V., Thierry, V., Xing, X., 2019. A BGC-Argo guide: planning, deployment, data handling and usage. Front. Mar. Sci. 6, 502.
Bollmann, J., 2014. Technical note: weight approximation of coccoliths using a circular polarizer and interference colour derived retardation estimates – (The CPR Method). Biogeosciences 11, 1899–1910. https://doi.org/10.5194/bg-11-1899-2014.
Boss, E., Slade, W.H., Behrenfeld, M., Dall, G., Gardner, D., Walsh, I.D., Richardson, M.J., Bogucki, D.J., Domaradzki, J.A., Stramski, D., Zaneveld, R.V., Zaneveld, J.R., Barnard, A.H., Twardowski, M.S., Chang, G.C., Dickey, T.D., 2009. Acceptance angle effects on the beam attenuation in the ocean. Opt. Express 17 (3), 1535–1550. https://doi.org/10.1364/OE.17.001535.
Boyd, P.W., Claustre, H., Levy, M., Siegel, D.A., Weber, T., 2019. Multi-faceted particle pumps drive carbon sequestration in the ocean. Nature. https://doi.org/10.1038/s41586-019-1098-2.
Brewin, R.J.W., Sathyendranath, S., Platt, T., Bouman, H., Ciavatta, S., Dall'Olmo, G., Dingle, J., Groom, S., Jönsson, B., Kostadinov, T.S., Kulk, G., Laine, M., Martínez-Vicente, V., Psarra, S., Raitsos, D.E., Richardson, K., Rio, M.H., Rousseaux, C.S., Salisbury, J., Shutler, J.D., Walker, P., 2021. Sensing the ocean biological carbon pump from space: A review of capabilities, concepts, research gaps and future developments. Earth-Sci. Rev. 217.
Briggs, N., Dall'Olmo, G., Claustre, H., 2020. Major role of particle fragmentation in regulating biological sequestration of CO2 by the oceans. Science (80-.) 367, 791–793. https://doi.org/10.1126/science.aay1790.
Broecker, W.S., 1971. Calcite accumulation rates and glacial to interglacial changes in oceanic mixing. In: Turekian, K.K. (Ed.), The Late Cenozoic Glacial Ages. Yale Univ. Press, New Haven, Conn, pp. 239–265.
Broecker, W., Clark, E., 2009. Ratio of coccolith CaCO3 to foraminifera CaCO3 in late Holocene deep sea sediments. Paleoceanography 24. https://doi.org/10.1029/2009PA001731.
Broecker, W.S., Peng, T.-H., 1982. Tracers in the Sea. Lamont- Doherty Geol. Obs., Palisades, N. Y., p. 690
Broerse, A.T.C., Brummer, G.-J.A., Hinte, J.E.V., 2000a. Coccolithophore export production in response to monsoonal upwelling off Somalia (northwestern Indian Ocean). Deep Sea Res.Part II Top. Stud. Oceanogr. 47, 2179–2205. https://doi.org/10.1016/S0967-0645(00)00021-7.
Broerse, A.T.C., Ziveri, P., Honjo, S., 2000b. Coccolithophore (–CaCO3) flux in the Sea of Okhotsk: seasonality, settling and alteration processes. Mar. Micropaleontol. 39, 179–200. https://doi.org/10.1016/S0377-8398(00)00020-7.
Broerse, A.T.C., Ziveri, P., van Hinte, J.E., Honjo, S., 2000c. Coccolithophore export production, species composition, and coccolith-CaCO3 fluxes in the NE Atlantic (34°N21°W and 48°N21°W). Deep Sea Res.Part II Top. Stud. Oceanogr. 47, 1877–1905. https://doi.org/10.1016/S0967-0645(00)00010-2.
Buesseler, K., Ball, L., Andrews, J., Benitez-Nelson, C., Belastock, R., Chai, F., Chao, Y., 1998. Upper Ocean export of particulate organic carbon in the Arabian Sea derived from thorium-234. Deep. Sea Res.Part II Top. Stud. Oceanogr. 45, 2461–2487. https://doi.org/10.1016/S0967-0645(98)80022-2.
Buesseler, K.O., Boyd, P.W., 2009. Shedding light on processes that control particle export and flux attenuation in the twilight zone of the open ocean. Limnol. Oceanogr. 54, 1210–1232. https://doi.org/10.4319/lo.2009.54.4.1210.
Buesseler, K.O., Boyd, P.W., Black, E.E., Siegel, D.A., 2020. Metrics that matter for assessing the ocean biological carbon pump. Proc. Natl. Acad. Sci. U. S. A. https://doi.org/10.1073/pnas.1918114117.
Buesseler, K.O., Lamborg, C.H., Boyd, P.W., Lam, P.J., Trull, T.W., Bidigare, R.R., Bishop, J.K.B., Casciotti, K.L., Dehairs, F., Elskens, M., Honda, M., Karl, D.M., Siegel, D.A., Silver, M.W., Steinberg, D.K., Valdes, J., Van Mooy, B., Wilson, S., 2007. Revisiting carbon flux through the ocean's twilight zone. <sb:title>Science </sb:title>(80-.) 316, 567–570. https://doi.org/10.1126/science.1137959.
Buitenhuis, E.T., Le Quéré, C., Bednaršek, N., Schiebel, R., 2019. Large contribution of pteropods to shallow CaCO3 export. Glob. Biogeochem. Cycles 33, 458–468. https://doi.org/10.1029/2018GB006110.
Busch, K., Bauerfeind, E., Nöthig, E.-M., 2015. Pteropod sedimentation patterns in different water depths observed with moored sediment traps over a 4-year period at the LTER station HAUSGARTEN in eastern Fram Strait. Polar Biol. 38 (6), 845–859.
Cazzaniga, I., Zibordi, G., Mélin, F., 2021. Spectral variations of the remote sensing reflectance during coccolithophore blooms in the Western Black Sea. Remote Sens. Environ. 264, 112607 https://doi.org/10.1016/J.RSE.2021.112607.
Ceballos-Romero, E., Buesseler, K.O., Villa-Alfageme, M., 2022. Revisiting five decades of ^{234}Th data: a comprehensive global oceanic compilation. Earth Syst. Sci. Data 14, 2639–2679. https://doi.org/10.5194/essd-14-2639-2022.
Cetinić, I., Perry, M.J., Briggs, N.T., Kallin, E., D'Asaro, E.A., Lee, C.M., 2012. Particulate organic carbon and inherent optical properties during 2008 North Atlantic Bloom Experiment. J. Geophys. Res. Ocean. 117, C06028. https://doi.org/10.1029/2011JC007771.
Claustre, H., Johnson, K.S., Takeshita, Y., 2020. Observing the global ocean with biogeochemical-argo. Annu. Rev. Mar. Sci. 12, 23–48. https://doi.org/10.1146/annurev-marine-010419-010956.
Claustre, H., Legendre, L., Boyd, P.W., Levy, M., 2021. The oceans' biological carbon pumps: framework for a research observational community approach. Front. Mar. Sci. 8, 780052. https://doi.org/10.3389/fmars.2021.780052.
Collier, R., Dymond, J., Honjo, S., Manganini, S., Francois, R., Dunbar, R., 2000. The vertical flux of biogenic and lithogenic material in the Ross Sea: moored sediment trap observations 1996–1998. DeepRes. Part II Top. Stud. Oceanogr. 47, 3491–3520. https://doi.org/10.1016/S0967-0645(00)00076-X.
Cornec, M., Claustre, H., Mignot, A., Guidi, L., Lacour, L., Poteau, A., D'Ortenzio, F., Gentili, B., Schmechtig, C., 2021. Deep chlorophyll maxima in the global ocean: occurrencesdrivers and characteristics. Glob. Biogeochem. Cycles 35. https://doi.org/10.1029/2020GB006759.
Dall'Olmo, G., Dingle, J., Polimene, L., Brewin, R.J.W., Claustre, H., 2016. Substantial energy input to the mesopelagic ecosystem from the seasonal mixed-layer pump. Nat. Geosci. 9, 820–823. https://doi.org/10.1038/ngeo2818.
Dall'Olmo, G., Mork, K.A., 2014. Carbon export by small particles in the Norwegian Sea. Geophys. Res. Lett. 41, 2921–2927. https://doi.org/10.1002/2014GL059244.
Deuser, W.G., Ross, E.H., 1989. Seasonally abundant planktonic Foraminifera of the Sargasso Sea: succession, deep-water fluxes, isotopic compositions, and paleoceanographic implications. J. Foraminifer. Res. 19, 268–293. https://doi.org/10.2113/gsjfr.19.4.268.
DeVries, T., Holzer, M., Primeau, F., 2017. Recent increase in oceanic carbon uptake driven by weaker upper-ocean overturning. Nature 542, 215–218. https://doi.org/10.1038/nature21068.
DeVries, T., Liang, J.-H., Deutsch, C., 2014. A mechanistic particle flux model applied to the oceanic phosphorus cycle. Biogeosciences 11, 5381–5398. https://doi.org/10.5194/bg-11-5381-2014.

DeVries, T., Weber, T., 2017. The export and fate of organic matter in the ocean: new constraints from combining satellite and oceanographic tracer observations. Glob. Biogeochem. Cycles 31, 535–555. https://doi.org/10.1002/2016GB005551.
Doney, S.C., Fabry, V.J., Feely, R.A., Kleypas, J.A., 2009. Ocean acidification: the other CO 2 problem. Annu. Rev. Mar. Sci. 1, 169–192. https://doi.org/10.1146/annurev.marine.010908.163834.
Eikrem, W., Medlin, L.K., Henderiks, J., Rokitta, S., Rost, B., Probert, I., Throndsen, J., Edvardsen, B., 2017. Haptophyta. In: Handbook of the Protists. Springer, pp. 1–61. https://doi.org/10.1007/978-3-319-32669-6_38-1.
Emerson, S., 2014. Annual net community production and the biological carbon flux in the ocean. Glob. Biogeochem. Cycles 28, 14–28. https://doi.org/10.1002/2013GB004680.
Engel, A., Szlosek, J., Abramson, L., Liu, Z., Lee, C., 2009. Investigating the effect of ballasting by CaCO3 in Emiliania huxleyi: I. Formation, settling velocities and physical properties of aggregates. Deep Sea Res.Part II Top. Stud. Oceanogr. 56, 1396–1407. https://doi.org/10.1016/J.DSR2.2008.11.027.
Estapa, M., Durkin, C., Buesseler, K., Johnson, R., Feen, M., 2017. Carbon flux from bio-optical profiling floats: calibrating transmissometers for use as optical sediment traps. Deep Sea Res.Part I Oceanogr. Res. Pap. 120, 100–111. https://doi.org/10.1016/J.DSR.2016.12.003.
Estapa, M.L., Buesseler, K., Boss, E., Gerbi, G., 2013. Autonomous, high-resolution observations of particle flux in the oligotrophic ocean. Biogeosciences 10, 5517–5531. https://doi.org/10.5194/bg-10-5517-2013.
Estapa, M.L., Feen, M.L., Breves, E., 2019. Direct observations of biological carbon export from profiling floats in the subtropical North Atlantic. Glob. Biogeochem. Cycles 33, 282–300. https://doi.org/10.1029/2018GB006098.
Fabry, V.J., Deuser, W.G., 1992. Seasonal Changes in the Isotopic Compositions and Sinking Fluxes of Euthecosomatous Pteropod Shells in the Sargasso Sea. Paleoceanography 7 (2), 195–213. https://doi.org/10.1029/91PA03138.
Fabry, V.J., Seibel, B.A., Feely, R.A., Orr, J.C., 2008. Impacts of ocean acidification on marine fauna and ecosystem processes. ICES J. Mar. Sci. 65, 414–432. https://doi.org/10.1093/icesjms/fsn048.
Fender, C.K., Kelly, T.B., Guidi, L., Ohman, M.D., Smith, M.C., Stukel, M.R., 2019. Investigating particle size-flux relationships and the biological pump across a range of Plankton ecosystem states from coastal to oligotrophic. Front. Mar.Sci. 6, 603. https://doi.org/10.3389/fmars.2019.00603.
Fischer, K., Dymond, J., Moser, C., Murray, D., Matherne, A., 1988. Seasonal variation in particulate flux in an offshore area adjacent to coastal upwelling. In: Suess, E., Thiede, J. (Eds.), Coastal Upwelling Its Sediment Record: Part A: Responses of the Sedimentary Regime to Present Coastal Upwelling. Springer US, Boston, MA, pp. 209–224.
Fischer, G., Karakas, G., Karakas, K., 2009. Sinking rates and ballast composition of particles in the Atlantic Ocean: implications for the organic carbon fluxes to the deep ocean. Biogeosciences 6, 85–102.
Fournier, G., Neukermans, G., 2018. Polarized light scattering properties of Emiliania Huxleyi coccoliths and coccospheres. In: Proceedings of Ocean Optics Conference XXIV. Oceanography Society, Dubrovnik.
Fournier, G., Neukermans, G., 2017. An analytical model for light backscattering by coccoliths and coccospheres of Emiliania huxleyi. Opt. Express 25, 14996. https://doi.org/10.1364/OE.25.014996.
Francois, R., Honjo, S., Krishfield, R., Manganini, S., 2002. Factors controlling the flux of organic carbon to the bathypelagic zone of the ocean. Glob. Biogeochem. Cycles 16. https://doi.org/10.1029/2001GB001722, 34–1-34–20.
Frankignoulle, M., Canon, C., Gattuso, J.-P., 1994. Marine calcification as a source of carbon dioxide: positive feedback of increasing atmospheric CO 2. Limnol. Oceanogr. 39, 458–462. https://doi.org/10.4319/lo.1994.39.2.0458.
Friedlingstein, P., Jones, M.W., O'Sullivan, M., Andrew, R.M., Bakker, D.C.E., Hauck, J., Le Quéré, C., Peters, G.P., Peters, W., Pongratz, J., Sitch, S., Canadell, J.G., Ciais, P., Jackson, R.B., Alin, S.R., Anthoni, P., Bates, N.R., Becker, M., Bellouin, N., Bopp, L., Chau, T.T.T., Chevallier, F., Chini, L.P., Cronin, M., Currie, K.I., Decharme, B., Djeutchouang, L.M., Dou, X., Evans, W., Feely, R.A., Feng, L., Gasser, T., Gilfillan, D., Gkritzalis, T., Grassi, G., Gregor, L., Gruber, N., Gürses, Ö., Harris, I., Houghton, R. A., Hurtt, G.C., Iida, Y., Ilyina, T., Luijkx, I.T., Jain, A., Jones, S.D., Kato, E., Kennedy, D., Goldewijk, K.K., Knauer, J., Korsbakken, J.I., Körtzinger, A., Landschützer, P., Lauvset, S.K., Lefèvre, N., Lienert, S., Liu, J., Marland, G., McGuire, P.C., Melton, J.R., Munro, D.R., Nabel, J.E.M.S., Nakaoka, S.I., Niwa, Y., Ono, T., Pierrot, D., Poulter, B., Rehder, G., Resplandy, L., Robertson, E., Rödenbeck, C., Rosan, T.M., Schwinger, J., Schwingshackl, C., Séférian, R., Sutton, A.J., Sweeney, C., Tanhua, T., Tans, P.P., Tian, H., Tilbrook, B., Tubiello, F., Van Der Werf, G.R., Vuichard, N., Wada, C., Wanninkhof, R., Watson, A.J., Willis, D., Wiltshire, A.J., Yuan, W., Yue, C., Yue, X., Zaehle, S., Zeng, J., 2022. Global Carbon Budget 2021. Earth Syst. Sci. Data 14, 1917–2005. https://doi.org/10.5194/essd-14-1917-2022.
Fuertes, M.-Á., Flores, J.-A., Sierro, F.J., 2014. The use of circularly polarized light for biometry, identification and estimation of mass of coccoliths. Mar. Micropaleontol. 113, 44–55. https://doi.org/10.1016/J.MARMICRO.2014.08.007.
Galí, M., Falls, M., Claustre, H., Aumont, O., Bernardello, R., 2022. Bridging the gaps between particulate backscattering measurements and modeled particulate organic carbon in the ocean. Biogeosciences 19, 1245–1275. https://doi.org/10.5194/BG-19-1245-2022.
Garcia, C.A.E., Garcia, V.M.T., Dogliotti, A.I., Ferreira, A., Romero, S.I., Mannino, A., Souza, M.S., Mata, M.M., 2011. Environmental conditions and bio-optical signature of a coccolithophorid bloom in the Patagonian shelf. J. Geophys. Res. Ocean. 116 https://doi.org/10.1029/2010JC006595.
Gehlen, M., Bopp, L., Emprin, N., Aumont, O., Heinze, C., Ragueneau, O., 2006. Reconciling surface ocean productivity, export fluxes and sediment composition in a global biogeochemical ocean model. Biogeosciences 3, 521–537. https://doi.org/10.5194/bg-3-521-2006.
Gilmer, R.W., Harbison, G.R., 1986. Morphology and field behavior of pteropod molluscs: feeding methods in the families Cavoliniidae, Limacinidae and Peraclididae (Gastropoda: Thecosomata). Mar. Biol. 911 (91), 47–57. https://doi.org/10.1007/BF00397570, 1986.
Giraudeau, J., Bailey, G.W., Pujol, C., 2000. A high-resolution time-series analyses of particle fluxes in the Northern Benguela coastal upwelling system: carbonate record of changes in biogenic production and particle transfer processes. Deep Sea Res.Part II Top. Stud. Oceanogr. 47, 1999–2028. https://doi.org/10.1016/S0967-0645(00)00014-X.
González-Lemos, S., Guitián, J., Fuertes, M.-Á., Flores, J.-A., Stoll, H.M., 2018. Technical note: an empirical method for absolute calibration of coccolith thickness. Biogeosciences 15, 1079–1091. https://doi.org/10.5194/bg-15-1079-2018.
Gordon, H.R., Boynton, G.C., Balch, W.M., Groom, S.B., Harbour, D.S., Smyth, T.J., 2001. Retrieval of coccolithophore calcite concentration from SeaWiFS Imagery. Geophys. Res. Lett. 28, 1587–1590. https://doi.org/10.1029/2000GL012025.
Gordon, H.R., Du, T., 2001. Light scattering by nonspherical particles: application to coccoliths detached from Emiliania huxleyi. Limnol. Oceanogr. 46, 1438–1454. https://doi.org/10.4319/lo.2001.46.6.1438.
Gordon, H.R., McCluney, W.R., 1975. Estimation of the depth of sunlight penetration in the sea for remote sensing. Appl. Opt. 14 (2), 413–416. https://doi.org/10.1364/AO.14.000413.
Greco, M., Morard, R., Kucera, M., 2021. Single-cell metabarcoding reveals biotic interactions of the Arctic calcifier Neogloboquadrina pachyderma with the eukaryotic pelagic community. J. Plankton Res. 43, 113–125. https://doi.org/10.1093/PLANKT/FBAB015.
Grigoratou, M., Monteiro, F.M., Schmidt, D.N., Wilson, J.D., Ward, B.A., Ridgwell, A., 2019. A trait-based modelling approach to planktonic foraminifera ecology. Biogeosciences 16, 1469–1492. https://doi.org/10.5194/BG-16-1469-2019.
Guay, C.K., Bishop, J.K., 2002. A rapid birefringence method for measuring suspended CaCO3 concentrations in seawater. Deep Sea Res.Part I Oceanogr. Res. Pap. 49, 197–210. https://doi.org/10.1016/S0967-0637(01)00049-8.
Guerreiro, C.V., Baumann, K.H., Brummer, G.J.A., Korte, L.F., Sá, C., Stuut, J.B.W., 2019. Transatlantic gradients in calcifying phytoplankton (coccolithophore) fluxes. Prog. Oceanogr. 176, 102140 https://doi.org/10.1016/J.POCEAN.2019.102140.
Guerreiro, C.V., Baumann, K.H., Brummer, G.J.A., Valente, A., Fischer, G., Ziveri, P., Brotas, V., Stuut, J.B.W., 2021. Carbonate fluxes by coccolithophore species between NW Africa and the Caribbean: implications for the biological carbon pump. Limnol. Oceanogr. 66, 3190–3208. https://doi.org/10.1002/LNO.11872.
Guidi, L., Legendre, L., Reygondeau, G., Uitz, J., Stemmann, L., Henson, S.A., 2015. A new look at ocean carbon remineralization for estimating deepwater sequestration. Glob. Biogeochem. Cycles 29, 1044–1059. https://doi.org/10.1002/2014GB005063.
Haidar, A.T., Thierstein, H.R., Deuser, W.G., 2000. Calcareous phytoplankton standing stocks, fluxes and accumulation in Holocene sediments off Bermuda (N. Atlantic). DeepRes. Part II Top. Stud. Oceanogr. 47, 1907–1938. https://doi.org/10.1016/S0967-0645(00)00011-4.
Heinze, C., 2004. Simulating oceanic CaCO 3 export production in the greenhouse. Geophys. Res. Lett. 31, L16308. https://doi.org/10.1029/2004GL020613.
Hense, I., Stemmler, I., Sonntag, S., 2017. Ideas and perspectives: climate-relevant marine biologically driven mechanisms in Earth system models. Biogeosciences 14, 403–413. https://doi.org/10.5194/bg-14-403-2017.
Henson, S.A., Sanders, R., Madsen, E., 2012. Global patterns in efficiency of particulate organic carbon export and transfer to the deep ocean. Glob. Biogeochem. Cycles 26, GB1028. https://doi.org/10.1029/2011GB004099.
Henson, S.A., Yool, A., Sanders, R., 2015. Variability in efficiency of particulate organic carbon export: a model study. Glob. Biogeochem. Cycles 29, 33–45. https://doi.org/10.1002/2014GB004965.
Hermoso, M., Minoletti, F., 2018. Mass and fine-scale morphological changes induced by changing seawaterpH in the Coccolith Gephyrocapsa oceanica. J. Geophys. Res. Biogeosci. 123, 2761–2774. https://doi.org/10.1029/2018JG004535.
Hofmann, M., Schellnhuber, H.-J., 2009. Oceanic acidification affects marine carbon pump and triggers extended marine oxygen holes. Proc. Natl. Acad. Sci. U. S. A. 106, 3017–3022. https://doi.org/10.1073/pnas.0813384106.
Holligan, P.M., Fernández, E., Aiken, J., Balch, W.M., Boyd, P., Burkill, P.H., Finch, M., Groom, S.B., Malin, G., Muller, K., Purdie, D.A., Robinson, C., Trees, C.C., Turner, S. M., van der Wal, P., 1993. A biogeochemical study of the coccolithophore, Emiliania huxleyi, in the North Atlantic. Glob. Biogeochem. Cycles 7, 879–900. https://doi.org/10.1029/93GB01731.
Holligan, P.M., Viollier, M., Harbour, D.S., Camus, P., Champagne-Philippe, M., 1983. Satellite and ship studies of coccolithophore production along a continental shelf edge. Nature 304, 339–342. https://doi.org/10.1038/304339a0.
Honjo, S., 1978. Sedimentation of materials int he Sargasso Sea at a 5,367 m deep station. J. Mar. Res. 36, 469–492.
Honjo, S., Manganini, S.J., 1993. Annual biogenic particle fluxes to the interior of the North Atlantic Ocean; studied at 34 N 21 W and 48 N 21 W. Deep Sea Res. Part II Top. Stud. Oceanogr. 40 (1–2), 587–607.
Honjo, S., Manganini, S.J., Krishfield, R.A., Francois, R., 2008. Particulate organic carbon fluxes to the ocean interior and factors controlling the biological pump: a synthesis of global sediment trap programs since 1983. Prog. Oceanogr. 76, 217–285. https://doi.org/10.1016/J.POCEAN.2007.11.003.
Hopkins, J., Balch, W.M., 2018. A new approach to estimating coccolithophore calcification rates from Space. J. Geophys. Res. Biogeosciences 123, 1447–1459. https://doi.org/10.1002/2017JG004235.

Howard, W., Roberts, D., Moy, A., Lindsay, M., Hopcroft, R., Trull, T., Bray, S., 2011. Distribution, abundance and seasonal flux of pteropods in the Sub-Antarctic Zone. Deep-Sea Res. II Top. Stud. Oceanogr. 58 (21–22), 2293–2300.

Iglesias-Rodriguez, M.D., Brown, C.W.C.W., Doney, S.C.S.C., Kleypas, J., Kolber, D., Kolber, Z., Hayes, P.K.P.K., Falkowski, P.G.P.G., Iglesias-Rodríguez, M.D., Brown, C. W.C.W., Doney, S.C.S.C., Kleypas, J., Kolber, D., Kolber, Z., Hayes, P.K.P.K., Falkowski, P.G.P.G., 2002. Representing key phytoplankton functional groups in ocean carbon cycle models: Coccolithophorids. Glob. Biogeochem. Cycles 16. https://doi.org/10.1029/2001GB001454, 47–1-47–.

IPCC, 2013. Climate Change 2013: The Physical Science Basis. Contribution of Working Group I to the Fifth Assessment Report of the Intergovernmental Panel on Climate Change. Cambridge University Press, Cambridge, United Kingdom and New York, NY, USA. https://doi.org/10.1017/CBO9781107415324.

Iversen, M.H., Ploug, H., 2010. Ballast minerals and the sinking carbon flux in the ocean: carbon-specific respiration rates and sinking velocity of marine snow aggregates. Biogeosciences 7, 2613–2624. https://doi.org/10.5194/bg-7-2613-2010.

Iversen, M.H., Robert, M.L., 2015. Ballasting effects of smectite on aggregate formation and export from a natural plankton community. Mar. Chem. 175, 18–27. https://doi.org/10.1016/J.MARCHEM.2015.04.009.

Jemai, A., Wollschläger, J., Voß, D., Zielinski, O., 2021. Radiometry on argo floats: from the multispectral State-of-the-Art on the step to hyperspectral technology. Front. Mar. Sci. 8, 676537. https://doi.org/10.3389/fmars.2021.676537.

Jin, X., Gruber, N., Dune, J.P., Sarmiento, J.L., Armstrong, R.A., 2006. Diagnosing the contribution of phytoplankton functional groups to the production and export of particulate organic carbon, CaCO3, and opal from global nutrient and alkalinity distributions. Global Biogeochem. Cycles 20. https://doi.org/10.1029/2005GB002532.

Johnson, K., Claustre, H., 2016. The scientific rationale, design, and Implementation Plan for a Biogeochemical-Argo float array. https://doi.org/10.13155/46601.

Johnson, K.S., Plant, J.N., Coletti, L.J., Jannasch, H.W., Sakamoto, C.M., Riser, S.C., Swift, D.D., Williams, N.L., Boss, E., Haëntjens, N., Talley, L.D., Sarmiento, J.L., 2017. Biogeochemical sensor performance in the SOCCOM profiling float array. J. Geophys. Res. Ocean. 122, 6416–6436. https://doi.org/10.1002/2017JC012838.

Jones, D.C., Ito, T., Takano, Y., Hsu, W.C., 2014. Spatial and seasonal variability of the air-sea equilibration timescale of carbon dioxide. Glob. Biogeochem. Cycles 28, 1163–1178. https://doi.org/10.1002/2014GB004813.

Kalberer, M., Fischer, G., Pätzold, J., Donner, B., Segl, M., Wefer, G., 1993. Seasonal sedimentation and stable isotope records of pteropods off Cap Blanc. Mar. Geol. 113 (3–4), 305–320.

Kiss, P., Jonkers, L., Hudáčková, N., Reuter, R.T., Donner, B., Fischer, G., Kucera, M., 2021. Determinants of planktonic foraminifera calcite flux: implications for the prediction of intra- and inter-annual pelagic carbonate budgets. Glob. Biogeochem. Cycles 35. https://doi.org/10.1029/2020GB006748.

Kitchen, J.C., Zaneveld, J.R.V., 1992. A three-layered sphere model of the optical properties of phytoplankton. Limnol. Oceanogr. 37, 1680–1690. https://doi.org/10.4319/lo.1992.37.8.1680.

Klaas, C., Archer, D.E., 2002. Association of sinking organic matter with various types of mineral ballast in the deep sea: implications for the rain ratio. Glob. Biogeochem. Cycles 16. https://doi.org/10.1029/2001GB001765, 63–1-63–14.

Köbrich, M., Baumann, K.H., 2009. Coccolithophore flux in a sediment trap off Cape Blanc (NW Africa). J. Nannoplankt. Res. 30, 83–96.

Koestner, D., Stramski, D., Reynolds, R.A., 2022. A multivariable empirical algorithm for estimating particulate organic carbon concentration in marine environments from optical backscattering and chlorophyll-a measurements. Front. Mar. Sci. 9, 941950 https://doi.org/10.3389/FMARS.2022.941950.

Koeve, W., 2002. Upper Ocean carbon fluxes in the Atlantic Ocean: the importance of the POC:PIC ratio. Glob. Biogeochem. Cycles 16. https://doi.org/10.1029/2001GB001836, 4–1-4–17.

Kondrik, D., Kazakov, E., Pozdnyakov, D., 2019. A synthetic satellite dataset of the spatio-temporal distributions of Emiliania huxleyi blooms and their impacts on Arctic and sub-Arctic marine environments (1998–2016). Earth Syst. Sci. Data 11, 119–128. https://doi.org/10.5194/ESSD-11-119-2019.

Kondrik, D.V., Pozdnyakov, D.V., Johannessen, O.M., 2018. Satellite evidence that E. huxleyi phytoplankton blooms weaken marine carbon sinks. Geophys. Res. Lett. 45, 846–854. https://doi.org/10.1002/2017GL076240.

Koppelmann, R., Schäfer, P., Schiebel, R., 2000. Organic carbon losses measured by heterotrophic activity of mesozooplankton and CaCO3 flux in the bathypelagic zone of the Arabian Sea. Deep-Sea Res. II Top. Stud. Oceanogr. 47 (1–2), 169–187.

Krumhardt, K.M., Lovenduski, N.S., Long, M.C., Levy, M., Lindsay, K., Moore, J.K., Nissen, C., 2019. Coccolithophore growth and calcification in an acidified ocean: insights from community earth system model simulations. J. Adv. Model. Earth Syst. 11, 1418–1437. https://doi.org/10.1029/2018MS001483.

Kwon, E.Y., Primeau, F., Sarmiento, J.L., 2009. The impact of remineralization depth on the air–sea carbon balance. Nat. Geosci. 2, 630–635. https://doi.org/10.1038/ngeo612.

Lacour, L., Briggs, N., Claustre, H., Ardyna, M., Dall'Olmo, G., 2019. The intraseasonal dynamics of the mixed layer pump in the subpolar North Atlantic Ocean: a biogeochemical-argo float approach. Global Biogeochem. Cycles 33, 266–281. https://doi.org/10.1029/2018GB005997.

Lacour, L., Claustre, H., Prieur, L., D'Ortenzio, F., 2015. Phytoplankton biomass cycles in the North Atlantic subpolar gyre: a similar mechanism for two different blooms in the Labrador Sea. Geophys. Res. Lett. 42, 5403–5410. https://doi.org/10.1002/2015GL064540.

Lacour, T., Larivière, J., Babin, M., 2017. Growth, Chl a content, photosynthesis, and elemental composition in polar and temperate microalgae. Limnol. Oceanogr. 62, 43–58. https://doi.org/10.1002/lno.10369.

Lampitt, R.S., Salter, I., de Cuevas, B.A., Hartman, S., Larkin, K.E., Pebody, C.A., 2010. Long-term variability of downward particle flux in the deep Northeast Atlantic: causes and trends. DeepRes. Part II Top. Stud. Oceanogr. 57, 1346–1361. https://doi.org/10.1016/J.DSR2.2010.01.011.

Langley, B., Halloran, P.R., Power, A., Rickaby, R.E.M., Chana, P., Diver, P., Thornalley, D., Hacker, C., Love, J., 2020. A new method for isolating and analysing coccospheres within sediment. Sci. Rep. 10 https://doi.org/10.1038/S41598-020-77473-5.

Laurenceau-Cornec, E.C., Le Moigne, F.A.C., Gallinari, M., Moriceau, B., Toullec, J., Iversen, M.H., Engel, A., De La Rocha, C.L., 2020. New guidelines for the application of Stokes' models to the sinking velocity of marine aggregates. Limnol. Oceanogr. 65, 1264–1285. https://doi.org/10.1002/lno.11388.

Le Moigne, F.A.C., Gallinari, M., Laurenceau, E., De La Rocha, C.L., 2013a. Enhanced rates of particulate organic matter remineralization by microzooplankton are diminished by added ballast minerals. Biogeosciences 10, 5755–5765. https://doi.org/10.5194/BG-10-5755-2013.

Le Moigne, F.A.C., Henson, S.A., Sanders, R.J., Madsen, E., 2013b. Global database of surface ocean particulate organic carbon export fluxes diagnosed from the 234Th technique. Earth Syst. Sci. Data 5, 295–304. https://doi.org/10.5194/essd-5-295-2013.

Le Moigne, F.A.C., Pabortsava, K., Marcinko, C.L.J., Martin, P., Sanders, R.J., 2014. Where is mineral ballast important for surface export of particulate organic carbon in the ocean? Geophys. Res. Lett. 41, 8460–8468. https://doi.org/10.1002/2014GL061678.

Lee, K., 2001. Global net community production estimated from the annual cycle of surface water total dissolved inorganic carbon. Limnol. Oceanogr. 46, 1287–1297.

Lee, Z.P., Weidemann, A., Kindle, J., Arnone, R., Carder, K.L., Davis, C., 2007. Euphotic zone depth: its derivation and implication to ocean-color remote sensing. J. Geophys. Res. Ocean. 112, 3009. https://doi.org/10.1029/2006JC003802.

Li, Y.H., Takahashi, T., Broecker, W.S., 1969. Degree of saturation of $CaCO_3$ in the oceans. J. Geophys. Res. 74, 5507–5525.

Loisel, H., Morel, A., 1998. Light scattering and chlorophyll concentration in case 1 waters: a reexamination. Limnol. Oceanogr. 43, 847–858. https://doi.org/10.4319/LO.1998.43.5.0847.

Loisel, H., Vantrepotte, V., Norkvist, K., Mériaux, X., Kheireddine, M., Ras, J., Pujo-Pay, M., Combet, Y., Leblanc, K., Dall'olmo, G., Mauriac, R., Dessailly, D., Moutin, T., 2011. Characterization of the bio-optical anomaly and diurnal variability of particulate matter, as seen from scattering and backscattering coefficients, in ultra-oligotrophic eddies of the Mediterranean Sea. Biogeosciences 8, 3295–3317. https://doi.org/10.5194/bg-8-3295-2011.

Lowenstam, H.A., Weiner, S., 1989. On Biomineralization. Oxford University Press, New York.

Lutz, M.J., Caldeira, K., Dunbar, R.B., Behrenfeld, M.J., 2007. Seasonal rhythms of net primary production andparticulate organic carbon flux to depth describe the efficiency of biological pump in the global ocean. J. Geophys. Res.112, C10011. https://doi.org/10.1029/2006JC003706.

Maier-Reimer, E., Mikolajewicz, U., Winguth, A., 1996. Future Ocean uptake of CO 2: interaction between ocean circulation and biology. Clim. Dyn. 12, 711–721.

Manno, C., Giglio, F., Stowasser, G., Fielding, S., Enderlein, P., Tarling, G.A., 2018. Threatened species drive the strength of the carbonate pump in the northern Scotia Sea. Nat. Commun. 91 (9), 1–7. https://doi.org/10.1038/s41467-018-07088-y.

Marchant, M., Hebbeln, D., Wefer, G., 1998. Seasonal flux patterns of planktic foraminifera in the Peru-Chile current. DeepRes. Part I Oceanogr. Res. Pap. 45, 1161–1185. https://doi.org/10.1016/S0967-0637(98)00009-0.

Marchant, M., Hebbeln, D., Wefer, G., 1998. Seasonal flux patterns of planktic foraminifera in the Peru–Chile Current. Deep Sea Res. Part I Oceanogr. Res. Pap. 45 (7), 1161–1185.

Marsay, C.M., Sanders, R.J., Henson, S.A., Pabortsava, K., Achterberg, E.P., Lampitt, R.S., 2015. Attenuation of sinking particulate organic carbon flux through the mesopelagic ocean. Proc. Natl. Acad. Sci. U. S. A. 112, 1089–1094. https://doi.org/10.1073/pnas.1415311112.

Mayer, L.M., 1994. Surface area control of organic carbon accumulation in continental shelf sediments. Geochim. Cosmochim. Acta 58, 1271–1284. https://doi.org/10.1016/0016-7037(94)90381-6.

Meilland, J., Schiebel, R., Monaco, C.L., Sanchez, S., Howa, H., 2018. Abundances and test weights of living planktic foraminifers across the Southwest Indian Ocean: implications for carbon fluxes. Deep-Sea Res. I Oceanogr. Res. Pap. 131, 27–40.

Menschel, E., González, H.E., Giesecke, R., 2016. Coastal-oceanic distribution gradient of coccolithophores and their role in the carbonate flux of the upwelling system off Concepción, Chile (36°S). J. Plankton Res. 38, 798–817. https://doi.org/10.1093/plankt/fbw037.

Mergulhao, L.P., Guptha, M.V.S., Unger, D., Murty, V.S.N., 2013. Seasonality and variability of coccolithophore fluxes in response to diverse oceanographic regimes in the Bay of Bengal: sediment trap results. Palaeogeogr. Palaeoclimatol. Palaeoecol. 371, 119–135.

Mergulhao, L.P., Mohan, R., Murty, V.S.N., Guptha, M.V.S., Sinha, D.K., 2006. Coccolithophores from the central Arabian Sea: sediment trap results. J. Earth Syst. Sci. 115, 415–428. https://doi.org/10.1007/BF02702870.

Meinecke, G., Wefer, G., 1990. Seasonal pteropod sedimentation in the Norwegian Sea. Palaeogeogr. Palaeoclimatol. Palaeoecol. 79 (1–2), 129–147.

Mignot, A., Ferrari, R., Claustre, H., 2018. Floats with bio-optical sensors reveal what processes trigger the North Atlantic bloom. Nat. Commun. 9, 190. https://doi.org/10.1038/s41467-017-02143-6.

Milliman, J.D., Droxler, A.W., 1996. Neritic and pelagic carbonate sedimentation in the marine environment: ignorance is not bliss. Geol. Rundschau 85, 496–504. https://doi.org/10.1007/BF02369004.

Milliman, J.D., Troy, P.J., Balch, W.M., Adams, A.K., Li, Y.H., Mackenzie, F.T., 1999. Biologically mediated dissolution of calcium carbonate above the chemical lysocline? DeepRes. Part I Oceanogr. Res. Pap. 46, 1653–1669. https://doi.org/10.1016/S0967-0637(99)00034-5.

Monteiro, F.M., Bach, L.T., Brownlee, C., Bown, P., Rickaby, R.E.M., Poulton, A.J., Tyrrell, T., Beaufort, L., Dutkiewicz, S., Gibbs, S., Gutowska, M.A., Lee, R., Riebesell, U., Young, J., Ridgwell, A., 2016. Why marine phytoplankton calcify. Sci. Adv. 2 https://doi.org/10.1126/sciadv.1501822 e1501822-e1501822.

Moore, T.S., Dowell, M.D., Franz, B.A., 2012. Detection of coccolithophore blooms in ocean color satellite imagery: a generalized approach for use with multiple sensors. Remote Sens. Environ. 117, 249–263. https://doi.org/10.1016/j.rse.2011.10.001.

Morel, A., Bricaud, A., 1986. Inherent optical properties of algal cells, including picoplankton. Theoretical and experimental results. Can. Bull. Fish. Aquat. Sci. 214, 521–559.

Mucci, A., 1983. The solubility of calcite and aragonite in seawater at various salinities, temperatures, and one atmosphere total pressure. Am. J. Sci. 283, 780–799. https://doi.org/10.2475/AJS.283.7.780.

Murnane, R., Sarmiento, J.L., Le Quéré, C., 1999. Spatial distribution of airsea CO2 fluxes and the interhemispheric transport of carbon by the oceans. Global Biogeochem. Cycles 13 (2), 287–305.

Neukermans, G., Fournier, G., 2018. Optical modeling of spectral backscattering and remote sensing reflectance from Emiliania huxleyi Blooms. Front. Mar. Sci. 5, 146. https://doi.org/10.3389/fmars.2018.00146.

Neukermans, G., Fournier, G.R., 2022. A method to produce a matched pair of polarizing filters and a method and apparatus to determine the concentration of birefringent particles using a pair of polarizing filters. International patent application number WO/2022/002939. https://patentscope.wipo.int/search/en/detail.jsf?docId=WO2022002939.

Neukermans, G., Loisel, H., Mériaux, X., Astoreca, R., McKee, D., 2012. In situ variability of mass-specific beam attenuation and backscattering of marine particles with respect to particle size, density, and composition. Limnol. Oceanogr. 57, 124–144. https://doi.org/10.4319/lo.2011.57.1.0124.

Neukermans, G., Reynolds, R.A., Stramski, D., 2016. Optical classification and characterization of marine particle assemblages within the western Arctic Ocean. Limnol. Oceanogr. 61, 1472–1494. https://doi.org/10.1002/lno.10316.

Nowicki, M., DeVries, T., Siegel, D.A., 2022. Quantifying the carbon export and sequestration pathways of the ocean's biological carbon pump. Glob. Biogeochem. Cycles 36. https://doi.org/10.1029/2021GB007083 e2021GB007083.

Olson, R.J., Zettler, E.R., Anderson, O.K., 1989. Discrimination of eukaryotic phytoplankton cell types from light scatter and autofluorescence properties measured by flow cytometry. Cytometry 10, 636–643. https://doi.org/10.1002/cyto.990100520.

Organelli, E., Dall'Olmo, G., Brewin, R.J.W., Tarran, G.A., Boss, E., Bricaud, A., 2018. The open-ocean missing backscattering is in the structural complexity of particles. Nat. Commun. 91 (9), 1–11.

Organelli, E., Leymarie, E., Zielinski, O., Uitz, J., D'ortenzio, F., Claustre, H., 2021. Hyperspectral radiometry on biogeochemical-argo floats: a bright perspective for phytoplankton diversity. Oceanography 34, 90–91. https://doi.org/10.5670/OCEANOG.2021.SUPPLEMENT.02-33.

Orr, J.C., Fabry, V.J., Aumont, O., Bopp, L., Doney, S.C., Feely, R.A., Gnanadesikan, A., Gruber, N., Ishida, A., Joos, F., Key, R.M., Lindsay, K., Maier-Reimer, E., Matear, R., Monfray, P., Mouchet, A., Najjar, R.G., Plattner, G.-K., Rodgers, K.B., Sabine, C.L., Sarmiento, J.L., Schlitzer, R., Slater, R.D., Totterdell, I.J., Weirig, M.-F., Yamanaka, Y., Yool, A., 2005. Anthropogenic ocean acidification over the twenty-first century and its impact on calcifying organisms. Nature 437, 681–686. https://doi.org/10.1038/nature04095.

Owens, W.B., Zilberman, N., Johnson, K.S., Claustre, H., Scanderbeg, M., Wijffels, S., Suga, T., 2022. OneArgo: a new paradigm for observing the global ocean. Mar. Technol. Soc. J. 56, 84–90. https://doi.org/10.4031/MTSJ.56.3.8.

Paasche, E., 2001. A review of the coccolithophorid Emiliania huxleyi (Prymnesiophyceae), with particular reference to growth, coccolith formation, and calcification-photosynthesis interactions. Phycologia 40, 503–529. https://doi.org/10.2216/i0031-8884-40-6-503.1.

Passow, U., De La Rocha, C.L., 2006. Accumulation of mineral ballast on organic aggregates. Glob. Biogeochem. Cycles 20, GB1013. https://doi.org/10.1029/2005GB002579.

Peeters, F., Ivanova, E., Conan, S., Brummer, G.-J., Ganssen, G., Troelstra, S., van Hinte, J., 1999. A size analysis of planktic foraminifera from the Arabian Sea. Mar. Micropaleontol. 36 (1), 31–63.

Picheral, M., Catalano, C., Brousseau, D., Claustre, H., Coppola, L., Leymarie, E., Coindat, J., Dias, F., Fevre, S., Guidi, L., Irisson, J.O., Legendre, L., Lombard, F., Mortier, L., Penkerch, C., Rogge, A., Schmechtig, C., Thibault, S., Tixier, T., Waite, A., Stemmann, L., 2022. The Underwater Vision Profiler 6: an imaging sensor of particle size spectra and plankton, for autonomous and cabled platforms. Limnol. Oceanogr. Methods 20, 115–129. https://doi.org/10.1002/LOM3.10475.

Pilskaln, C.H., Neumann, A.C., Bane, J.M., 1989. Periplatform carbonate flux in the northern Bahamas. Deep Sea Res. Part A. Oceanogr.Res.Papers 36 (9), 1391–1406.

Pinsonneault, A.J., Matthews, H.D., Galbraith, E.D., Schmittner, A., 2012. Calcium carbonate production response to future ocean warming and acidification. Biogeosciences 9, 2351–2364. https://doi.org/10.5194/BG-9-2351-2012.

Ploug, H., Iversen, M.H., Koski, M., Buitenhuis, E.T., 2008. Production, oxygen respiration rates, and sinking velocity of copepod fecal pellets: direct measurements of ballasting by opal and calcite. Limnol. Oceanogr. 53, 469–476. https://doi.org/10.4319/LO.2008.53.2.0469.

Poulton, A.J., Adey, T.R., Balch, W.M., Holligan, P.M., 2007. Relating coccolithophore calcification rates to phytoplankton community dynamics: regional differences and implications for carbon export. DeepRes. Part II Top. Stud. Oceanogr. 54, 538–557. https://doi.org/10.1016/J.DSR2.2006.12.003.

Poulton, A.J., Holligan, P.M., Charalampopoulou, A., Adey, T.R., 2017. Coccolithophore ecology in the tropical and subtropical Atlantic Ocean: new perspectives from the Atlantic meridional transect (AMT) programme. Prog. Oceanogr. 158, 150–170. https://doi.org/10.1016/J.POCEAN.2017.01.003.

Puigcorbé, V., Masqué, P., Le Moigne, F.A.C., 2020. Global database of ratios of particulate organic carbon to thorium-234 in the ocean: improving estimates of the biological carbon pump. Earth Syst. Sci. Data 12, 1267–1285. https://doi.org/10.5194/essd-12-1267-2020.

Ramaswamy, V., Gaye, B., 2006. Regional variations in the fluxes of foraminifera carbonate, coccolithophorid carbonate and biogenic opal in the northern Indian Ocean. DeepRes. Part I Oceanogr. Res. Pap. 53, 271–293. https://doi.org/10.1016/J.DSR.2005.11.003.

Rembauville, M., Briggs, N., Ardyna, M., Uitz, J., Catala, P., Penkerc'h, C., Poteau, A., Claustre, H., Blain, S., 2017. Plankton assemblage estimated with BGC-Argo floats in the southern ocean: implications for seasonal successions and particle export. J. Geophys. Res. Ocean. 122, 8278–8292.

Rembauville, M., Meilland, J., Ziveri, P., Schiebel, R., Blain, S., Salter, I., 2016. Planktic foraminifer and coccolith contribution to carbonate export fluxes over the Central Kerguelen Plateau. Deep Sea ResPart I Oceanogr. Res. Pap. 111, 91–101. https://doi.org/10.1016/J.DSR.2016.02.017.

Reynolds, L., Thunell, R.C., 1985. Seasonal succession of planktonic foraminifera in the subpolar North Pacific. J. Foraminiferal Res. 15 (4), 282–301.

Reynolds, R.A., Stramski, D., Neukermans, G., 2016. Optical backscattering by particles in Arctic seawater and relationships to particle mass concentration, size distribution, and bulk composition. Limnol. Oceanogr. 61, 1869–1890. https://doi.org/10.1002/lno.10341.

Riebesell, U., Körtzinger, A., Oschlies, A., 2009. Sensitivities of marine carbon fluxes to ocean change. Proc. Natl. Acad. Sci. U. S. A. 106, 20602–20609. https://doi.org/10.1073/pnas.0813291106.

Rigual Hernández, A.S., Trull, T.W., Nodder, S.D., Flores, J.A., Bostock, H., Abrantes, F., Eriksen, R.S., Sierro, F.J., Davies, D.M., Ballegeer, A.-M., 2020. Coccolithophore biodiversity controls carbonate export in the Southern Ocean. Biogeosciences 17 (1), 245–263.

Roberts, D., Howard, W.R., Moy, A.D., Roberts, J.L., Trull, T.W., Bray, S.G., Hopcroft, R. R., 2011. Interannual pteropod variability in sediment traps deployed above and below the aragonite saturation horizon in the Sub-Antarctic Southern Ocean. Polar Biol. 34 (11), 1739–1750.

Roberts, D., Howard, W.R., Roberts, J.L., Bray, S.G., Moy, A.D., Trull, T.W., Hopcroft, R. R., 2014. Diverse trends in shell weight of three Southern Ocean pteropod taxa collected with Polar Frontal Zone sediment traps from 1997 to 2007. Polar Biol. 37 (10), 1445–1458.

Robertson, J.E., Robinson, C., Turner, D.R., Holligan, P., Watson, A.J., Boyd, P., Fernandez, E., Finch, M., 1994. The impact of a coccolithophore bloom on oceanic carbon uptake in the Northeast Atlantic during summer 1991. Deep Sea ResPart I Oceanogr. Res. Pap. 41, 297–314. https://doi.org/10.1016/0967-0637(94)90005-1.

Roemmich, D., Alford, M.H., Claustre, H., Johnson, K., King, B., Moum, J., Oke, P., Owens, W.B., Pouliquen, S., Purkey, S., Scanderbeg, M., Suga, T., Wijffels, S., Zilberman, N., Bakker, D., Baringer, M., Belbeoch, M., Bittig, H.C., Boss, E., Calil, P., Carse, F., Carval, T., Chai, F., Conchubhair, D.Ó., d'Ortenzio, F., Dall'Olmo, G., Desbruyeres, D., Fennel, K., Fer, I., Ferrari, R., Forget, G., Freeland, H., Fujiki, T., Gehlen, M., Greenan, B., Hallberg, R., Hibiya, T., Hosoda, S., Jayne, S., Jochum, M., Johnson, G.C., Kang, K., Kolodziejczyk, N., Körtzinger, A., Traon, P.-Y. Le, Lenn, Y.-D., Maze, G., Mork, K.A., Morris, T., Nagai, T., Nash, J., Garabato, A.N., Olsen, A., Pattabhi, R.R., Prakash, S., Riser, S., Schmechtig, C., Schmid, C., Shroyer, E., Sterl, A., Sutton, P., Talley, L., Tanhua, T., Thierry, V., Thomalla, S., Toole, J., Troisi, A., Trull, T.W., Turton, J., Velez-Belchi, P.J., Walczowski, W., Wang, H., Wanninkhof, R., Waterhouse, A.F., Waterman, S., Watson, A., Wilson, C., Wong, A.P. S., Xu, J., Yasuda, I., 2019. On the future of argo: a global, full-depth, multi-disciplinary array. Front. Mar. Sci. 6, 439. https://doi.org/10.3389/fmars.2019.00439.

Roesler, C., Uitz, J., Claustre, H., Boss, E., Xing, X., Organelli, E., Briggs, N., Bricaud, A., Schmechtig, C., Poteau, A., D'Ortenzio, F., Ras, J., Drapeau, S., Haëntjens, N., Barbieux, M., 2017. Recommendations for obtaining unbiased chlorophyll estimates from in situ chlorophyll fluorometers: a global analysis of WET Labs ECO sensors. Limnol. Oceanogr. Methods 15, 572–585. https://doi.org/10.1002/LOM3.10185.

Rosengard, S.Z., Lam, P.J., Balch, W.M., Auro, M.E., Pike, S., Drapeau, D., Bowler, B., 2015. Carbon export and transfer to depth across the Southern Ocean Great Calcite Belt. Biogeosciences 12, 3953–3971. https://doi.org/10.5194/bg-12-3953-2015.

Rost, B., Riebesell, U., 2004. Coccolithophores and the biological pump: responses to environmental changes. In: Coccolithophores. Springer Berlin Heidelberg, Berlin, Heidelberg, pp. 99–125. https://doi.org/10.1007/978-3-662-06278-4_5.

Salmon, K.H., Anand, P., Sexton, P.F., Conte, M., 2015. Upper Ocean mixing controls the seasonality of planktonic foraminifer fluxes and associated strength of the carbonate pump in the oligotrophic North Atlantic. Biogeosciences 12, 223–235. https://doi.org/10.5194/BG-12-223-2015.

Salter, I., Schiebel, R., Ziveri, P., Movellan, A., Lampitt, R., Wolff, G.A., 2014. Carbonate counter pump stimulated by natural iron fertilization in the Polar Frontal Zone. Nat. Geosci. 7, 885–889. https://doi.org/10.1038/ngeo2285.

Samtleben, C., Bickert, T., 1990. Coccoliths in sediment traps from the Norwegian Sea. Mar. Micropaleontol. 16 (1–2), 39–64.

Sarmiento, J.L., Gruber, N., 2006. Ocean Biogeochemical Dynamics. Princeton University Press, Princeton, New Jersey. https://doi.org/10.2307/j.ctt3fgxqx.

Sarmiento, J.L., Dunne, J., Gnanadesikan, A., Key, R.M., Matsumoto, K., Slater, R., 2002. A new estimate of the CaCO 3 to organic carbon export ratio. Glob. Biogeochem. Cycles 16. https://doi.org/10.1029/2002GB001919, 54–1-54–12.
Schiebel, R., Hemleben, C., 2000. Interannual variability of planktic foraminiferal populations and test flux in the eastern North Atlantic Ocean (JGOFS). Deep-Sea Res. II Top. Stud. Oceanogr. 47 (9–11), 1809–1852.
Schiebel, R., 2002. Planktic foraminiferal sedimentation and the marine calcite budget. Glob. Biogeochem. Cycles 16. https://doi.org/10.1029/2001GB001459, 3–1-3–21.
Schiebel, R., Hemleben, C., 2017. Planktic foraminifers in the modern ocean. Planktic Foraminifers Mod. Ocean 1–358. https://doi.org/10.1007/978-3-662-50297-6/COVER.
Schiebel, R., Hiller, B., Hemleben, C., 1995. Impacts of storms on recent planktic foraminiferal test production and CaCO3 flux in the North Atlantic at 47 N, 20 W (JGOFS). Mar. Micropaleontol. 26 (1–4), 115–129.
Schiebel, R., Movellan, A., 2012. First-order estimate of the planktic foraminifer biomass in the modern ocean. Earth Syst. Sci. Data 4, 75–89. https://doi.org/10.5194/essd-4-75-2012.
Schmidt, K., De La Rocha, C.L., Gallinari, M., Cortese, G., 2014. Not all calcite ballast is created equal: differing effects of foraminiferan and coccolith calcite on the formation and sinking of aggregates. Biogeosciences 11, 135–145. https://doi.org/10.5194/bg-11-135-2014.
Scholten, J.C., Fietzke, J., Vogler, S., Rutgers van der Loeff, M.M., Mangini, A., Koeve, W., Waniek, J., Stoffers, P., Antia, A., Kuss, J., 2001. Trapping efficiencies of sediment traps from the deep Eastern North Atlantic: the 230Th calibration. Deep Sea Res. Part II Top. Stud. Oceanogr. 48, 10, 2383–2408. https://doi.org/10.1016/S0967-0645(00)00176-4.
Shutler, J.D., Land, P.E., Brown, C.W., Findlay, H.S., Donlon, C.J., Medland, M., Snooke, R., Blackford, J.C., 2013. Coccolithophore surface distributions in the North Atlantic and their modulation of the air-sea flux of CO2 from 10 years of satellite Earth observation data. Biogeosciences 10, 2699–2709. https://doi.org/10.5194/bg-10-2699-2013.
Siegel, D.A., Buesseler, K.O., Behrenfeld, M.J., Benitez-Nelson, C.R., Boss, E., Brzezinski, M.A., Burd, A., Carlson, C.A., D'Asaro, E.A., Doney, S.C., Perry, M.J., Stanley, R.H.R., Steinberg, D.K., 2016. Prediction of the export and fate of Global Ocean net primary production: the EXPORTS science plan. Front. Mar. Sci. 3, 22. https://doi.org/10.3389/fmars.2016.00022.
Siegel, D.A., Buesseler, K.O., Doney, S.C., Sailley, S.F., Behrenfeld, M.J., Boyd, P.W., 2014. Global assessment of ocean carbon export by combining satellite observations and food-web models. Glob. Biogeochem. Cycles 28, 181–196. https://doi.org/10.1002/2013GB004743.
Siegel, D.A., Devries, T., Doney, S.C., Bell, T., 2021. Assessing the sequestration time scales of some ocean-based carbon dioxide reduction strategies. Environ. Res. Lett. 16, 104003 https://doi.org/10.1088/1748-9326/AC0BE0.
Singh, A., Conan, S.-H., 2008. Aragonite pteropod flux to the Somali Basin, NW Arabian Sea. Deep Sea Res. Part I Oceanogr. Res. Pap. 55 (5), 661–669.
Smith, S.V., 2013. Parsing the oceanic calcium carbonate cycle : a net atmospheric carbon dioxide source or a sink? Association for the Sciences of Limnology and Oceanography. https://doi.org/10.4319/svsmith.2013.978-0-9845591-2-1.
Smith, S.V., Gattuso, J.-P., 2011. Balancing the Oceanic calcium carbonate cycle: consequences of variable water columnΨ. Aquat. Geochem. 17, 327–337. https://doi.org/10.1007/s10498-010-9109-9.
Smith, S.V., Mackenzie, F.T., 2016. The role of CaCO3 reactions in the contemporary oceanic CO2 cycle. Aquat. Geochem. 22, 153–175. https://doi.org/10.1007/s10498-015-9282-y.
Sprengel, C., Baumann, K.-H., Neuer, S., 2000. Seasonal and interannual variation of coccolithophore fluxes and species composition in sediment traps north of Gran Canaria (29 N 15 W). Mar. Micropaleontol 39 (1–4), 157–178.
Stramski, D., Reynolds, R.A., Babin, M., Kaczmarek, S., Lewis, M.R., Röttgers, R., Sciandra, A., Stramska, M., Twardowski, M.S., Franz, B.A., Claustre, H., 2008. Relationships between the surface concentration of particulate organic carbon and optical properties in the eastern South Pacific and eastern Atlantic Oceans. Biogeosciences 5, 171–201. https://doi.org/10.5194/BG-5-171-2008.
Stramski, D., Reynolds, R.A., Kahru, M., Mitchell, B.G., 1999. Estimation of particulate organic carbon in the ocean from satellite remote sensing. <sb:title>Science </sb:title>(80-.) 285, 239–242. https://doi.org/10.1126/science.285.5425.239.
Subhas, A.V., Dong, S., Naviaux, J.D., Rollins, N.E., Ziveri, P., Gray, W., Rae, J.W.B., Liu, X., Byrne, R.H., Chen, S., Moore, C., Martell-Bonet, L., Steiner, Z., Antler, G., Hu, H., Lunstrum, A., Hou, Y., Kemnitz, N., Stutsman, J., Pallacks, S., Dugenne, M., Quay, P.D., Berelson, W.M., Adkins, J.F., 2022. Shallow calcium carbonate cycling in the North Pacific Ocean. Glob. Biogeochem. Cycles 36. https://doi.org/10.1029/2022GB007388.
Sulpis, O., Jeansson, E., Dinauer, A., Lauvset, S.K., Middelburg, J.J., 2021. Calcium carbonate dissolution patterns in the ocean. Nat. Geosci. 146 (14), 423–428. https://doi.org/10.1038/s41561-021-00743-y, 2021.
Takahashi, T., Sutherland, S.C., Chipman, D.W., Goddard, J.G., Ho, C., Newberger, T., Sweeney, C., Munro, D.R., 2014. Climatological distributions of pH, pCO2, total CO2, alkalinity, and CaCO3 saturation in the global surface ocean, and temporal changes at selected locations. Mar. Chem. 164, 95–125. https://doi.org/10.1016/J.MARCHEM.2014.06.004.
Tanaka, Y., Kawahata, H., 2001. Seasonal occurrence of coccoliths in sediment traps from West Caroline Basin, equatorial West Pacific Ocean. Mar. Micropaleontol. 43, 273–284. https://doi.org/10.1016/S0377-8398(01)00027-5.
Terrats, L., Claustre, H., Cornec, M., Mangin, A., Neukermans, G., 2020. Detection of coccolithophore blooms with BioGeoChemical-argo floats. Geophys. Res. Lett. 47 https://doi.org/10.1029/2020GL090559 e2020GL090559.
Thunell, R.C., Honjo, S., 1981. Planktonic foraminiferal flux to the deep ocean: Sediment trap results from the tropical Atlantic and the central Pacific. Mar. Geol. 40 (3), 237–253.
Thunell, R.C., Honjo, S., 1987. Seasonal and interannual changes in planktonic foraminiferal production in the North Pacific. Nature 328 (6128), 335–337.
Thunell, R.C., Reynolds, L.A., 1984. Sedimentation of Planktonic Foraminifera: seasonal changes in species flux in the Panama Basin. Micropaleontology 243–262.
Torres Valdés, S., Painter, S.C., Martin, A.P., Sanders, R., Felden, J., 2014. Data compilation of fluxes of sedimenting material from sediment traps in the Atlantic Ocean. Earth Syst. Sci. Data 6, 123–145. https://doi.org/10.5194/ESSD-6-123-2014.
Tsurumi, M., Mackas, D., Whitney, F., DiBacco, C., Galbraith, M., Wong, C., 2005. Pteropods, eddies, carbon flux, and climate variability in the Alaska Gyre. Deep-Sea Res. II Top. Stud. Oceanogr. 52 (7–8), 1037–1053.
Twardowski, M.S., Boss, E., Macdonald, J.B., Pegau, W.S., Barnard, A.H., Zaneveld, J.R. V., 2001. A model for estimating bulk refractive index from the optical backscattering ratio and the implications for understanding particle composition in case I and case II waters. J. Geophys. Res. Ocean. 106, 14129–14142. https://doi.org/10.1029/2000JC000404.
Ulloa, O., Sathyendranath, S., Platt, T., 1994. Effect of the particle-size distribution on the backscattering ratio in seawater. Appl. Opt. 33 (30), 7070–7077. https://doi.org/10.1364/AO.33.007070.
Volk, T., Hoffert, M.I., 1985. Ocean carbon pumps: analysis of relative strengths and efficiencies in ocean-driven atmospheric CO 2 changes. In: Sundquist, E.T., Broecker, W.S. (Eds.), The Carbon Cycle and Atmospheric CO2: Natural Variations Archean to Present. American Geophysical Union, pp. 99–110. https://doi.org/10.1029/GM032p0099.
von Dassow, P., van den Engh, G., Iglesias-Rodriguez, D., Gittins, J.R., 2012. Calcification state of coccolithophores can be assessed by light scatter depolarization measurements with flow cytometry. J. Plankton Res. 34, 1011–1027. https://doi.org/10.1093/plankt/fbs061.
Wefer, G., Suess, E., Balzer, W., Liebezeit, G., Müller, P.J., Ungerer, C.A., Zenk, W., 1982. Fluxes of biogenic components from sediment trap deployment in circumpolar waters of the Drake Passage. Nature 299 (5879), 145–147.
Wilson, J.D., Barker, S., Ridgwell, A., 2012. Assessment of the spatial variability in particulate organic matter and mineral sinking fluxes in the ocean interior: implications for the ballast hypothesis. Glob. Biogeochem. Cycles 26, GB4011. https://doi.org/10.1029/2012GB004398.
Wilson, R., Millero, F., Taylor, J., Walsh, P., Christensen, V., Jennings, S., Grosell, M., 2009. Contribution of fish to the marine inorganic carbon cycle. Science 323 (5912), 359–362.
Winter, A., Henderiks, J., Beaufort, L., Rickaby, R.E.M., Brown, C.W., 2014. Poleward expansion of the coccolithophore Emiliania huxleyi. J. Plankton Res. 36, 316–325. https://doi.org/10.1093/plankt/fbt110.
Winter, A., Siesser, W.G., 1994. Coccolithophores. Cambridge University Press, Cambridge;New York NY.
Wong, C.S., Whitney, F.A., Crawford, D.W., Iseki, K., Matear, R.J., Johnson, W.K., Page, J.S., Timothy, D., 1999. Seasonal and interannual variability in particle fluxes of carbon, nitrogen and silicon from time series of sediment traps at Ocean Station P, 1982– 1993: Relationship to changes in subarctic primary productivity. Deep Sea Res. Part II 46, 2735–2760.
Xing, X., Boss, E., Zhang, J., Chai, F., 2020. Evaluation of ocean color remote sensing algorithms for diffuse attenuation coefficients and optical depths with data collected on BGC-argo floats. Remote Sens. https://doi.org/10.3390/rs12152367.
Xing, X., Briggs, N., Boss, E., Claustre, H., 2018. Improved correction for non-photochemical quenching of in situ chlorophyll fluorescence based on a synchronous irradiance profile. Opt. Express 26, 24734. https://doi.org/10.1364/OE.26.024734.
Xing, X., Claustre, H., Uitz, J., Mignot, A., Poteau, A., Wang, H., 2014. Seasonal variations of bio-optical properties and their interrelationships observed by Bio-Argo floats in the subpolar North Atlantic. J. Geophys. Res. Ocean. 119, 7372–7388. https://doi.org/10.1002/2014JC010189.
Yamanaka, Y., Tajika, E., 1996. The role of the vertical fluxes of particulate organic matter and calcite in the ocean carbon cycle: Studies using an ocean biogeochemical general circulation model. Global Biogeochem. Cycles 10 (2), 361–382.
Young, J.R., Didymus, J.M., Brown, P.R., Prins, B., Mann, S., 1992. Crystal assembly and phylogenetic evolution in heterococcoliths. Nature 356, 516–518. https://doi.org/10.1038/356516a0.
Young, J.R., Poulton, A.J., Tyrrell, T., 2014. Morphology of Emiliania huxleyi coccoliths on the northwestern European shelf – is there an influence of carbonate chemistry? Biogeosciences 11, 4771–4782. https://doi.org/10.5194/bg-11-4771-2014.
Young, J.R., Ziveri, P., 2000. Calculation of coccolith volume and it use in calibration of carbonate flux estimates. Deep Sea ResPart II Top. Stud. Oceanogr. 47, 1679–1700. https://doi.org/10.1016/S0967-0645(00)00003-5.
Zeebe, R.E., Wolf-Gladrow, D., 2001. CO2 in Seawater: Equilibrium, Kinetics, Isotopes: Equilibrium, Kinetics, Isotopes. Elsevier.
Zhai, P.-W., Hu, Y., Trepte, C.R., Winker, D.M., Josset, D.B., Lucker, P.L., Kattawar, G.W., 2013. Inherent optical properties of the coccolithophore: Emiliania huxleyi. Opt. Express 21, 17625. https://doi.org/10.1364/OE.21.017625.
Ziveri, P., Broerse, A.T.C., van Hinte, J.E., Westbroek, P., Honjo, S., 2000. The fate of coccoliths at 48°N 21°W, Northeastern Atlantic. Deep Sea Res. Part II Top. Stud. Oceanogr. 47, 1853–1875. https://doi.org/10.1016/S0967-0645(00)00009-6.
Ziveri, P., de Bernardi, B., Baumann, K.H., Stoll, H.M., Mortyn, P.G., 2007. Sinking of coccolith carbonate and potential contribution to organic carbon ballasting in the

deep ocean. DeepRes. Part II Top. Stud. Oceanogr. 54, 659–675. https://doi.org/10.1016/J.DSR2.2007.01.006.

Ziveri, P., Thunell, R., 2000. Coccolithophore export production in Guaymas Basin, Gulf of California: response to climate forcing. Deep Sea Res. Part II Top. Stud. Oceanogr. 47 (9–11), 2073–2100.

Ziveri, P., Thunell, R.C., Rio, D., 1995. Export production of coccolithophores in an upwelling region: results from San Pedro Basin,Southern California Borderlands. Marine Micropaleontol. 24 (3–4), 335–358.